KAUNAS UNIVERSITY OF TECHNOLOGY

LINA RAMANAUSKAITĖ

THE SYNTHESIS, CHARACTERISATION AND APPLICATION OF PLASMONIC NANOSTRUCTURES FOR SURFACE ENHANCED RAMAN SPECTROSCOPY

Doctoral dissertation
Physical Sciences, Chemistry (03P)

2016, Kaunas

UDK 543.064 + 543.424.2] (043.3)

Doctoral dissertation was prepared in Kaunas University of Technology, Faculty of Mathematics and Natural Sciences, Research Centre for Microsystems and Nanotechnology during the period of 2012 – 2016. The studies were supported by Research Council of Lithuania.

Scientific Supervisor:

Prof. Habil. Dr Valentinas SNITKA (Kaunas University of Technology, Physical Sciences, Chemistry – 03 P).

Doctoral dissertation has been published in:
http://ktu.edu

English Language Editor:

UAB “Synergium”

ISBN

KAUNO TECHNOLOGIJOS UNIVERSITETAS

LINA RAMANAUSKAITĖ

PLAZMONINIŲ NANOSTRUKTŪRŲ SINTEZĖ, CHARAKTERIZAVIMAS IR TAIKYMAS PAVIRŠIUMI STIMULIUOTAI RAMANO SPEKTROSKOPIJAI

Daktaro disertacija
Fiziniai mokslai, chemija (03P)

2016, Kaunas

UDK 543.064 + 543.424.2] (043.3)

Disertacija rengta 2012–2016 metais Kauno technologijos universiteto, Matematikos ir gamtos mokslų fakulteto Mikrosistemų ir nanotechnologijų mokslo centre. Mokslinius tyrimus rėmė Lietuvos mokslo taryba.

Mokslinis vadovas:

Prof. habil. dr. Valentinas SNITKA (Kauno technologijos universitetas, fiziniai mokslai, chemija – 03 P).

Interneto svetainės, kurioje skelbiama disertacija, adresas:
http://ktu.edu

Redagavo:

UAB “Synergium”

ISBN

TABLE OF CONTENTS

A LIST OF ABBREVIATIONS

AFM – atomic force microscopy
BP – benzylpenicillin
EDX – energy dispersive X-ray spectroscopy
EF – enhancement factor
GO – graphene oxide
I-V – current-voltage characteristics
LSP – local surface plasmon
LSPR – localised surface plasmon resonance
PEG – polyethylene glycol
PEG 400 – polyethylene glycol 400
R6G – rhodamine dye
SD – standard deviation
SEM – scanning electron microscopy
SERS – surface enhanced Raman spectroscopy
SPR – surface plasmon resonance
TEOS – tetraethyl orthosilicate
TERS – tip enhanced Raman spectroscopy

A LIST OF FIGURES

Fig. 3.8. The statistical evaluation of spherical silver nanoparticle formation repeatability: (A) AFM image of spherical silver nanoparticles and their height histogram (1); (B) grain image of spherical silver nanoparticles; (C) a graph showing the average diameter of spherical silver nanoparticles on 5 samples

Fig. 3.9. The statistical evaluation of silver self-assembled networks: (A) AFM image of self-assembled silver nanoparticles formed on the silica film; (B) fractal dimensions of roughness of 5 samples

Fig. 3.10. The simulation of EM distribution: for a single silver nanoring (A); for a system consisting of three silver nanorings (B)

Fig. 3.11. The average spectra of crystal violet analyte collected at 50 randomly selected points of the sample: (A) Raman spectra obtained on microscopic glass; (B) SERS spectra obtained on silver nanoring decorated SERS substrate; (C) SERS spectra obtained on silver nanosphere decorated SERS substrate; (D) SERS spectra obtained on silver self-assembled nanoparticle decorated SERS substrate. The acquisition time for the collection of Raman and SERS spectra was 1s

Fig. 3.12. The AFM images of the silver SERS substrates and the height histograms of silver nanoparticles distribution. For the evaluation of nanoparticles shapes and height repeatability, 10 samples (marked 1-10) were characterised in the scanning area of 3 × 3μm

Fig. 3.13. EDX spectrum of silver SERS substrate (A); SEM image of the SERS substrate demonstrating the silver nanoparticles of irregular shapes (B) (magnification: 30000×; high vacuum mode ((30.00 kV)); UV-Vis spectra showing a plasmon at 447 nm that confirms the presence of silver nanoparticles

Fig. 3.14. The AFM images of the silver SERS substrates and the height histograms of silver nanoparticles distribution. For the evaluation of nanoparticles shapes and height repeatability, 10 samples (marked 1-10) were characterised in the scanning area of 3 × 3μm

Fig. 3.15. EDX spectrum of silver SERS substrate (A); SEM image of silver nanotriangle (magnification: 400000×; high vacuum mode ((30.00 kV)); (B) UV-Vis spectra showing a plasmon at 490 nm that confirms the presence of silver nanoparticles

Fig. 3.16. Enhancement of electromagnetic field intensity in a logarithmic scale for a pair of nanotriangles in two cross-sections: (A) and (C) in the z = 0 plane, (B) and (D) in the z = 50 nm plane. The incident light is polarised in the x-axis for (A) and (B) and in the y-axis for (C) and (D)

Fig. 3.17 The AFM images of the gold SERS substrates and the height histograms of gold nanoparticles distribution. For the evaluation of nanoparticles shapes and height repeatability, 10 samples (marked 1-10) were characterised in the scanning area of 3 × 3μm

Fig. 3.18. EDX spectrum of gold SERS substrate (A); SEM image of gold SERS substrate (magnification: 30000×; high vacuum mode ((30.00 kV)); (B) UV-Vis spectra showing a plasmon at 490 nm that confirms the presence of silver nanoparticles

Fig. 3.19. Raman spectra of pentacene obtained on a blank silicon wafer (A); the SERS spectra of pentacene obtained on gold SERS substrate (B); the SERS spectra of pentacene obtained on a SERS substrate decorated with irregular shapes of silver nanoparticles (C); the SERS spectra of pentacene obtained on triangular silver nanoparticle decorated SERS substrate (D). In all the cases the acquisition time for Raman signal collection was 1 s

Fig. 3.20. Raman spectra of R6G obtained on blank silicon wafer (A); the SERS spectra of R6G obtained on gold SERS substrate (B); the SERS spectra of R6G obtained on SERS substrate decorated with irregular shapes of silver nanoparticles (C); the SERS spectra of R6G obtained on triangular silver nanoparticle decorated SERS substrate (D). In all the cases the acquisition time for Raman signal collection was 1 s

Fig. 3.21. SERS spectra of α-synuclein of different concentrations in aqueous solutions

Fig. 3.22. AFM images of the silver nanotriangle decorated SERS substrate: (A) height image of silver nanotriangles measured at the first randomly selected point of the sample and

A LIST OF TABLES

INTRODUCTION

The relevance of the work. In recent years, research in nanotechnology has grown rapidly, thus proposing novel solutions and innovations in analytical science. Most of the existing devices and methods used for the characterisation of the target objects at the nanoscale provide information about the shapes, surface morphology, electrical and mechanical properties of the nanoobjects. These include atomic force microscopy (AFM), scanning electron microscopy (SEM), transmission electron microscopy (TEM), and scanning tunnelling microscopy (STM). However, there is a lack of devices providing complementary information about the physical properties and chemical composition of the objects (including bio-objects) with a nanometric resolution at the same time. Surface enhanced Raman spectroscopy (SERS) is a powerful analytical tool enabling diverse information to be obtained about the conformation of molecules as well as their chemical composition with a high sensitivity. Such capabilities make SERS attractive for the detection of molecular traces (explosives, drugs or toxic substances) on surfaces, vapours or liquids. Moreover, the increasing numbers of products that contain nanoparticles require extensive research focused on their influence on human health, and mechanisms by which they affect biochemical processes in the body. However, SERS still faces challenges, such as low reproducibility and sensitivity of the SERS substrates, while commercially available SERS substrates are expensive and require special storage and measurements conditions. Additionally, most of such substrates are two dimensional (2D) planar systems limiting the SERS-active area to a single Cartesian plane. For this reason, the fabrication of 3D SERS sensors with the goal to expand the content of hot spots in the third dimension along the z-axis is an important issue in the development of highly-sensitive SERS substrates. Considering this, the key point of this work is to design, develop and investigate the novel SERS sensors for emerging areas such as highly sensitive detection of molecular traces as well as the interaction mechanisms at the bio-nano interface. Moreover, the novel methodologies for the local modification of materials at a nano-level can provide ground breaking solutions for the development of the next generation devices, such as nanostructured organic semiconductors.

During the last decade, the number of scientific publications in the field of SERS has grown intensively (Fig. 1). Such tendency shows that the SERS technique is going to be a new breakthrough in analytical science in various areas of applications, including medicine, diagnostics, food and the cosmetics industry, ecology, forensic expertise, and even space. Therefore, the development of new methodologies for the fabrication of inexpensive, reproducible and highly-sensitive SERS substrates is of great importance.

The aim of the work. To synthesise and investigate porous hybrid plasmonic nanostructures for shape-controllable and highly efficient 3D SERS substrates and to apply them for the detection of molecular traces, investigation of biomolecule interactions with nanostructured surfaces and investigation of phenomena of local plasmon stimulated chemical reactions.

The work addresses the following five objectives:

1. To investigate the formation of sol-gel based nanostructured hybrid films with the potential applicability for the development of novel 3D SERS substrates.

2. To investigate the formation of noble metals plasmonic nanostructures on silicon wafers that would open up the possibility for the development of large area, inexpensive, highly sensitive and reproducible SERS substrates.

3. To investigate the effectiveness of the synthesised SERS substrates for the detection of molecular traces.

4. To investigate the behaviour of the biomolecules at the bio-nano interface that would provide a unique opportunity for the detailed understanding of biomolecules dynamic processes, their orientation and location on the nanostructured surfaces.

5. To investigate the mechanism of the nano-chemical reactions, driven by localised surface plasmon (LSP).

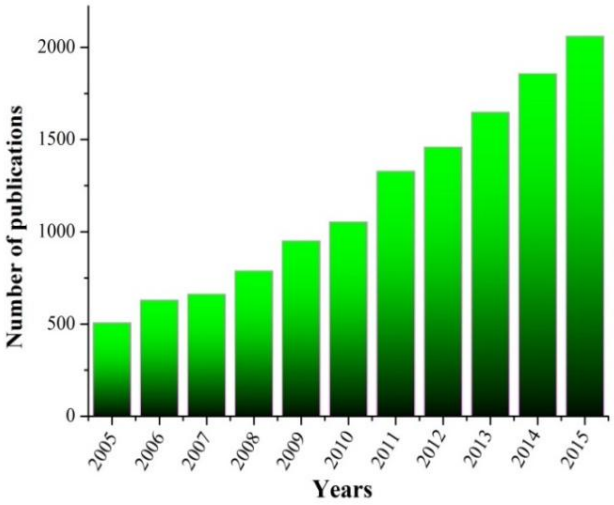

Fig. 1. Growing interest in SERS technique. The plot shows the number of publications during the period 2005-2015. The data are obtained from *Thomson Reuters*^{TM} *Web of Science* citation indexing service for the key words "*surface enhanced Raman spectroscopy*" (accessed on 11 February 2016)

Scientific novelty of the dissertation. In this work, novel methodologies for the synthesis of hybrid porous nanostructures have been proposed. From the analytical chemistry point of view, the interaction of L-alanyl-L-tryptophan dipeptide with a nanostructured silver surface has been investigated for the first time. The possibility to perform nanochemical reactions on the SERS substrate has been demonstrated. The novel methodology for the local reduction of graphene oxide (GO) on the nanostructured silver surface has been developed. The novel methodology for the LSP stimulated synthesis of polyaromatic hydrocarbons (PAHs) has been developed.

Practical significance of the dissertation. The results presented in this work propose inexpensive and reproducible approaches for the fabrication of the SERS sensors applicable for the detection of molecular traces; expand the knowledge of protein interactions with nanostructured surfaces; propose the novel method for the local modification of electrical conductivity of GO, which can be used for the further development of nanostructured organic semiconductors on graphene substrate. Part of the results obtained during the preparation of the dissertation was used in the successfully implemented project *"Nanoscopic investigation of structural transformations of proteins at the nano-bio-interfaces" (NanoProt, 2013-2015)*. The new knowledge and experience gained during the PhD research are applied in the project *"Development of advanced methods for molecular contamination analysis by surface and tip enhanced Raman for space applications" (CONRAM, 2016-2017)* funded by the European Space Agency (ESA).

Approval and publication of research results. The results of the research are presented in 5 publications. All of them are published in the journals listed in the *Thomson Reuters™ Web of Science* publications database with citation index. The results of the research are presented in 13 international conferences (4 of them are invited talks) and 2 seminars.

Overview of the dissertation. The dissertation consists of an introduction, review of literature associated with the topic of the dissertation, applied methods and materials, the results and discussion section, conclusions and a list of references which includes 265 literature sources. The dissertation comprises 110 pages, 47 illustrations, and 9 tables.

Statements for defence:

1. The novel methodology for the synthesis of sol-gel technique based porous hybrid organic-inorganic films for SERS applications has been developed.
2. The novel methodology for the synthesis of noble metals nanostructures on the silicon wafers for SERS applications has been developed. The enhancement of the Raman signal for the rhodamine dye analyte deposited on triangular silver nanoparticle decorated SERS substrate was found to be 10^7. Such enhancement factor is sufficient for the detection of molecular traces on the surface and in liquid.
3. The SERS substrates based on developed methodology allow the detection of α-synuclein (up to 1 fM) and benzylpenicillin (up to 0.25 pM) traces in water and milk respectively.
4. The mechanism of the L-alanyl-L-tryptophan interaction with nanostructured silver surface and its orientation on silver SERS substrate has been investigated and the relationship with Raman (SERS) spectra has been established.
5. The novel methodology for the LSP stimulated reduction of GO and its local chemical-physical characteristics modification has been developed.
6. The possibility to perform nanochemical synthesis on the silver SERS substrate based on the developed methodology has been demonstrated.

1. A LITERATURE REVIEW

1.1. Background of Raman scattering

In 1930, the Indian scientist Sir C.V. Raman was awarded the Nobel Prize in Physics for his discovery of the "Raman effect", which is defined as the change of the light wavelength occurring when a light beam is deflected by molecules (Bumbrah, Sharma, 2015). Such wavelength shift corresponds to the oscillation frequency of a particular molecule, and provides information about its structure. Fundamentally, Raman spectroscopy is an analytical technique based on inelastic scattering of monochromatic light (Hanlon et al., 2000). When a sample is irradiated with a source of monochromatic radiation, usually in the visible part of the spectrum, it interacts with the molecules and results in a scattered light. Photons interacting with the molecules mostly scatter elastically and have the same energy as the incident photons. This process is described as Rayleigh scattering. However, if nuclear motion is induced during the scattering process, energy is transferred from the incident photon to the molecule or, oppositely, from the molecule to the scattered photon. These processes are inelastic and the energy of the scattered photon is different from that of the incident photon by one vibrational unit (Smith, Dent, 2013). This phenomenon is called Raman scattering.

At room temperature, most of the molecules exist in the ground (lowest energy) vibrational state. When the sample is irradiated with a source of light, usually a laser, a photon interacts with the molecule, polarises the cloud of electrons around the nuclei and raises it to a "virtual" (excited) energy state. Since this state is not stable the molecule loses energy and returns to a lower level with the emission of a photon. If the molecule returns to its start position (ground state), there is no frequency shift in the emitted photon and the scattered light is of the same wavelength (Rayleigh scattering). However, if the molecule falls to a distinct level, the energy of the emitted photon is different to that of the incident one. Therefore, if the incident photon gives up energy to the sample it is scattered with a red-shifted frequency (Stokes photons). Alternatively, when the molecule is already in an excited state and gives energy to the scattered photon, the output has a blue-shifted frequency corresponding to anti-Stokes photons (Wang, 2013). Usually, Stokes lines are the most common type of scattering probed within Raman spectroscopy and is of higher intensity compared to anti-Stokes (Tüysüz, Chan, 2015).

Raman, as well as infrared (IR), are the most common vibrational spectroscopies providing information about the specific vibrational and rotational modes of the molecules, also referred to as "fingerprints". However, these methods are based on the different selection rules (Colthup, 2012). In IR spectroscopy, the frequency of the incident light must match the energy differences between the ground and excited vibrational state, leading to the detection of the energy loss of the incident light. The vibrational motion can be IR-active only when the molecular vibration causes a change in the dipole moment of the molecule, while in Raman spectroscopy, Raman-active vibrations must be accompanied by the change in the polarizability of the molecule. Therefore, the activity of a particular vibrational

mode strongly depends on its symmetry and the symmetry of the molecule (Skoog, Holler, and Nieman 1998). Despite the fundamental differences of IR and Raman spectroscopies, these techniques are complementary because the vibrational modes that are allowed in Raman are forbidden in IR, while other vibrations can be observed by both methods.

In chemistry, Raman spectroscopy is an effective tool used for the qualitative (O'Connell et al., 2010; Stone et al., 2004; Rosch et al., 2005) and/or quantitative (Strachan et al., 2007; Lee, Herrman and Yun; 2014, Pratiwi et al., 2002) analysis, offering a number of advantages compared to other analytical techniques. For example, gas or high performance liquid chromatography coupled to mass spectrometry is the basic instrument used for the chemical identification of materials. However, these methods require a long time-consuming preparation of the sample (Kast, Auner, 2015), in some cases the use of hazard solvents, while Raman spectroscopy does not. A major advantage of Raman spectroscopy compared to IR is that water is a strong IR-absorbing medium. For this reason, the IR analysis of samples prepared in aqueous medium is complicated, while Raman spectroscopy allows this problem to be avoided. This aspect is important regarding the biological samples that are required to maintain native conditions.

1.2. Surface Enhanced Raman Scattering

Normal Raman scattering is a weak effect because only 1 of a million photons are scattered in-elastically. Therefore, Raman spectroscopy is not a sensitive technique for the detection of molecular traces in liquids and/or on surfaces. Thus, a weak Raman Effect can be one of the reasons why Raman spectroscopy has been discovered so late. In 1974, a group of researchers reported a surprisingly strong Raman signals from pyridine adsorbed on an electrochemically roughened silver electrode surface (Fleischmann, Hendra and McQuillan, 1974). These observations were the beginning of a new epoch in spectroscopy. A new kind of spectroscopy has been called Surface Enhanced Raman Scattering (SERS). This phenomenon is described as a significant increase in the peaks intensity in the Raman spectrum when molecules are adsorbed on rough metal surfaces. It is now generally accepted that SERS effect is a result of two major enhancement mechanisms: electromagnetic (EM) and chemical effect (CE) (Levin, 2009). Both EM and CE models are thought to operate separately. However, in some systems both enhancements can occur simultaneously and in such cases, they are complementary (Faulds, Hernandez-Santana and Smith, 2010).

EM provides the main contribution, where the local electromagnetic field close to a metal surface is enhanced due to the excitation of the conduction electrons of the nanoparticle. The collective oscillation of such electrons is called localised surface plasmon resonance (LSPR, Fig. 1.1) (Kelly et al., 2003). LSPR arises when the dimensions of the nanoparticles are significantly smaller than the wavelength of the exciting light.

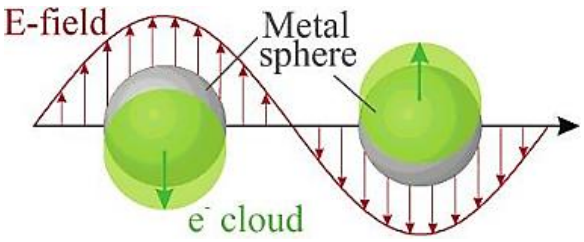

Fig. 1.1. Scheme of plasmon oscillation for a nanosphere. In the case of LSPR, light interacts with nanoparticles smaller than the incident wavelength. This leads to a plasmon that oscillates locally around the nanoparticle with a frequency known as the LSPR (Kelly et al., 2003)

Chemical enhancement usually results from charge-transfer when the analyte interacts with the metal surface on which it is adsorbed. This type of enhancement can be explained as the changes of the adsorbate electronic states due to the chemisorption of the analyte (Weaver, Zou and Chan, 2000). In the case of CE, the molecule chemically interacts with the surface of the metal and, as a result, the molecule-metal complex is formed. The appearance of such complex increases the Raman cross-section and leads to the resonances in the visible region of the spectra due to the metal to molecule or molecule to metal transitions. In most molecules, the Fermi energy of the noble metal surface is situated in between the HOMO (highest occupied molecular orbital) and LUMO (lowest unoccupied molecular orbital) of the intramolecular transition. Therefore, the new energy states can contribute resonantly to the Raman scattering cross-section of the surface complex thus increasing its magnitude (Lai-Kwan, Chang, 2012).

1.2.1. Plasmonic nanomaterials

Plasmonics, as a science concerned with the study of light interaction with metallic nanostructures, has a broad scope. The understanding of the different types of plasmon resonance (PR) has a great interest in the development and application of plasmonic nanomaterials: colloidal nanoparticles or substrates. One type of PR occurs when plane, polarised light hits a metal film under total internal reflection conditions and the light couples to electrons, thus forming a wave bounded to the surface of the metal (Kausaite et al., 2007). Such wave is called surface plasmon resonance (SPR). On the contrary to SPR, LSPR arises in the nanostructures or nanoparticles of the noble metals. It is important to mention that all Raman experiments carried out in this work were based on LSPR.

The classic metals used for the preparation of plasmonic nanoparticles or substrates are silver (Eom et al., 2013; Fan, Brolo, 2009; Harraz et al., 2015; Kashmery et al., 2015; Novara et al., 2014), gold (Shi et al., 2015; Butler et al., 2015; Zheng et al., 2014; Ngo, Simon and Garnier, 2012; Tsvetkov et al., 2013) and copper (Muniz-Miranda, Gellini and Giorgetti, 2011; Cejkova et al., 2009; Dendisova-Vyskovska, Prokopec and Člupek, 2012). This is because of their ability to support LSPR at the visible and near-infrared wavelength range. However, recently it has been shown that the SERS effect can also be obtained on the other metals such as gallium (Wu et al., 2009), palladium (Chen et al., 2010), platinum

(Abdelsalam et. al., 2007) and the combination of different metals (Fu et al., 2015; Chen et al., 2015; Fleger and Rosenbluh, 2009). Unfortunately, some of these metals are not desirable for the SERS measurements due to their specific features. For example, copper tends to corrode and that makes it difficult to perform the measurements in the air, while palladium has a low enhancement factor (Faulds, Hernandez-Santana and Smith, 2010).

A few groups have begun to explore graphene (Xu, Mao and Zhang, 2013), quantum dots (Livingstone et al., 2005) or the combined systems, such as graphene/graphene oxide (GO) decorated with silver (Ding et al., 2015; Song et al., 2014; Lin-jun et al., 2016) or gold (Mevold et al., 2015; Benitez-Martinez, Lopez-Lorente and Valcarcel, 2015) nanoparticles as plasmonic materials for SERS measurements. In such nanocomposites, graphene oxide nanosheets are the supporting substrates that allow nanoparticles to be embedded uniformly with the controlled size of the nanogaps between them. Meanwhile, GO contains oxygen-rich species (-hydroxyl, -epoxy, -carboxyl) on its basal planes and edges. Such feature makes GO attractive for its functionalisation with metal nanoparticles, thus creating the desired nanostructures on GO nanosheets.

As the combined systems, bimetallic nanomaterials have attracted enormous attention from the SERS community (Sivanesan et al., 2014; Bi et al., 2013; Shen et al., 2015). Previous reports demonstrated that bimetallic nanocomposites consisting of Au and Ag nanoparticles show higher SERS activity compared to the nanoparticles fabricated of pure gold or silver. The reason for that can be explained by the pin-hole theory stating that the local electromagnetic field can increase by a factor of 4 within pin-holes in the core-shell nanoparticles, leading to the better SERS efficiency (Fan et al., 2013).

SERS typically uses solid rough surfaces as plasmonic SERS substrates instead of colloidal nanoparticles. This is because nanoparticles are usually synthesised in solutions, which makes it difficult to assemble them in an ordered and controllable way (Abdelsalam et al., 2007). Another problem is the aggregation of the nanoparticles in the solution. In order to avoid this phenomenon, nanoparticles are usually stabilised with additional reagents, such as sodium citrate, polyvinyl alcohol, cetyltrimethylammonium bromide, etc. Nevertheless, some groups showed the SERS effect from the aggregated nanoparticles (Bell, McCourt, 2009; Karvonen et al., 2011). The reason for this is the great number of the particle junctions of the aggregates (Schwartzberg et al., 2004) where the electromagnetic field is higher than on the single nanoparticle.

1.2.2. Enhancement factor

The quantitative parameter characterising the ability of the SERS substrate or colloidal nanoparticles to enhance the Raman signal of a particular molecule is the enhancement factor (EF). This parameter can be estimated through the following equation (Camargo et al., 2010):

$$EF = \frac{I_{SERS} \times N_{normal}}{I_{normal} \times N_{SERS}}; \quad (1.1)$$

Where I_{sers} and I_{normal} - the intensities of the same Raman band in the SERS and normal Raman spectra respectively;
N_{normal} - the number of molecules probed for a normal Raman scattering;
N_{sers} - the number of molecules probed in SERS.

The EF depends on the number of factors such as size and shape of nanoparticles, their arrangement on the surface of the substrate, the type of the metal and resonance conditions. One of the most important parameters determining the high EF of the SERS substrate is the roughness of the surface. On the smooth surfaces of the metals an oscillation of the electrons takes place along the plane of the surface. For this reason, no scattering occurs. In order to obtain the scattering, an oscillation of the electrons must be perpendicular to the metal surface (Smith, Dent 2005). This can be achieved by roughening the metal surface. The high-curvature of the SERS substrate leads to the high density of nanometric gaps (usually ~1-2 nm) between nanoparticles known as "hot spots". The EM field generated in such gaps is one of the main enhancement mechanisms to realise a single molecule SERS. As seen in Fig.1.2 (A), the EF strongly depends on the size of the "hot spot". There is a decrease of EF with the increase of the nanogap size. The maximum EF can be reached when the distance between nanoparticles is a few nanometres. Therefore, the gap size is a crucial parameter of the SERS substrates because of the strong EM coupling effect at the nanometric scale (Wei, Wang and Chen, 2015). A high EF of the SERS substrate is an important criterion for its selection. As shown in Fig.1.2 (B), the highest EF can be obtained on the SERS substrates coated with Au, Ag and Cu nanoparticles.

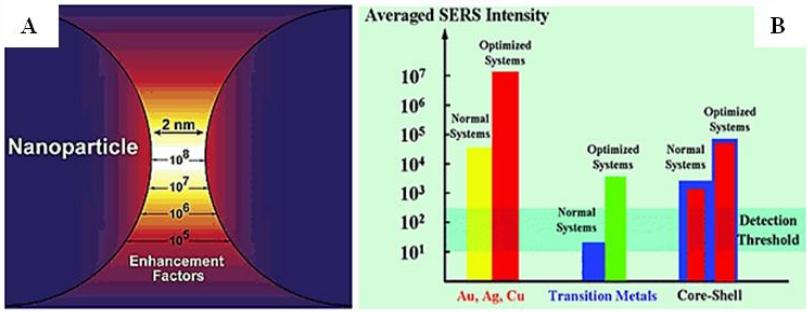

Fig. 1.2. The enhancement factor dependence on: A) the nanogap size between separate nanoparticles (Petryayeva, Krull, 2011); B) the SERS substrates fabricated of different types of metals (Tian et al., 2007)

1.2.3. Enhancement dependency on the nanoparticles properties

1.2.3.1. Effect of the nanoparticles shape

The shape of the nanoparticles is one of the key factors strongly affecting the sensitivity of the SERS substrate. Chemically synthesised Au or Ag nanospheres are the oldest and still most frequently used substrates for SERS applications due to their rapid, easy and inexpensive synthesis (Kumar, 2012; Zhang et al., 2015). However, computer simulations show that a single spherical nanoparticle does not generate a strong localised electric field on its surface (Chung et al., 2011). Therefore, a single nanoparticle is non-SERS active leading to the complicated detection of low concentrations of the molecules or even more – molecular traces. As seen in Fig.1.2 (A), the SERS activity changes dramatically in the case of two spherical nanoparticles that are in close proximity (~2 nm) with each other. Such structures act as dipole plasmonic nanoantennas producing a high intensity electromagnetic field and resulting in a high enhancement of the Raman signal. In recent years, a few groups have demonstrated the enhancement factor of 10^4-10^7 obtained from the spherical dimer type structures (Xia et al., 2013; Zou, Schatz, 2006; Li et al., 2008). However, the formation of dimer type structures with a nanogap between them suffers from the salt-induced aggregation as well as from the difficulty in bringing the separate nanoparticles together with the size of the nanogap down to a few nanometers.

According to Kumar (2012), a good SERS substrate usually has an enhancement factor between the values of 10^6-10^{11}. Therefore, the researchers still focus on the search for the optimal plasmonic nanostructures exhibiting the highest EF. Some of these structures are nanocubes, nanotriangles, nanoprisms, nanostars, nanorods or nanowires (Fig 1.3.). All these shapes have an advantage over the spherical nanoparticles because of their sharp corners or tips. The electric field generated at the sharp apexes is much stronger than on the other areas of the surface.

In 2009, Sajanlal and Pradeep demonstrated that the EF of gold nanotriangles can reach 10^8 (Sajanlal, Pradeep, 2009). A similar result has been published by Feng et al. (2015) who observed the EF of 10^9 obtained from silver coated bowtie nanoantennas. An interesting comparison of the EFs observed from spherical silver nanoparticles and silver nanoprisms has been reported by Ciou et al. (2009). The SERS measurements were performed in colloidal solutions where the analyte of nanomolar concentration has been introduced. The results revealed that the EF of silver nanospheres was 10^3, while the EF of silver nanoprisms was found to be 10^5.

Another promising shape of nanoparticles for SERS applications is nanocubes. Rycenga et al. (2011) reported an interesting way to increase the content of hot spots by depositing Ag nanocubes on Ag or Au surfaces. Hot spots were formed at the corners of silver nanocubes in a close proximity with the metal substrate. They showed that the EF of such structures is 10^8 and could be used for the single molecule detection under resonant conditions. An excellent EF has been observed by the other research group who suggested using gold nanocube–nanosphere dimers (Lee, Yoon, 2015). They demonstrated that the EF of 1,8-octanedithiol deposited on such shape–hybrid structure is 10^{10}, which is larger than that observed on the

nanoassemblies consisting only of nanospheres (EF = 10^8) or nanoclusters (EF = 10^7). One of the latest works reporting the nanocubes application for SERS measurements was published by Banchelli et al. (2016). The researchers demonstrated that silver nanocubes/graphene hybrid nanocomposites show a higher intensity of the Raman signal of the analyte compared to that observed on the individual components: only on silver nanocubes or only on graphene.

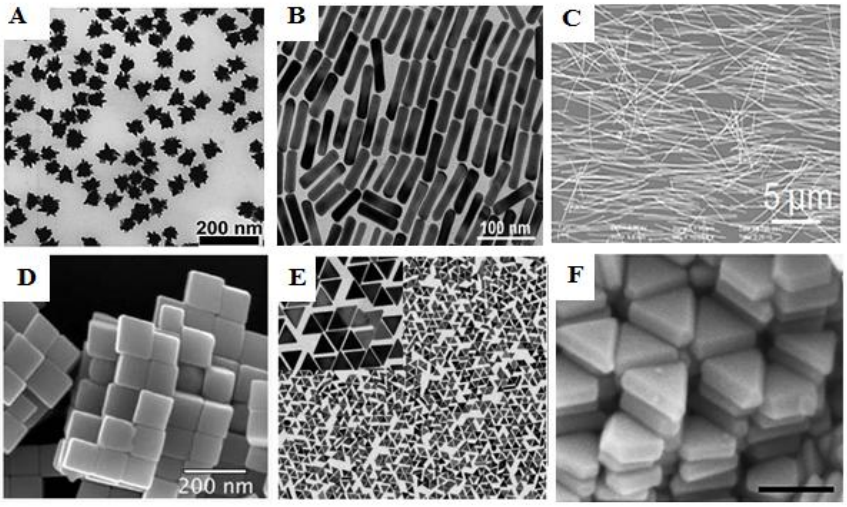

Fig. 1.3. The SEM images of different shapes of nanoparticles: (A) Gold nanostars (Kumar et al., 2007); (B) gold nanorods (Bao et al., 2011); (C) silver nanowires (Liu et al., 2012); (D) silver nanocubes (Rycenga, McLellan and Xia, 2008); (E) gold nanotriangles (Scarabelli et al., 2014); (F) silver nanoprisms (Xue et al., 2015)

Another important category of the nanoparticles shapes applicable for the SERS study is nanostars. Researchers are working on the methods allowing the improvement of the sharpness of the nanostars spikes in order to maximise the sensitivity of the SERS substrate. Among all the shapes of the nanoparticles, nanostars are a promising nanoplatform for bio-applications. Star-shaped nanoparticles have plasmon bands tunable in the IR spectral range. Also, their sharp branches act as hot spots due to the "lightning rod" effect. As it was shown before, gold nanostars demonstrated an EF of 10^9 with the concentration of the analyte of 10^{-15} M (Indrasekara et al., 2014), whereas the other research groups reported that the plasmonic nanostars showed an EF of 10^5 (Su et al., 2011) and 10^6 (Yuan et al., 2013). A significant result has been demonstrated by Rodriguez-Lorenzo et al. (2009). They showed that the usage of the star-shaped gold nanoparticles allows the detection of the analyte of zeptomolar (zM) concentration.

Among the various shapes of the nanoparticles, nanorods are one of the most intensively studied plasmonic geometries. Because of their anisotropic geometry, the nanorods show several plasmon modes: transverse and longitudinal. Such feature expands the possibilities to work with lasers of different wavelengths under the resonance conditions. This is especially important while working, for example, with gold nanoparticles and biological samples which exhibit a strong fluorescence

background in the case when a green laser (532 nm) is used. In recent years, it has been shown that the aligned silver nanorods are suitable for SERS study because of their high EF which was found to be in the range of 10^7-10^8 (Chaney et al., 2005; Liu, Chu and Zhao, 2010; Oh et al., 2015). In these studies, the authors focus on the synthesis of various lengths and arrangements of the nanorods in order to obtain a high concentration of "hot spots", and to improve the EF of such nanoarchitectures. As a great example, the work of Samanta et al. (2014) should be mentioned. They investigated the EF dependency on the gold nanoparticle's geometry. As seen in Fig. 1.4 the control of the gold nanorod's size allowed them to optimise the EF. However, the most effective structures for the enhancement of the Raman signal were found to be gold nanostars.

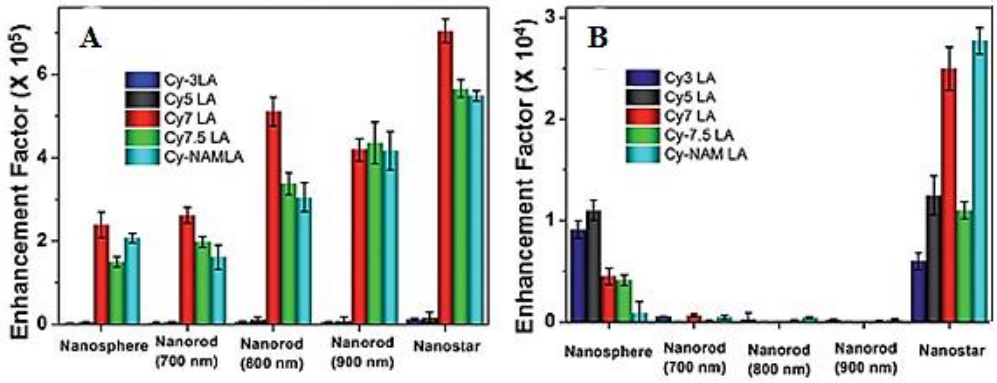

Fig. 1.4. The EF comparison of the different geometries of gold nanoparticles: (A) under the excitation source at 785 nm and (B) under the excitation source at 633 nm (Samanta et al., 2014)

With regard to oblong structures, nanowires should be mentioned as an excellent plasmonic nanoshape. As it was reported by Chikkaraddy, Singh and Kumar (2012), the SERS hot spots can be obtained at the junction of the nanowires. The experimentally obtained EF of 10^6 obtained from the gold functionalised anodised aluminium oxide nanowires was demonstrated by Jiwei (2013) and his co–workers. They claimed that the observed EF was 14% higher compared to the commercial Klarite® substrates. The close-packed silver nanowire monolayers as the SERS substrates were also tested by Tao et al. (2003). They found that the EF of the nanowires for thiol molecules was 10^5 and for rhodamine dye (R6G) – 10^9.

Ring-shaped nanostructures with various diameters have also attracted the attention as SERS sensors. Such noble metal nanoshapes demonstrate multipolar plasmon modes in the visible and NIR regions. The application of nanorings for SERS measurements is attractive because of their ability to adsorb high volumes of molecules and provide a uniform electric field inside their cavities (Yi et al., 2015). Bechelany et al. (2009) proposed a method for the preparation of 100 nm silver grains that tend to form ring-shaped nanostructures. They demonstrated that the EF of such organisations is around 10^5. Meanwhile, another group reported the EF of 10^6 observed on gold nanoring dimers (Banaee, Crozier, 2010).

1.2.3.2. Effect of the nanoparticles size

Another important parameter determining the ability of the SERS substrate to enhance the Raman signal is the size of the nanoparticles, which has been investigated by several researchers. In recent studies, it has been shown that the highest EF can be reached when the nanoparticles are around 50–60 nm (Stamplecoskie et al., 2011; Hong, Li, 2013; Wang et al., 2012), while others have demonstrated the EF of 10^6 obtained from nanospheres of 90 nm (Sugawa et al., 2015). An interesting work has been published by Kahraman, Aydin and Culha (2009) who investigated the size influence of 3D silver nanoparticle aggregates for the enhancement of the Raman signal. They showed that an EF of 10^7 can be achieved when the sizes of the nanoparticles containing the aggregate are less than 200 nm. A similar result was obtained by another research group who reported that the highest SERS activity can be observed from nanoparticles of 130 nm (Yi et al., 2014). Based on the previous experiments it can be assumed that the highest EFs are achieved when the sizes of the nanoparticles vary from 50 nm to 200 nm. According to Isralsaen, Hanson and Vargis (2015), there is an effective range of nanoparticle sizes for optimal enhancement. In the case when the nanoparticles are too small the conductivity and light scattering properties, required for SERS enhancement, diminish. As the size of the nanoparticles increase, the SERS effect gets better because of the increment of the electrons available. However, if the nanoparticle size is similar to the excitation wavelength they are excited in non-radiative modes and result in a weak SERS effect.

1.2.4. Effect of the synthesis parameters on the geometry, dimensions and arrangement of plasmonic nanoparticles

Colloidal nanoparticles. In chemical synthesis, the concentrations of the reagents as well as reaction time, temperature and pH are the crucial parameters determining the size and geometry of the plasmonic nanoparticles. Sobczak-Kupiec et al. (2011) studied the influence of silver nitrate concentrations on the synthesis rate and optical properties of silver nanoparticles. During the synthesis they changed the silver salt concentrations in the reaction system and observed the UV-Vis spectra. It was found that the usage of high concentrations of $AgNO_3$ resulted in the increment of the nanoparticles size. This was confirmed by UV-Vis spectra showing the red-shifted plasmon. Meanwhile, the use of low concentrations determines the formation of small nanoparticles. This was also confirmed by UV-Vis observations showing the blue-shifted plasmon. According to the authors, the use of a high concentration of $AgNO_3$ leads to the rapid reduction process resulting in the formation of a larger number of silver nuclei. Consequently, the large number of silver atoms leads to the fast growth of the nucleated particles and results in the formation of the aggregates. In another study, Pris (2014) investigated the effects of temperature and tri-sodium citrate concentrations for the synthesis of silver nanoparticles. It has been shown that at low ratios of reducing agent to silver nitrate (1:1 and 1:2) and low temperatures (20-40^oC) the reaction solutions were colourless, meaning that the formation of silver nanoparticles did not take place. However, after one week the solutions turned dark red indicating the enormously slow formation of

the nanoparticle aggregates in the reaction system. This phenomenon occurred because of the low ratios of tri-sodium citrate to silver nitrate. Given that tri-sodium citrate acts a as reducing and stabilising agent, its concentration was too low to effectively stabilise the nanoparticles. Moreover, at low concentrations of this reductant, Ag^+ ions tend to form complexes with tri-sodium citrate resulting in the formation of silver clusters. The experiment was repeated by keeping the same ratios of both reagents but using higher temperatures (70-100^{o}C). Again, the silver aggregates were formed in the solution. However, in this case the aggregates were formed after a few days, indicating the faster formation of the nanoparticles due to the faster reaction kinetics.

Mansouri and Ghader (2009) studied the influence of tri-sodium citrate, silver nitrate and hydrazine concentrations as well as the effect of pH value on the formation of triangular silver nanoparticles. According to the authors, when the silver precursor concentration reached 0.5 mM, the formation of triangular nanoparticles did not take place. However, when the solution was left unstirred for a few months, the colloidal solution colour changed from yellow to green indicating the change of the nanoparticles' size and shape. Based on the UV-Vis results, the authors concluded that the ageing of the solution containing small nanospheres resulted in the formation of silver nanotriangles. Additionally, the reduced supersaturation of the silver precursor allows a higher yield of triangular silver nanoparticles to be obtained. Meanwhile, another experiment showed that triangular nanoparticles were formed at any tri-sodium citrate concentration. The authors also investigated the effect of hydrazine solution pH on the formation of silver nanotriangles. Given that the original pH value of hydrazine solution was 9.2, the authors have chosen nitric acid and sodium hydroxide to reach pH values of 2-8 and 10-12 respectively. At pH 2 an almost colourless solution was obtained indicating the low amount of silver nanoparticles in the reaction system. Based on this result the authors confirmed the important role of hydrazine in the formation of triangular silver nanoparticles. At low pH values, most of the hydrazine is removed resulting in a decrease in the amount of nanotriangles (Mansouri and Ghader, 2009). Therefore, the obtained results allowed it to be concluded that hydrazine acts not only as reductant but also plays a key role in the control of nanoparticle shapes.

Drogat et al. (2010) proposed a protocol for the synthesis of colloidal silver nanorings. The authors found that the synthesis conditions strongly affect the final shape of the nanoparticles. For example, silver nanorings were obtained at temperatures between 19-22^{o}C. Meanwhile, the increment of the temperature resulted in the formation of hollow spherical silver nanoparticles. In order to reveal the formation mechanism of silver nanotriangles, NaOH, sodium tri-citrate and $AgNO_3$ were mixed and the obtained solution was quickly cryogenised in liquid nitrogen. The sample was characterised by Cryo-electron microscopy (Cryo-SEM). The results showed that Ag_2O particles resulted from the reaction of $AgNO_3$ and NaOH tend to produce ring-shaped aggregates. Therefore, such aggregates must be further reduced by $NaBH_4$ in order to obtain SERS-active silver nanorings.

In 2014, Zhang et al. reviewed several multistep approaches such as the double reduction method, etching technique and construction of core-shell composite

structures for the chemical synthesis of silver nanostructures with well-controlled shapes. The authors discussed the nanoparticle shapes transformation depending on the reactions conditions such as reagent concentrations or types of reducing agents.

Solid SERS substrates. Sol-gel technique is a wet chemical process involving the formation of colloidal system and its gelation. It is a promising route for the formation of 3D silica porous matrixes serving as template substrates for the immobilisation of metal nanoparticles in order to obtain SERS-active films. In general, the sol-gel process can be described in three reactions: hydrolysis, water condensation and alcohol condensation, as shown in equations 1.2, 1.3, 1.4 and 1.5:

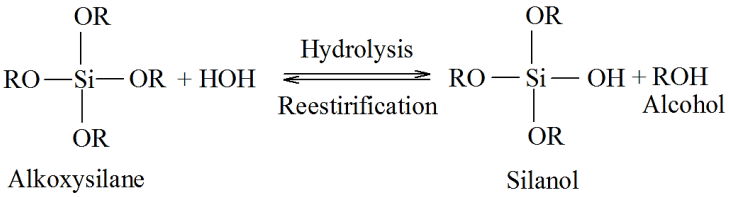

(1.2)

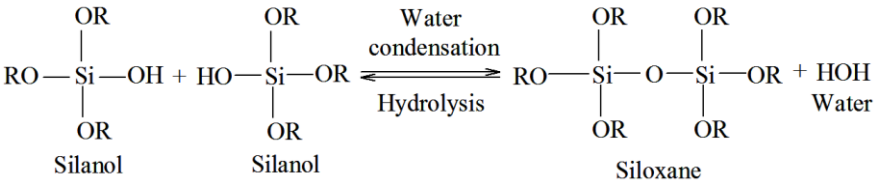

(1.3)

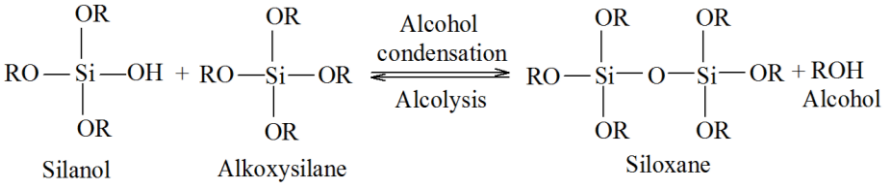

(1.4)

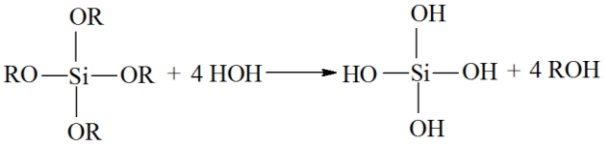

(1.5)

Where R = C_2H_5

This process contains three main stages: the polymerisation of the monomers to form particles, the growth of the particles and the formation of the polymeric network. The sol-gel process starts with a solution containing alkoxysilane, water as the hydrolysis agent, alcohol as the solvent and the base or acid as the catalyst. During the hydrolysis reaction, the alkoxysilane ligands are replaced with hydroxyl groups and release the alcohol molecules (equation 1.2). Further, the condensation reactions occur between the already formed silanols (equation 1.3) or silanol and

alkoxysilane (equation 1.4). During this stage the molecular weight of the product is increasing. Complete hydrolysis of alkoxysilane (equation 1.5) occurs in the case when the stoichiometric molar ratio of water to alkoxysilane is 1:4 respectively (Milea, Bogatu and Duta, 2011).

In order to use the sol-gel process for the synthesis of porous silica films, the careful control of the synthesis parameters such as temperature or pH is required. For example, the final structure of the film fabricated by sol-gel technique depends on the hydrolysis and condensation reactions that are particularly controlled by pH (Milea et al., 2011). Under the acid-catalysed conditions, the silica tends to form linear molecules that are occasionally cross-linked. Meanwhile, in alkali-catalysed reactions a highly branched cluster formation takes place. Fardad (2000) studied the effect of different catalysts on the porosity of the films produced by sol-gel technology. He found that H_2SO_4 and H_3PO_4 increase the hydrolysis rate of the TEOS ethoxy groups and leads to the formation of low porosity films. The porosity of the silica films can be increased by using organic templates. Previously, Dutta, Ellateif and Maitra (2011) synthesised porous silica films by the sol-gel process under alkaline conditions in the presence of glycerol. In another study, 3D arrays were prepared by the template directed sol-gel method. In this work the authors used poly-methyl methacrylate (PMMA) spheres as the template for the preparation of the well-ordered three-dimensional structures (Li, Lin and Guliants, 2010). Such structures are very promising for SERS applications because the incorporation of plasmonic nanoparticles (e.g. directly from the colloidal solution or evaporation) into such matrix allows the fabrication of 3D SERS-active nanoarchitectures.

Another important parameter for the formation of porous structures is the thermal treatment of the fabricated films. When the hydrolysis and condensation reactions are not completed, reactive silanols remain in the system or wet film. Therefore, thermal treatment is required for the removal of residual solvents and the formation of covalent Si-O-Si bonds. These bonds are not stable at a temperature below 450^{o}C. For this reason, temperatures higher than 1000^{o}C are required to achieve bonding energy close to the bulk fracture one. However, the extremely high temperatures (600^{o}C) lead to the shrinkage of the pores (Sinko, 2010; Dutta et al., 2011) resulting in the formation of dense silica film.

1.2.5. The synthesis of the SERS substrates

There are a number of ways used for the preparation of the SERS substrates. Their synthesis is usually based on physical, biological and chemical methods (Table 1.1). All these methods allow nanostructures of desirable sizes or shapes to be obtained, which are the key factors for high-sensitive SERS measurements. Iravani et al. (2014) published a review of the above-mentioned approaches for the preparation of plasmonic silver nanoparticles. They identified several advantages of the physical synthesis over the chemical processes. For example, the production of the nanoparticles by the most common methods such as laser ablation, evaporation/condensation or magnetron sputtering allows the residual reagents on their surfaces to be avoided. This ensures the cleanness of the SERS substrate and the quality of the measurements. As environmental pollution is a huge problem that

the world is facing today, the mentioned methods allow the usage of hazard chemicals to be avoided. However, these arguments do not diminish the chemical methods being superior in the fabrication of 3D nanoarchitectures. In order to avoid toxic chemicals, modern chemical or biochemical synthesis of plasmonic nanostructures is based on natural agents, such as sugars, plant extracts, honey, fungi or microorganisms. Moreover, most of the chemical methods do not require sophisticated systems, equipment or special skills, and in many cases are cheaper than the mentioned physical methods. Another important aspect is that chemical synthesis allows for the functionalisation of the nanoparticles straight in the reaction pot, while for physical synthesis it should be an additional action.

Table 1.1. The most common approaches for the synthesis of plasmonic nanoparticles and nanostructures

Physical	Chemical	Biological
Evaporation/condensation approach	Traditional reduction (tri-sodium citrate, sodium borohydride)	Bacteria
Laser ablation	Green reduction (Polymers and polysaccharides)	Fungi
Sputtering	Photochemical reduction	Yeast
Lithography	Micro-emulsion technique	Plants
Laser induced etching	Sol-gel technology	
	Electrochemical synthesis	
	Microwave assisted synthesis	
	Tollens method	

1.2.5.1. Physical approach

Within a few years, the researchers demonstrated the synthesis of colloidal nanoparticles and nanostructured SERS substrates by laser ablation. Highly monodisperse silver and gold nanoparticles were fabricated in water by Vinod and Gopchandran (2014). The authors reported spherical-shaped nanostructures that were inclined to join with each other thus forming the "hot spots". The same method was used for the preparation of 3D micro-square silicon arrays decorated with silver nanoparticles (Yang et al., 2014). The EF of the above mentioned structures was found to be in the range of 10^5-10^6. Pulsed laser ablation, for the preparation of plasmonic nanoarchitectures, was also selected by other researchers who studied their ability to enhance the Raman signal (Herrera, Padilla and Hernandez-Rivera, 2013; Agarwal et al., 2011). One of the latest works was published by Xu et al. (2015) who prepared the hybrid substrate of graphene and silver nanoparticles. They demonstrated that the fabricated substrate showed an EF of 10^8 for R6G molecules.

Previously, SERS-active substrates were prepared by sputtering gold nanotubes on polycarbonate-track etched membranes. The prepared SERS substrates were tested with R6G dye of 0.1 nM and demonstrated an EF of 10^5 (Rodriguez, Andrade and Temperini, 2013). In 2011, Li et al. applied unusual substrate for SERS

measurements. The substrate was based on nickel film fabricated by magnetron sputtering. Nickel has been chosen because it is cheaper than silver or gold and less reactive than copper. According to the authors, the sputtering technology allowed them to obtain the higher EF compared to that observed on an electrochemical nickel electrode.

Other physical methods used for the production of SERS substrates also include a laser induced dry etching technique (Csizmadia et al., 2013), physical vapour deposition (Yan et al., 2015) or electronic beam lithography (Huebner et al., 2010; Petti et al., 2016) allowing the fabrication of regular nanostructures due to their ability to precisely control the shapes and sizes of the nanoparticles. Despite the high sensitivity of such prepared SERS substrates, these techniques are time-consuming and expensive.

1.2.5.2. Chemical approach

The most common method for the synthesis of the plasmonic nanoparticles or nanostructures is a chemical reduction of metal ions by organic or inorganic agents. Given that most of the reduction reactions are carried out in the solutions, the SERS measurements can be performed in two ways. One of them is a wet method when the analyte is introduced straight into the colloidal solution. In such case, a drop of the nanoparticles-analyte solution can be placed on the solid substrate (silicon, mica, glass, etc.) and SERS spectra can be recorded in solution. This method is essential while working with biological samples, such as proteins or peptides because it allows their conformational changes that occur when the measurements are carried out under dry conditions to be avoided. Another way is to dry the drop of nanoparticles-analyte solution on the solid substrate. This method allows for the concentration of the analyte. It is important in these cases when the concentration of the analyte is nanomolar (10^{-9}), picomolar (10^{-12}), femtomolar (10^{-15}) or even zeptomolar (10^{-21}).

A classic way to synthesise spherical-shaped colloidal gold or silver nanoparticles is known as the Turkevich method introduced in the early 1950s (Turkevich, Stevenson and Hillier, 1951). Gold (III) chloride trihydrate or silver nitrate is used as a precursor that reacts with tri-sodium citrate and reduces gold or silver ions respectively. In such synthesis, sodium citrate act both as a reducing and capping agent. The final oxidation products of citrate anions adsorb on the surface of the synthesised nanoparticles thus preventing them from aggregation (Creanga et al., 2013). The general reduction reaction of silver ions can be expressed as follows

$$3\,Na^{+}(aq) + 2\,Ag^{+}(aq) + C_6H_5O_7^{-3}(aq) \longrightarrow 2\,Ag^{0}(s) + C_5H_4O_5^{2-}(aq) + CO_2(g) + 3\,Na^{+}(aq) + H^{+}(aq) \quad (1.6)$$

Previously, the Turkevich method has been applied not only for the synthesis of gold and silver nanoparticles (Li et al., 2011; Krpetić et al. 2012; Rashid, Bhuiyan and Quayum, 2013), but also for hybrid nanostructures such as silver/gold nanoshells (Stevenson et al., 2012; Samal et al., 2013) or the SiO_2/Au nanoparticles (Saini et al., 2015). Moreover, Shulz et al. (2014) proposed the modification of the Turkevich method which allowed them to improve the shape uniformity of the gold nanoparticles. However, the citrate colloids are known to have a broad size

distribution of the synthesised metallic nanoparticles. Therefore, the sodium borohydride ($NaBH_4$) or ascorbic acid ($C_6H_8O_6$) can be used as reducing agents instead of tri-sodium citrate (Mikac et al., 2014). The reduction of silver or gold by ice-cold $NaBH_4$ is one of the most popular and well known chemical methods for the preparation of the nanoparticles in solution. In such synthesis, an excess of $NaBH_4$ is required both for the reduction of ionic silver and for the stabilisation of the nanoparticles (Mavani, Shah, 2013). The reduction reaction of silver ions by $NaBH_4$ can be written as follows:

$$AgNO_3\,(aq) + NaBH_4\,(aq) \longrightarrow Ag^0\,(s) + 1/2\,H_2\,(g) + 1/2\,B_2H_6\,(g) + NaNO_3(aq) \quad (1.7)$$

Despite its popularity, sodium borohydride is a highly toxic and irritating agent having a negative impact on health and the environment. The harmful properties are also common for hydrazine (Nickel et al., 2000) and N, N-dimethylformamide (Pastoriza-Santos, Liz-Marzan, 1999) which is used for the synthesis of SERS-active nanoparticles as well. With regard to their toxicity, the classic chemical approaches were modernised in order to reduce or completely eliminate the hazardous reagents. Therefore, as an alternative, bio-friendly reducing reagents such as carbohydrates (Boitor et al., 2015; Osorio-Roman et al., 2011; Sivera et al., 2014), polyethylene glycols (Stiufiuc et al., 2013; Leopold et al., 2013;) or amino acids (Yang et al., 2014; Li et al., 2016) have been proposed. The eco- and bio- friendly protocols are highly desirable because of the possibility of avoiding the adverse effects of the nanoparticles or nanostructures, especially in biomedical applications. Such protocols have been proposed by a number of researchers. For example, the extracts obtained from different kind of leaves (Gaware, Kamble and Ankamwar, 2012; Loo et al., 2012; Sathyavathi, Krishna and Rao, 2011) have been used for the synthesis of nanoparticles. In such bio-synthesis, the reducing agents are glucose, ascorbic acid or proteins. The latest review, focused on the plant extract mediated synthesis of silver nanoparticles, has been published by Ahmed et al. (2016) and perfectly reflects the diversity of the plants used for the preparation of silver nanoparticles.

Another “green” reduction of ionic silver has been carried out by hyaluronic acid (HA) (Xia et al., 2011). This glycosaminoglycan is a natural compound found in the human body. HA has -OH groups which are responsible for the reduction of silver ions. Recently, it has been proposed to perform the bio-direct synthesis of gold nanoparticles by using honey (Philip, 2009; Haiza et al., 2013) as a “green” reducing and capping agent. Honey contains fructose and vitamin C possibly responsible for the gold ions reduction. Unusual “green materials” recently applied for the synthesis of spherical and triangular silver nanoparticles are the extracts of various mushrooms (Anthony et al., 2014; Sen et al., 2013). They contain different aromatic and bio-active compounds acting as reductants. Another interesting approach for the synthesis of the SERS-active nanoparticles is the usage of microorganisms (Shivaji, Madhu and Singh, 2011). Under the alkaline conditions, in the bio-reduction system, $[Ag(NH3)_2]^+$ reacts with the hydroxyl groups thus forming Ag_2O. Silver (I) oxide is further metabolised and finally reduced to Ag^0 by the biomass (Iravani, 2014).

The chemical synthesis of the SERS substrates also includes sol-gel technology (Kang et al., 2003; Fan, Brolo, 2009; Garcia-Macedo et al., 2004), attractive for many authors because of its inexpensiveness and simplicity. This method allows the fabrication of the films on different surfaces directly from the solution; controls the porosity of the films by varying synthesis parameters or using organic templates, functionalisation of the films with nanoparticles as well as the formation of self-assembled nanostructures. Moreover, the sol-gel method allows the fabrication of 3D plasmonic substrates leading to the extension of the hot spots in the third dimension along the z-axis. Most recently, Yang et al. (2016) reported a new generation of the solid SERS substrates the fabrication process of which includes the sol-gel technique. They demonstrated a unique SERS platform allowing the detection of the analytes down to femtomolar concentrations with a high sensitivity and specificity in liquid, solid or air.

Regardless of the synthesis method selected, the effective SERS substrate must meet the certain parameters such as high EF, repeatability of the nanostructure, stability on storage, applicability to various analytes and low cost. One of such chemical methods has been proposed by Khlebtsov et al. (2015). In the proposed protocol, gold nanoparticles are seeded on thiols modified silicon surface. After that, a standard reduction of gold (III) chloride trihydrate by AA is carried out in order to overgrow the seeds in the nano islands. The advantages of the proposed method include the possibility to control the size of the nano islands by controlling the concentrations of AA or gold (III) chloride trihydrate; it is also possible to prepare the SERS substrates on the transparent surfaces such as cover slips or microscopic objective glasses.

The method known as “silver mirror reaction” or the Tollens process has also been applied for the preparation of the SERS substrates (Leng et al., 2006; Kvítek et al., 2005). The reaction for silver ions reduction can be expressed as follows (Macijauskienė and Griškonis, 2015):

$$2\,AgNO_3\,(aq) + 2\,KOH\,(aq) \longrightarrow Ag_2O\,(s) + 2\,KNO_3\,(aq)$$

$$Ag_2O\,(s) + 4\,NH_3(aq) + H_2O\,(l) \longrightarrow 2[Ag(NH_3)_2]^+(aq) + 2\,OH^-(aq)$$

$$\underset{\text{D-glucose}}{C_6H_{12}O_6\,(aq)} + 2[Ag(NH_3)_2]^+(aq) + 3\,OH^-\,(aq) \longrightarrow \underset{\text{gluconate ion}}{C_6H_{11}O_7^-\,(aq)} + 2\,H_2O\,(l) + 4\,NH_3\,(aq) + 2\,Ag^0(s) \quad (1.8)$$

This approach allows the control of silver nanoparticles size (from tens to hundreds of nanometres) by change the ammonia concentration in the reaction system as well as to use a broad range of reducing sugars – glucose, fructose, maltose, ribose, galactose or xylose.

One of the possible methods to obtain bimetallic Ag-Au SERS substrates is the galvanic replacement reaction between silver nanoparticles and $HAuCl_4$ (Zhang et al., 2007). Given that the reduction potential of $AuCl^-_4/Au$ is higher than that of Ag^+/Ag, the silver nanoparticles synthesised in the presence of the reducing agent are oxidised to Ag^+ by aqueous $HAuCl_4$ solution as follows:

$$3\,Ag^{0}_{(s)} + AuCl^{+}_{4\,(aq)} \longrightarrow Au^{0}_{(s)} + 3\,Ag^{+}_{(aq)} + 4\,Cl^{-}_{(aq)}$$

$$Ag^{+}_{(aq)} + Cl^{-}_{(aq)} \rightleftharpoons AgCl_{(s)} \qquad (1.9)$$

This method is advantageous because of the possibility to synthesise different shapes of bimetallic composites such as Ag-Au hollow nanostructures (Yang et al., 2014) or triangular Ag-Au frameworks (Yi et al., 2011).

Plasmonic nanoparticles can be synthesised by the photochemical reduction of metal ions. This approach is a clean process allowing the synthesis of plasmonic nanoparticles in various mediums such as emulsions, polymer films or even cells (Iravani et al., 2014). Moreover, the control of the irradiation time opens the possibility to control the size and shape of the nanoparticles and the density of the SERS-active films. Sato-Berru et al. (2008) reported the photochemical reduction of silver ions in the presence of sodium citrate using different light sources, while Dong et al. (2004) studied the formation of gold nanoparticles under sunlight radiation. Another protocol proposed in the literature was found to be suitable for the synthesis of various shapes of gold nanoparticles (pentagonal, hexagonal, spherical and triangular) in the presence of ethylene glycol (Hsu, El-Sayed and Eustis, 2004). In such reaction, the gold salt absorbs the ultraviolet light to generate an excited electronic state and reacts with ethylene glycol. This organic compound acts as a solvent and reducing agent. After the formation of nucleation sites, gold nanoparticles grow until the polyvinylpyrrolidone (PVP) is introduced into the reaction solution. PVP terminates the further growth of the nanoparticles and stabilise the colloidal system.

The microwave assisted synthesis has also been utilised for the preparation of metallic nanoparticles (Seol et al., 2013; Manikprabhu and Lingappa, 2013). Microwave reactors allow high pressures and temperatures to be maintained (the driving force for the chemical reaction) that can replace the traditional heating process. Using microwave irradiation, it is possible to obtain nanoparticles of exact sizes or shapes in a short time. Recently, it has been shown that silver nanoparticles can be prepared using microwave irradiation in the presence of orange peel extract acting as a reducing and capping agent (Kahrilas et al., 2013). Another example demonstrates that the usage of a microwave reactor allows the synthesising of gold nanoparticles in a two-phase system in the presence of 1-dodecanethiol. According to this protocol, the gold nanoparticles of 1.8 nm in size tend to form self-supported superstructures (> 1 μm) which can be further used for SERS applications. In such synthesis, the energy supplied from the microwave source induce the formation of reducing species obtained from the dissociation of the chemicals capable of reducing Au^{3+} to Au^{0}.

1.2.6. Commercial SERS substrates

There are several types of the commercially available SERS substrates offered by the different companies (Fig. 1.5).

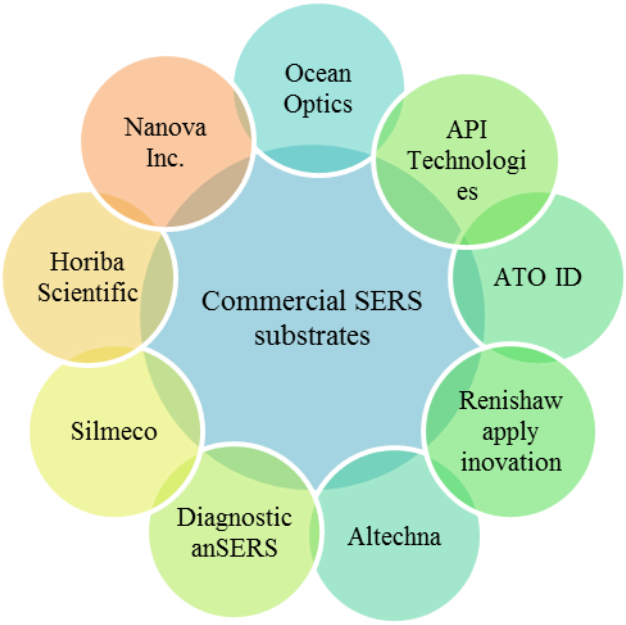

Fig. 1.5. The companies offering the SERS substrates

Horiba Scientific proposes SERS substrates with a high reproducibility and significant enhancement. These substrates are coated with gold and are of different sizes. Gold coated SERS sensors are also offered by *Ocean Optics*. According to this manufacturer, these substrates allow the performance of fast and repeatable SERS measurements for a wide range of analytes with a concentration sensitivity from one part per million (ppm) to one part per billion (ppb). The similar detection limits of various analytes are demonstrated on the silver and gold SERS substrates suggested by *Silmeco*. According to the manufacturer, the majority of the commercial SERS sensors fabrication techniques involve polymer mask deposition (lithography) or complex chemistry which dramatically increases the manufacturing costs. Meanwhile, *Silmeco* nanofabrication technology excludes lithography. It is important to mention that the methods, materials, equipment and other details relevant for the fabrication of the SERS substrates is *"know-how"*. Therefore, the comprehensive comparison of the fabrication techniques used by the different manufacturers is limited. In 2015, Owens et al. reported the comparison of Raman signal intensity of 2-naphthalene-thiol deposited on the different commercial SERS substrates. The highest Raman signal (10^4) of this organic material has been observed on the silver SERS substrate obtained from *Silmeco* (Owens et al., 2015).

Another example of the commercially available SERS substrates is *Klarite*® sensors. The surface of the *Klarite*® substrates is of a regular structure consisting of the uniform silicon pyramids with roughened gold deposited on their internal walls. As it was demonstrated before, the SERS spectra of benzenethiol and ibuprofen obtained from *Klarite*® showed the EF at least two orders of magnitude higher than the competitor SERS substrate consisting of randomly distributed gold aggregates.

The *Solas* SERS substrates are proposed by *API Technologies*. According to the manufacturer these SERS substrates can be applied for the detection of molecular traces, contaminants in water, drugs, melamine in milk or explosive residues. One of the major advantages of the proposed substrates is that they are designed in such a way that can be used with different Raman systems including portable Raman spectrometers. Therefore, this advantage allows the analysis to be performed immediately after sampling.

Lithuanian companies have also joined the SERS market. "*Altechna*" collaborates with Swinburne University (Australia) and develops the SERS substrates known as ripples. They fabricate the periodic nanostructures using ultra-short laser pulses. Recently, it has been shown that ripples demonstrated higher sensitivity and reproducibility compared to other commercial SERS substrates fabricated by lithography (Buividas, Stoddart and Juodkazis, 2012). For example, the SERS spectra of thiophenol monolayer were recorded on different, commercially available SERS substrates, under the same conditions. The highest intensity of Raman signal was observed on gold ripples, which was found to be 10^3 (Buividas, Day and Juodkazis, 2012).

Another example is *ATO ID*, a Lithuanian Start-up Company offering gold SERS substrates applicable for molecular detection and analysis in the red and NIR excitation wavelength range. The manufacturer claims that they fabricated the SERS substrates allowing them to obtain 8 times higher Raman intensity compared to other SERS substrates proposed in the market.

However, despite the high number of patents proposing novel SERS-active substrates, commercial sensors are still expensive; most of them are not highly sensitive, they also require special storage conditions in controlled atmospheres and rigorous handling to maintain their enhancement properties.

1.2.7. SERS applications in analytical chemistry

Detecting target analytes with a high sensitivity and specificity is of fundamental importance to analytical chemistry. Due to its sensitivity and the possibility to observe the molecular fingerprints of particular analytes of low concentrations, the SERS technique has been used for the detection of additives and antibiotics in food (He et al., 2015; Xie et al., 2012), the pollutants in water (Wang et al., 2014), drugs in body fluids (Han et al., 2015), explosives (Chou et al., 2012) as well as for the determination of the freshness of fruits and vegetables (Gopal et al., 2016). Recently, an interesting report has been published proposing the application of the SERS technique in the field of forensic analysis (Kurouski and Van Duyne, 2015). The authors suggested a protocol that allows the determination of whether hair is coloured or not and even to reveal the brand of the artificial dyes. SERS has been also used for the identification and analysis of pigments in historic paintings (Frano et al., 2014) and for the detection of surface contamination in spacecraft.

In recent years, a significant step has been made towards the investigation of the causes that determine Parkinson's and Alzheimer's diseases (Lee et al., 2011; Chou et al., 2008). Those diseases are directly connected to the conformational transitions and aggregation of amyloidogenic proteins (such as α-synuclein) on the brain lipid bilayer. The SERS technique is one of the analytical techniques finding great applications for studying structural changes of molecules based on vibrational fingerprints of separate amino acids (Podstawka, Ozaki and Proniewicz, 2005), peptides (Seballos et al., 2007) or proteins (Domenici, Bizzarri and Cannistraro, 2012) at low concentrations or/and for the analysis of interaction mechanisms at bio-nano interfaces. Researchers prefer several types of rough metal surfaces, such as Au, Cu or Ag not only because they generate the highest enhancement in the visible and NIR wavelength range, but also because they provide a better understanding of how and which molecular species bind to the surface and what is the orientation of an adsorbate (Castro et al., 2003). The understanding of the binding mechanism of amino acids or short peptides is significant for the development of the fundamental knowledge of peptide or protein conformational changes induced by nanoparticles or nanostructured surfaces that are important for the study of the causes of neurodegenerative disorders.

The development of the sensitive SERS sensors has led the possibility of extending the SERS technique into trace detection applications within the pharmaceutical field as well. With the advantage of easy sampling, the high measurement speed and the possibility to perform the analysis in liquids, SERS has become a promising technique for the analysis of pharmaceuticals. The method provides a possibility to determine the distribution of active pharmaceutical ingredients in the tablets as well as studying the drugs penetration through the cell membranes by applying Raman mapping (Gordon and McGoverin, 2011). Recently, the SERS technique has been successfully applied for the analysis of pharmaceuticals such as modafinil (Caglayan et al., 2015), doxorubicin (Abrahamsson, 2001), vitamins (Cinta Pinzaru et al., 2004) and not only as

individual substances, but also in different matrixes such as urine (Dong et al., 2015) or saliva (Farquharson et al., 2011). Given that the SERS sensors or colloidal nanoparticles can be functionalised with the molecules having the affinity for the particular compound, the SERS technique opens up the possibility to identify drugs of a similar structure.

1.2.8. Plasmon driven chemical reactions

Surface plasmon chemistry is becoming a fast-growing branch of catalysis chemistry. This is because surface plasmons can strongly harvest electromagnetic energy via LSPR when light hits the metal nanostructures (Zhang et al., 2014). In general, the irradiation of plasmonic nanoparticles contributes to significant heating which can be used to drive the chemical reactions. Plasmons are able not only to drive the chemical synthesis but also to cleave the chemical bonds as nano- scissors via plasmonic hot electrons (Cui et al., 2014).

LSP, as collective oscillations of free electrons, can be generated in the nanoparticles of noble metals and result in strong localised electric fields. 3D nano-architectures are known to produce stronger LSP than two-dimensional ones because 3D nanoparticles exhibit larger optical cross-sections and can selectively channel photon energy into “hot spots”. For this reason, chemical reactions can be facilitated and improved by the use of LSP. In recent years, it was demonstrated that LSP plays a key role in chemical reactions revealed by surface or tip–enhanced Raman spectroscopies (TERS). For example, Zhang et al. (2014) reported a plasmon induced sequential chemical reaction in which 4-nitrothioanisole (4NTA) adsorbed on rough silver surface was reduced to 4-nitrobenzenethiol (4NBT) via the dissociation of the CH_3 group of 4NTA. Meanwhile, another group demonstrated the dimerisation reaction of 4NBT to dimercaptoazobenzene (DMAB) using high vacuum TERS (Sun et al., 2012).

Over the last years, a number of reports were published demonstrating the use of LSP for the stimulation of the chemical reactions (Oshikiri, Ueno and Misawa, 2014; Zong et al., 2014; Kang et al., 2015; Dai et al., 2015). One of such examples is shown in Fig 1.6. It represents the mechanism of the plasmon assisted conversion of 4NBT to DMAB (Dong et al. 2011). In such synthesis, the four electrons ($4e^-$), required in the chemical reaction, are proposed to be “hot electrons” arising from the plasmon decay. These electrons have a high kinetic energy which is a “driving force” required for the performance of the chemical reaction.

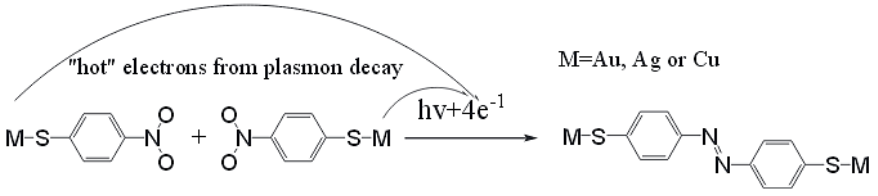

Fig. 1.6. Mechanism of the Plasmon-Assisted conversion of 4NBT to DMAB (Dong et al., 2011)

However, the application of both SERS and TERS methods for the realisation of plasmon assisted chemical reactions is a challenge. First, plasmonic nanostructures, as SERS substrates, must be fabricated in such a way that they have specific features, such as shape and the arrangement of nanoparticles due to the high density of “hot spots”. Secondly, one of the major difficulties of producing TERS probes is the low reproducibility of the plasmon-active coated metal (Ag or Au) tips with a fixed-size diameter since only the sharp tip in TERS can create a “hot site” to excite strong plasmon resonance at the tip apex. Despite these difficulties, LSP stimulated chemical reactions using both techniques are promising ways for the disruption of toxic pollutants or the local modification of molecules thus opening new routes for the development of the next generation molecular semiconductors.

2. MATERIALS AND METHODS

2.1. Materials

All the reagents used in the experiments (Table 2.1.) were used without further purification.

Table 2.1. The list of reagents and materials used in the experiments

Materials/Reagents	Manufacturer	Formula
1,2-Dioleoyl-*sn*-glycero-3-phosphocholine (DOPC)	Sigma Aldrich	$C_{44}H_{84}NO_8P$
1,2-dioleoyl-*sn*-glycero-3-phospho-L-serine (sodium salt), DOPS	Sigma Aldrich	$C_{42}H_{77}NO_{10}PNa$
11-mercaptoundecanoic acid 95%	Sigma Aldrich	$HS(CH_2)_{10}CO_2H$
2-Amino-2-hydroxymethylpropane-1,3-diol (Tris buffer)	Sigma Aldrich	$(HOCH_2)_3CNH_2$
Benzylpenicillin (penicillin G)	Sandoz GmbH	$C_{16}H_{17}N_2NaO_4S$
Chloroform	Sigma Aldrich	$CHCl_3$
Cover slips	Menzel Gläser	–
Crystal violet (dye)	Sigma Aldrich	$C_{25}H_{30}N_3Cl$
Ethyl alcohol	Sigma Aldrich	CH_3CH_2OH
Ethylenediaminetetraacetic acid (EDTA)	Sigma Aldrich	$C_{10}H_{16}N_2O_8$
Gold (III) chloride trihydrate	Sigma Aldrich	$HAuCl_4 \times 3H_2O$
Graphene oxide	Graphene Supermarket	$C_xO_yH_z$
Hydrochloric acid (36.5-38.0%)	Sigma Aldrich	HCl
Hydrofluoric acid (48 wt. % in H_2O)	Sigma Aldrich	HF
Hydrogen peroxide (30 wt. % in H_2O)	Sigma Aldrich	H_2O_2
L-alanyl-L-tryptophan dipeptide	Sigma Aldrich	$C_{14}H_{17}N_3O_3$
Microscopic glass	Menzel Gläser	–
Nitrogen gas	AGA	N_2
Pentacene	Sigma Aldrich	$C_{22}H_{14}$
Phosphate Buffered Saline System (PBS)	Sigma Aldrich	–
Polyethylene glycol (400)	Sigma Aldrich	$H(OCH_2CH_2)_nOH$
Rhodamine 6G	Sigma Aldrich	$C_{28}H_{31}N_2O_3Cl$
Silicone isolators 20 mm × 20 mm × 1 mm; 8 mm × 8 mm × 1 mm	Grace Bio-Labs	–
Silver nitrate	Sigma Aldrich	$AgNO_3$
Sulphuric acid	Sigma Aldrich	H_2SO_4
Tetraethyl orthosilicate (TEOS)	Acros Organics	$Si(OC_2H_5)_4$
Water	Sigma Aldrich	H_2O
α-Synuclein A30P human, lyophilized powder	Sigma Aldrich	–

2.2. The methods for the synthesis of SERS-active substrates

2.2.1. Synthesis of silver SERS substrates based on the sol-gel technique

The sol was prepared by mixing TEOS, ethanol and water in a flask with the ratios 0.2:0.4:1 respectively. Reaction was carried out under acidic conditions: hydrochloric acid was used to reach the pH value of 2.3. The solution was mixed for one hour maintaining a constant temperature of 60°C and finally divided into three flasks. Pure PEG 400 was added to reach sol/PEG 400 ratios of 1:0.05 (v:v), 1:0.10 (v:v) and 1:0.15 (v:v) in each flask respectively. All PEG 400 modified sols were aged for 48 hours at room temperature. The films were formed on the ethanol cleaned microscopic objective glasses by the spin coating method with a spin speed of 1,500 rpm and a spin time of 10 s, dried at room temperature and heated in air at 300°C for 2 hours. After the thermal treatment, all the films were cooled to room temperature, immersed in freshly prepared 1 M $AgNO_3$ solution for 17 hours, then removed from the solution and dried under the nitrogen flow. Schematic illustration of the synthesis is represented in Fig. 2.1.

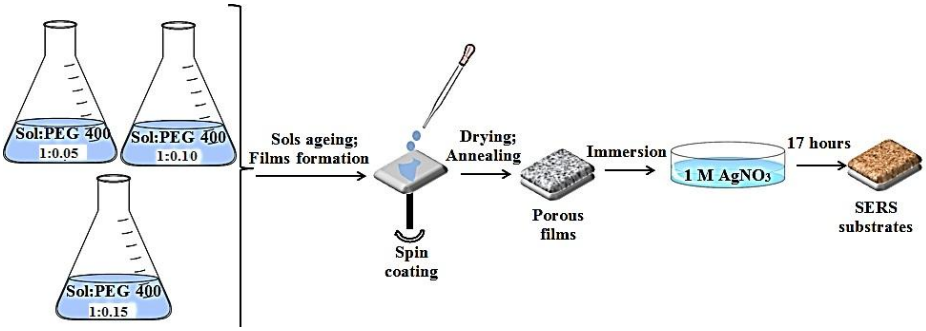

Fig. 2.1. A scheme illustrating the synthesis of silver SERS substrates based on sol-gel technique

2.2.2. Synthesis of silver and gold SERS substrates on silicon wafers

The preparation of silicon wafers. The synthesis of gold and silver SERS substrates was based on direct metal ion reduction by elemental silicon. Silicon wafers [111] were cut into small pieces (1.5 × 1.5 cm), cleaned by immersing them in pure ethanol and dried under the nitrogen flow. Such prepared silicon wafers were kept in the closed Petri dishes until use.

The synthesis of silver SERS substrates based (protocol No. 1). Hydrofluoric acid (HF) was diluted with water to the final concentration of 24%. The solution of silver precursor was prepared by dissolving $AgNO_3$ in water to the final concentration of 10 mM. The prepared HF (24%) and $AgNO_3$ (10 mM) solutions were mixed in a ratio of 1:1 (v:v). The silicon wafers were immersed in the reaction solution for 10 s, then immediately transferred to pure water and finally dried under the nitrogen flow.

The synthesis of silver SERS substrates (protocol No. 2). The solution of silver precursor was prepared by dissolving $AgNO_3$ in water to the final concentration of 2.5 mM. The prepared HF (24%) and $AgNO_3$ (2.5 mM) solutions were mixed in a

ratio of 1:1 (v:v). The silicon wafers were immersed in the reaction mixture for 5 s, then immediately transferred to pure water and finally dried under the nitrogen flow.

The synthesis of gold SERS substrates. The solution of gold precursor was prepared by dissolving gold (III) chloride trihydrate in water to the final concentration of 2.5 mM. The prepared HF (24%) and $HAuCl_4$ (2.5 mM) solutions were mixed in a ratio of 1:1 (v:v). The silicon wafers were immersed in the reaction mixture for 60 s, then immediately transferred to pure water and finally dried under the nitrogen flow.

The illustration of the synthesis of silver and gold SERS substrates is presented in Fig. 2.2. The synthesis conditions used for the preparation of the SERS substrates are listed in Table 2.2.

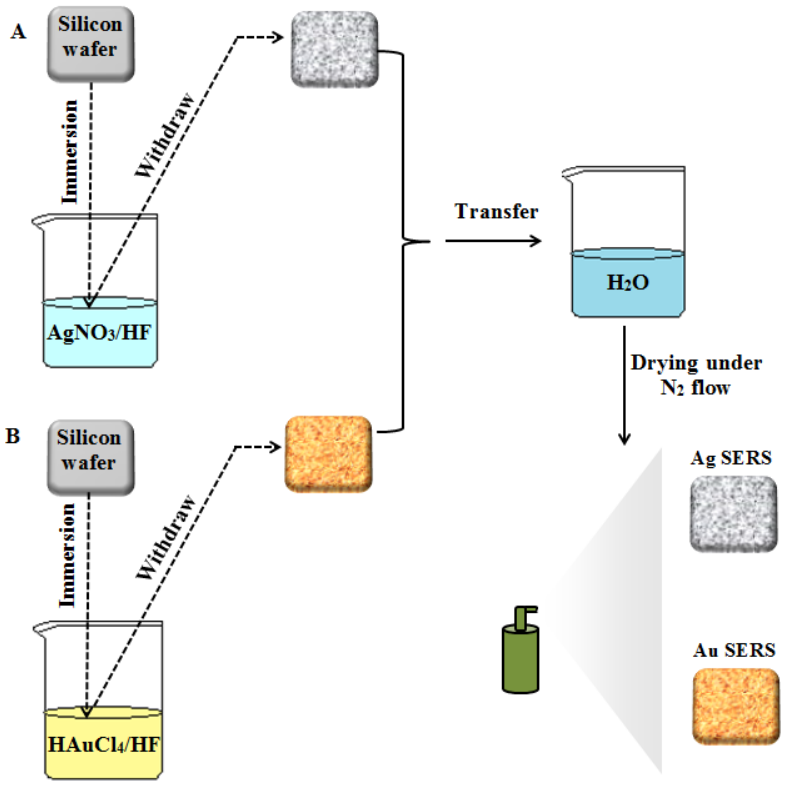

Fig. 2.2. The illustration of the synthesis of silver (A) and gold (B) SERS substrates on the silicon wafers

Table 2.2. The synthesis conditions for the preparation of silver and gold SERS substrates on silicon wafers

Silver SERS substrates				
Synthesis protocol No.	HF concentration, %	$AgNO_3$ concentration, mM	HF to $AgNO_3$ ratio	Immersion time, s
1	24	10	1:1	10
2	24	2.5	1:1	5
Gold SERS substrates				
HF concentration, %		$HAuCl_4$ concentration, mM	HF to $HAuCl_4$ ratio	Immersion time, s
24		2.5	1:1	60

2.3. Sample preparation for the experiments

2.3.1. The deposition of crystal violet analyte on the SERS substrates synthesised by the sol-gel technique

Silver nanoparticle decorated silica films were tested as substrates for Surface Enhanced Raman spectroscopy using 1% aqueous solution of crystal violet dye. 20 μl of the prepared solution was dropped on the surfaces of the SERS substrates. The prepared samples were dried at room temperature.

2.3.2. The deposition of pentacene monolayer on silver and gold SERS substrates

The monolayer of pentacene was deposited by vacuum evaporation on silver and gold SERS substrates. The thickness of the monolayer was 1-1.5 nm. The deposition of pentacene was performed at Istituto Officina dei Materiali - CNR (Trieste, Italy) in collaboration with Dr Denys Naumenko.

2.3.3. The deposition of R6G monolayer on silver and gold SERS substrates

The solution of R6G (1 mM) was prepared in methanol. The silver/gold SERS substrates were immersed in the R6G solution for 2 h. After 2 h, the SERS substrates were washed in methanol in order to remove the excess dye molecules. The method for the preparation of R6G monolayer was based on previous work reported by Sweetenham and Notingher (2011).

2.3.4. The preparation of the samples for the trace detection of α-Synuclein molecules in water

In order to avoid the additional peaks in SERS spectra characteristic for buffers, the stock solution (100 μM) of α-synuclein A30P human was prepared by dissolving it in water. The further dilutions with water were carried out in order to obtain the concentrations of α-synuclein A30P human of:

a) 100 nM
b) 1 nM;
c) 1 pM;
d) 1 fM.

The schematic illustration of the protein measurements is presented in Fig. 2.3.

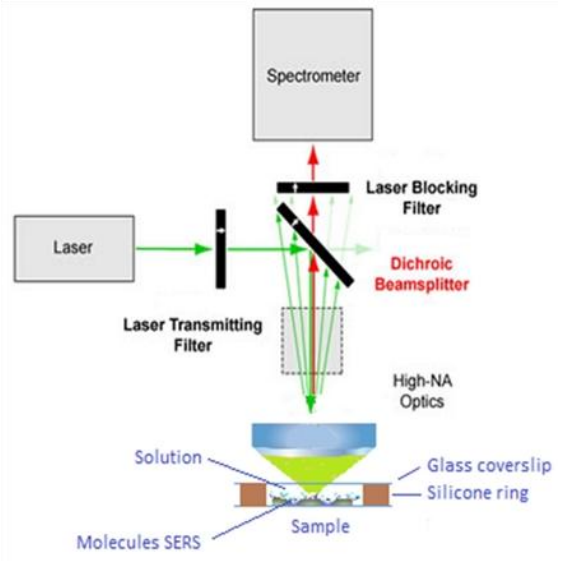

Fig. 2.3. Illustration of SERS measuring methodology

The samples preparation for SERS measurements were carried out as follows: The silicon isolators (8 mm × 8 mm × 1 mm) were attached to the silver SERS surfaces. 100 µl of the prepared α-synuclein A30P human solution was injected into the cavity of the silicone isolator and covered with the cover slip in order to avoid evaporation.

2.3.5. The preparation of L-alanyl-L-tryptophan samples for the investigation of dipeptide interaction with SERS surface

Aqueous solution of L-alanyl-L-tryptophan dipeptide was prepared by dissolving dipeptide in water to the final concentration of 10 mM. The pH of the prepared solution was found to be 6.3.

A silicon isolator (20 mm × 20 mm × 1 mm) was carefully attached to the surface of the silver SERS substrate. 0.5 ml of L-alanyl-L-tryptophan solution was injected into the cavity of the silicon isolator and covered with cover slip in order to avoid evaporation of the sample.

2.3.6. The deposition of lipid membrane on silver SERS substrates

Lipid membranes were deposited on the silver triangular nanoparticle decorated SERS substrates. The deposition was performed based on the modified methodology presented previously (Grinceviciute, Verdes and Snitka, 2015). Briefly, DOPS and DOPC in chloroform were used as received and mixed at a ratio of 1:4. The lipid was dried to remove the solvent and then resuspended in Tris buffer (149 mM NaCl, 5 mM $CaCl_2$, 10 mM Tris) to a final concentration of 0.1 g/l. The resulting solution was extruded 27 times through a membrane (pore size 0.1 µm) to

produce unilamellar vesicles. The vesicle solution was introduced directly in the measurement cell containing blank microscopic glass (control sample) or silver SERS substrate (test sample). The substrates were kept in the solution for 1 h, then it was replaced by pure Tris buffer. Subsequently, the solution was exchanged again by a Ca^{2+} free Tris buffer (10 mM Tris, 133 mM NaCl) containing 5 mM EDTA in order to remove the Ca^{2+} ions and finally by PBS. All buffers (pH 7.4) contained 0.05% NaN_3. The formation of the lipid membrane was carried out in collaboration with PhD student Nora Grinceviciute.

2.3.7. The preparation of the samples for the trace detection of benzylpenicillin molecules in cow's milk

The preparation of benzylpenicillin (BP) samples. Five solutions of different concentrations of BP (Table 2.3.) were prepared by dissolving it in water. 20 µl of each solution was deposited on the silver SERS substrates and dried at room temperature. The reference Raman spectra of BP was obtained from the concentrated solution of BP (1 M) deposited on the blank Si wafer (100 µl) and dried at room temperature.

The preparation of blank milk samples. Two types of cow's milk were selected for the experiment: raw milk obtained from an ecological farm and pasteurised commercial milk obtained from a supermarket. The untreated milk from the ecological farm was derived from healthy cows by the milking equipment; this kind of milk was selected as a reference. No further treatment of both types of milk has been performed. 20 µl of each type of milk was deposited on SERS substrates decorated with triangular silver nanoparticles. The samples were dried at room temperature.

The preparation of spiked milk samples. In order to identify Raman bands of BP in milk, the reference milk was spiked with different concentrations of aqueous BP solutions (Table 2.3.). The amount of spiking solutions to be added to the milk samples were calculated according to the following formula:

$$V_{std} = \frac{C_A \times V_0}{C_{std}} \quad (2.1)$$

Where V_{std} - volume of spike solution;
C_A – selected spike concentration;
V_0 – volume of the sample;
C_{std} – concentration of spike solution.

Table 2.3. The concentrations of BP used in the experiment

Concentration of BP in H_2O, pM	Concentration of BP in milk, pM
0.25	0.25
0.5	0.5
1	1
2.5	2.5
5	5

2.3.8. The preparation of the samples for the implementation of local chemical reaction on the silver SERS substrate

The concentrated GO (5 mg/l) solution was diluted with water in order to obtain a GO/H_2O ratio of 1/100. A diluted GO solution of 0.025 ml was placed on the triangular silver nanoparticle decorated SERS substrate. The prepared sample was kept at room temperature for 10 min in order to precipitate the GO on the SERS surface. For the control experiment the described procedure was repeated only on a blank silicon wafer.

2.4. Analytical methods

2.4.1. Structural characterisation

2.4.1.1. The structural analysis of the synthesised SERS substrates was carried out by Atomic Force Microscope (AFM) (NT-MDT Inc., Russia) using commercial silicon cantilevers (resonant frequency 150 kHz, tip radius < 10 nm, force constant 5 N/m). AFM was also used for the measurements of current-voltage (I-V) characteristics. I-V curves were obtained with spreading resistance mode AFM using commercial silicon cantilevers with conductive TiN coating (resonant frequency 150 kHz, tip radius: 35 nm, force constant 5.1 N/m).

2.4.1.2. A scanning electron microscope (SEM) (Helios NanoLab 650 FEI, Holland) was used for the structural investigation of the silver nanoparticle decorated silica films. The measurements were carried out at the Centre for Physical Sciences and Technology (Vilnius). A scanning electron microscope (FEI Quanta 200 FEG) was used for the structural characterisation of the SERS substrates prepared on the silicon wafers. The energy dispersive X-ray spectroscopy (EDX) was used for the elemental analysis of the SERS substrates. The analysis was performed using a spectrometer equipped with a Bruker XFlash® 4030 detector (Bruker AXS).

2.4.2. Optical characterisation

2.4.2.1. Optical characterisation of all the types of SERS substrates and colloidal silver solutions were performed using a UV-Vis USB 2000 optic spectrometer (Ocean-Optics Inc.).

2.4.2.2. Raman and SERS spectra were recorded using a Raman spectrometer (NTEGRA Spectra, NT-MDT Inc.). The objective magnification was $100\times$, numerical aperture NA = 1.49 and optical beam focus spot diameter – 500 nm. The excitation source was a laser with λ = 532 nm and optical beam power of 25 mW. The laser power on the samples was 1.7 mW.

2.4.3. Theoretical computation

The theoretical simulation of the EM field enhancement on the silver nanoring decorated silica films and silver nanotriangle decorated Si substrates, as well as the determination of their EF were performed using COMSOL Multiphysics® v4.3 (RF Module) software. The simulations were carried out in collaboration with

Dr Xu Huizhong at the Department of Physics, St. John's University (USA). The theoretical SERS enhancement was calculated with the following equation (Choi et al., 2010):

$$EF_{SERS} = \frac{|E_{loc}(\omega_{ex})|^2}{|E_0(\omega_{ex})|^2} \frac{|E_{loc}(\omega_s)|^2}{|E_0(\omega_s)|^2} \quad (2.2)$$

Where $E_{loc}(\omega_{ex})$ - the amplitude of the enhanced local electric field at the laser excitation frequency;

$E_0(\omega_{ex})$ - the amplitude of the incident electric field provided by the laser at the laser excitation frequency;

$E_{loc}(\omega_s)$ - the amplitude of the enhanced local electric field at the Raman scattered frequency;

$E_0(\omega_s)$ - the amplitude of the electric field at the Raman scattered frequency resulted by the analyte.

The wavelength of the incident light was 532 nm. Perfectly matched layer (PML) boundary conditions were used.

2.4.4. Software for data processing

The results were processed using Origin Pro 8.5.1, Nova MT-MDT SPM, Image J (2006), Jmol, HyperChem (Molecular Modeling System 5.0.2), ChemSketch (ACD 2012), SPIP Image Processing (V4. 02) and Crystal Sleuth (2008) software.

3. RESULTS AND DISCUSSION

3.1. The synthesis of the SERS substrates based on the sol-gel technique

3.1.1. The synthesis of PEG 400 modified porous hybrid silica films

The sol-gel technique is a promising way for the fabrication of 3D SERS substrates. Moreover, the usage of organic templates makes this method desirable because of the possibility to use organic templates allowing the size of the pores to be controlled and to immobilise nanoparticles directly from colloidal solutions. In the current experiment, the polyethylene glycol 400 (PEG 400) has been chosen as the porogen and the reducing agent of silver ions. Recently, a number of publications represented polyethylene glycol as a perfect substance for "green reduction" of silver ions and for the stabilisation of the silver nanoparticles (Stiufiuc et al., 2013; Luo et al., 2005). It also became attractive for its solubility in an aqueous medium, low toxicity and wide selection of molecular weights (Shameli et al., 2012). Recently, two publications dealing with the current experiment and the topic of the dissertation were published (Snitka et al., 2012; Snitka et al., 2011). It has been shown that the combination of the sol-gel technique and the usage of honey allow the synthesis of SERS-active hybrid silica films decorated with gold nanoparticles. In such synthesis, the "green" reduction of gold ions has been carried out using honey. It was demonstrated that the bio-active ingredients of honey, such as reducing sugars or proteins, can act as reducing agents and produce the gold nanoparticles.

The aim of the current experiment was to synthesise novel plasmonic nanostructures of controllable shapes by combining the sol-gel technique and direct silver ions reduction. The sol-gel process involves hydrolysis of the alkoxides, water and alcohol condensation. In a general case, hydrolysis of the TEOS is based on the replacement of alkoxide ligand by the hydroxyl group. During the condensation stage occurring between two silanols or silanol and alkoxide, the molecular weight of the synthesis product increases. When PEG 400 is introduced into the reaction system it interacts chemically with the sol particles and results in the formation of a hybrid polymeric network (Kuraoka et al., 2005), where part of the PEG 400 interacts physically with the sol particles and remains inside the pores and channels (Sun et al., 1998) (Fig. 3.1).

During the thermal annealing of hybrid silica films chemically unreacted PEG 400 is not fully removed from the polymeric matrix. This was confirmed by Raman measurements performed after thermal treatment of the films (Fig. 3.2).

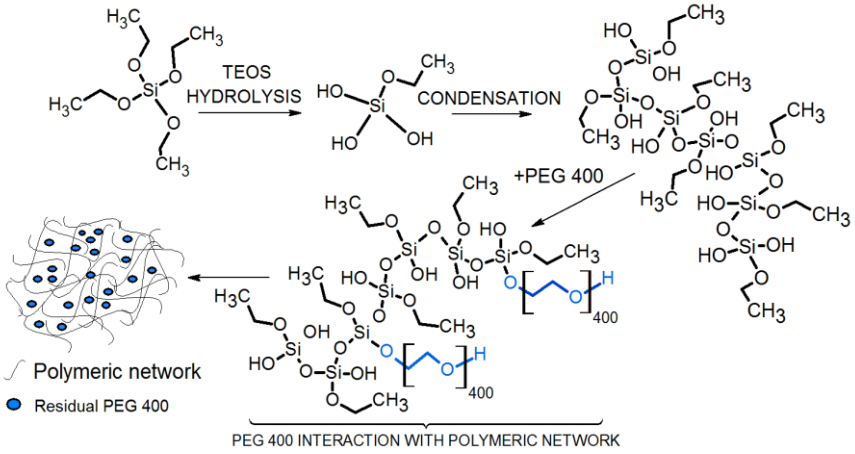

Fig. 3.1. Proposed mechanism of PEG 400 interaction with the silane network

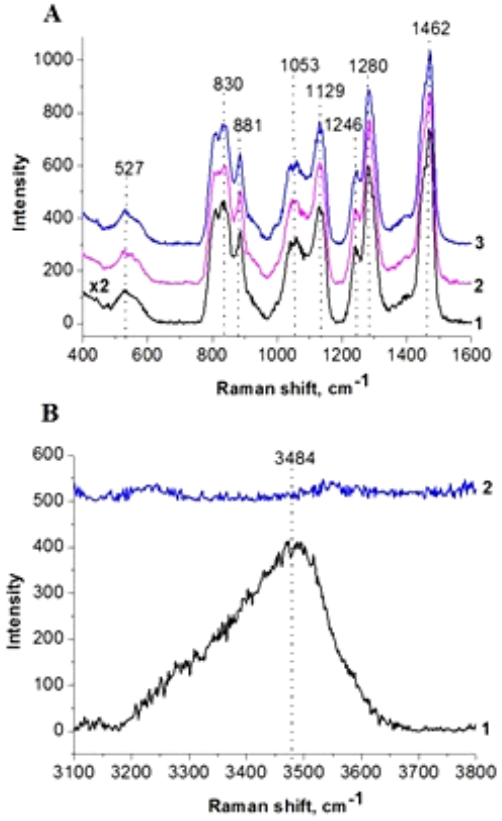

Fig. 3.2. Raman spectrum of PEG 400 modified silica films after thermal treatment at 300°C: (A) a film prepared at a volume ratio of sol:PEG 1:0.05 (1); a film prepared at a volume ratio of sol:PEG 1:0.10 (2); a film prepared at a volume ratio of sol:PEG 1:0.15 (3); (B) a film prepared at a volume ratio of sol:PEG 1:0.10 before the deposition of silver nanoparticles (1) and after the deposition of silver nanoparticles (2)

Raman spectra of organically modified silicates strongly depend on the hybrid materials preparation technique, molecular weight, concentration and nature of the modifying polymer. Considering this, the peaks at ~ 830 cm^{-1} and 881 cm^{-1} as well as at 1053 cm^{-1} and 1129 cm^{-1} were assigned to CH_2 bands from pure polyethylene glycol (Jung et al., 2005) (Fig. 3.2, A). The presence of the residual PEG 400 in porous silica matrix can be explained by insufficient temperature for the total removal of the organic template. More recently, other researchers showed that total elimination of PEG from the composites is available at the temperatures above 400°C (Fan et al., 2006; Ramírez-Santos, Acevedo-Peña and Córdoba, 2012). Thermal stability of PEG-silica hybrid systems is influenced by a strong interaction between PEG and silica. Therefore, silica prevents the heat transfer to the inner parts of PEG (Oh et al., 2009). For this reason, the vibrations of incorporated polymer chains are well expressed in the Raman spectra. The peaks observed at 1,462 cm^{-1} correspond to C-H vibrations while bands at 1,246 cm^{-1} and 1,280 cm^{-1} are assigned to C-O-C bonds of PEG 400. A broad band rising from 500-550 cm^{-1} represents mixed stretching and bending modes of Si-O-Si (Manara, Grandjean and Neuville, 2009). As seen in Fig. 3.2 (B), a shoulder at 3,484 cm^{-1} corresponding to -OH vibrations of PEG 400 is visible in the Raman spectra of the film before its immersion in the silver nitrate solution. However, this band disappears after the exposure of silica film in $AgNO_3$ solution for 17 h. This suggests that -OH groups of PEG 400 are responsible for the reduction of silver ions.

3.1.2. The modification of hybrid porous silica films with silver nanoparticles

The results of Raman measurements allowed the hypothesis that residual PEG 400 could act as a reducing agent for silver cations and results in the formation of silver nanoparticles on the films surface. Therefore, when such films were introduced into a silver nitrate solution, the reduction of silver ions occurred through the oxidation of PEG 400 hydroxyl groups to aldehyde groups (Nam et al., 2011). In order to confirm that PEG 400 is able to act as a reducing agent, 1 M $AgNO_3$ solution was mixed with pure PEG 400 (volume ratio 1:1). The reaction was monitored in real-time by using UV-Vis spectroscopy (Fig. 3.3). At the beginning of the reaction, no absorption peak characteristic for silver nanoparticles was recorded. However, a broad plasmon occurred in the spectra after 20 minutes from the moment when $AgNO_3$ and PEG 400 were mixed. The plasmon increased with an increase in the reaction time and was found to be located at 428 nm. The peak reached the maximum after 50 minutes and did not rise with a longer reaction time that indicated that the reduction reaction was completed. The colour of the reaction solution changed from colourless to yellowish that also suggested the successful formation of silver nanoparticles.

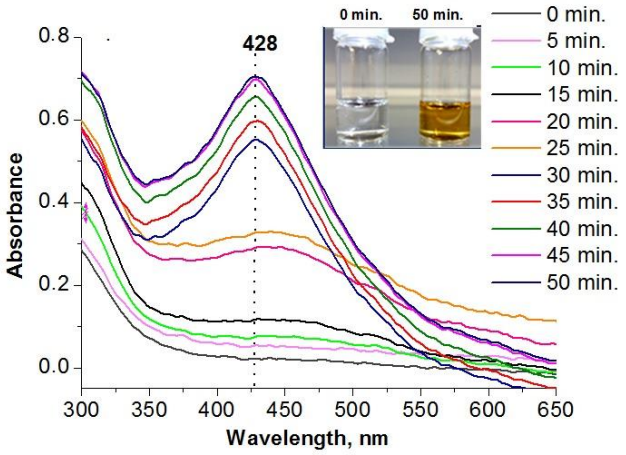

Fig. 3.3. Time-dependent UV-Vis spectra showing the reduction of silver ions with PEG 400

The reduction of silver ions both in the solution and on the surface of the films can be expressed by the following reaction:

$$Ag^{+}(aq) + e^{-} \longrightarrow Ag^{0}(s)$$
$$NO_3^{-}(aq) + e^{-} + 2H^{+}(aq) \longrightarrow NO_2\uparrow + H_2O \quad \Big\} \text{ (reduction half-reactions)}$$
$$*PEG_{400}(aq) - 2e^{-} \longrightarrow **\text{Aldehyde-}PEG_{400}\text{-Aldehyde (aq)} + 2H^{+}(aq) \text{ (oxidation half-reaction)}$$

$$Ag^{+}(aq) + NO_3^{-}(aq) + *PEG_{400}(aq) \longrightarrow Ag^{0}(s) + **\text{Aldehyde-}PEG_{400}\text{-Aldehyde}(aq) + H_2O + NO_2\uparrow$$

(overall redox reaction)

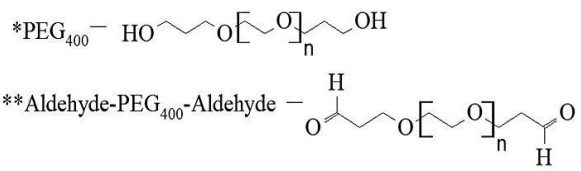

Fig. 3.4 shows the morphological characterisation of the films by AFM before (A, C, E) and after (B, D, F) their immersion in the silver nitrate solution. AFM characterisation revealed that the change of PEG 400 amount in the sol resulted in the different structures of silver nanoparticles formed on the films surfaces. Silica films, prepared by using a sol/PEG 400 ratio 1:0.05 (v:v) were decorated with nanosized silver rings, while the films prepared using a sol/PEG 400 ratio 1:0.10 (v:v) were found to have spherical silver nanoparticles on the surface. The third type of the films (sol/PEG 400 ratio 1:0.15 (v:v) was found to have the network of silver nanoparticles formed on the surface of the film.

In all the cases, the reduction of silver ions starts inside the pores, where the formation of primary nanoparticles takes place. Those particles are the nucleation centres and catalyse the reduction of other Ag cations around them. The lowest amount of organic template leads to the growth of silver nanoparticles along the

edges of the pores thus resulting in nanosized ring-like silver structures. When the amount of PEG 400 is increased, reduction continues and results in spherical silver nanoparticle filled pores. The high amount of polyethylene glycol template influences the increase of interconnections between pores (Ramírez-Santos, Acevedo-Peña and Córdoba, 2012) and self-assembled structures of silver nanoparticles are formed on the surface of the third type of film.

The formation of nanosized silver rings, spherical and self-assembled silver nanoparticles on the films surfaces were also confirmed by the SEM measurements (Fig. 3.5., A, B, C).

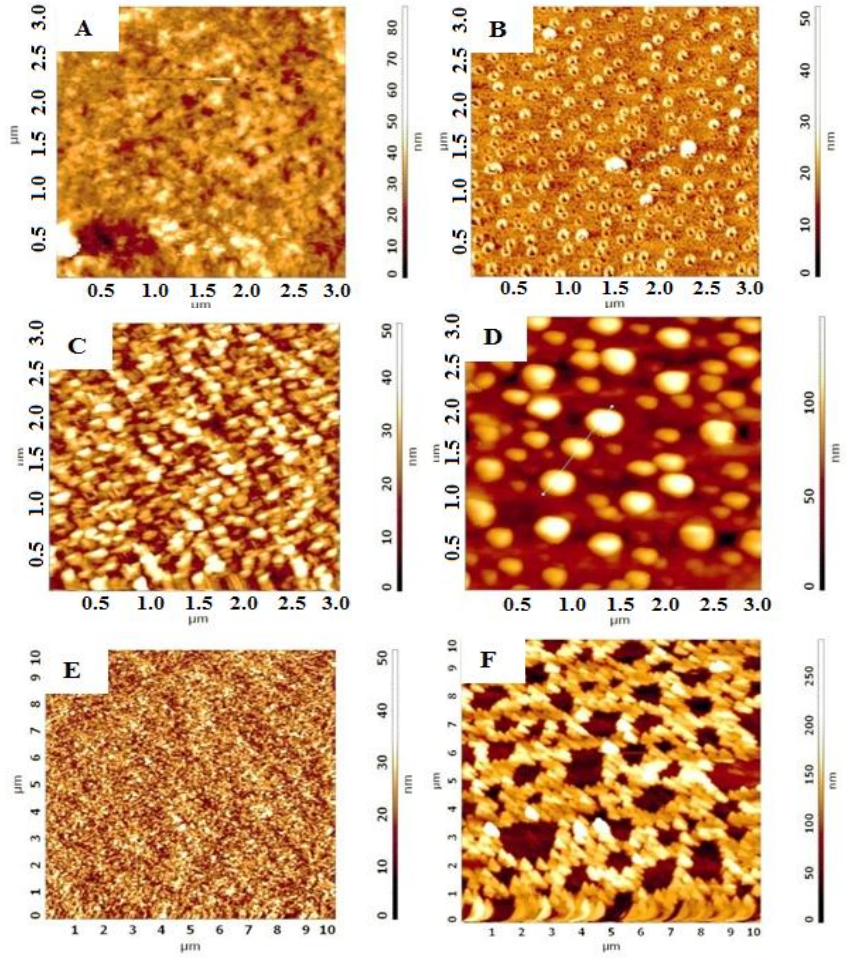

Fig. 3.4. AFM images showing the morphology of the films: (A) a film prepared at a volume ratio of sol:PEG 1:0.05 after thermal treatment and (B) after exposure in silver nitrate solution for 17 hours (C) a film prepared at a volume ratio of sol:PEG 1:0.10 after thermal treatment and (D) after exposure in silver nitrate solution for 17 hours; (E) a film prepared at a volume ratio of sol:PEG 1:0.15 after thermal treatment and (F) after exposure in silver nitrate solution for 17 hours

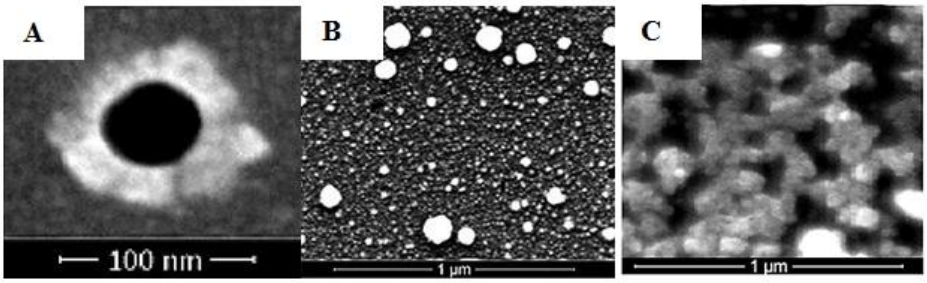

Fig. 3.5. SEM images of silver nanoparticle decorated silica films: (A) SEM image of a nanosized silver ring; (B) SEM image of spherical silver nanoparticle decorated silica film; (C) SEM image of a self-assembled silver nanoparticle decorated silica film

The optical characterisation of all types of films is presented in Fig. 3.6. Broad shoulders located at around 472-478 nm are typical for silver nanostructures. Recently, it has been shown that various nanostructures, such as silver spheres, rods, discs, triangles or truncated structures exhibit mono-, di-, tri-, tetra- or multiple surface plasmon resonances in UV-Vis absorption spectra respectively that result from individual dipole and/or quadrupole plasmon modes (Jiang, Zeng and Yu, 2006). Due to the size and/or the shapes of the nanoparticles the resonance conditions change and result in a shifted or broadened UV-Vis spectra.

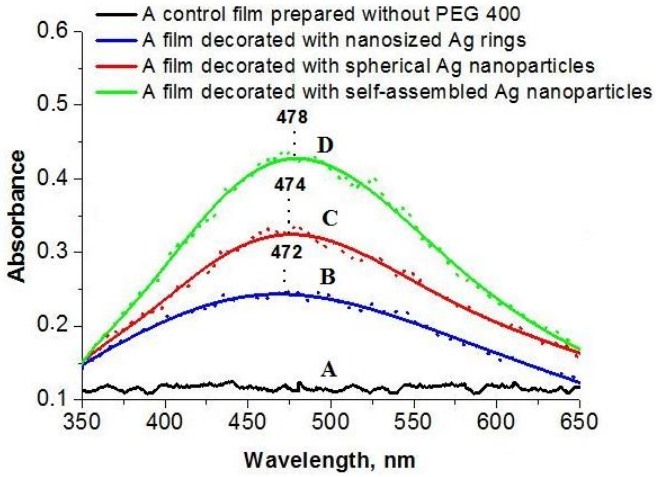

Fig.3.6. UV-Vis spectra of the films fabricated by the sol-gel technique: a control film prepared without PEG 400 (A); a film decorated with silver nanorings (B); a film decorated with spherical silver nanoparticles (C); a film decorated with self-assembled silver nanoparticles (D)

It is obvious from the UV-Vis measurements that the absorption of the hybrid films increases with an increase in the amount of PEG 400. The reason for such phenomenon is that after the thermal treatment of the films more residual PEG 400 remains entrapped in the pore channels and results in an increase in the density of the silver nanoparticles on the films surface. In order to confirm that silver ions are

reduced by PEG 400, the control UV-Vis spectra of PEG 400-free film was recorded. No plasmon in the range common for silver nanoparticles was observed. This result confirmed that PEG 400 is responsible for the reduction of silver ions.

3.1.3. Statistical evaluation of nanostructures repeatability

In order to determine the repeatability of the silver nanostructures formed on the silica films, grain analysis was performed using NT-MDT software. The grain analysis function provides automatic grains determination and evaluation. For the evaluation of the repeatability of the obtained silver nanorings and spherical nanostructures the *"grain diameter parameter"* was selected. As seen in Fig. 3.7 (B) and 3.8 (B) such parameter allowed the mean diameter of the silver nanorings and spherical nanoparticles formed on the silica films to be calculated. For the statistical evaluation of the nanostructures repeatability, 5 samples of silver nanorings and 5 samples of spherical silver nanoparticle decorated silica films were prepared. The threshold level was selected according to the nanoparticles height histograms (Fig. 3.7, A (1) and Fig. 3.8, A (1)). The average height histogram of silver nanorings was found to be ~19 nm and for silver spherical nanoparticles ~53 nm. The average diameter of silver nanorings of all 5 samples was found to be ~95 nm and the calculated standard deviation (SD) was 9.8 nm. The average diameter of spherical silver nanoparticles of all 5 samples was found to be ~170 nm and the calculated SD was 8.3 nm. The SD was calculated according to the following equation:

$$SD = \sqrt{\frac{\sum(x-\bar{x})^2}{N-1}} \tag{3.1}$$

Where:
SD – standard deviation;
N – number of value in the data set;
x – each value of the selected evaluation parameter;
$\bar{x}$ − mean value of the selected evaluation parameter of all the samples.

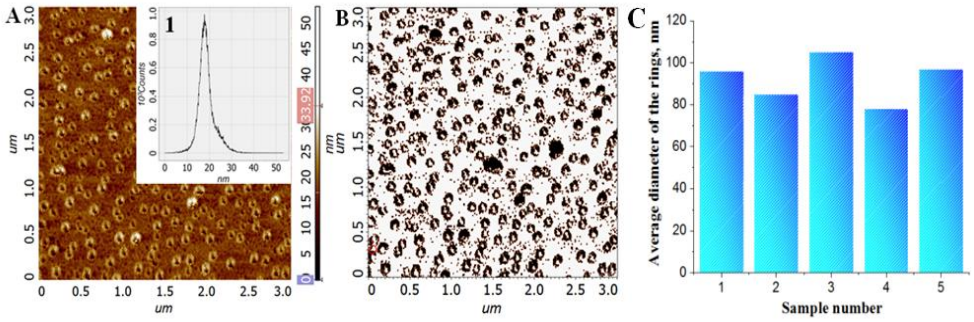

Fig. 3.7. The statistical evaluation of silver nanoring formation repeatability: (A) AFM image of silver nanorings and their height histogram (1); (B) grain image of silver nanorings; (C) a graph showing the average diameter of silver nanorings on 5 samples

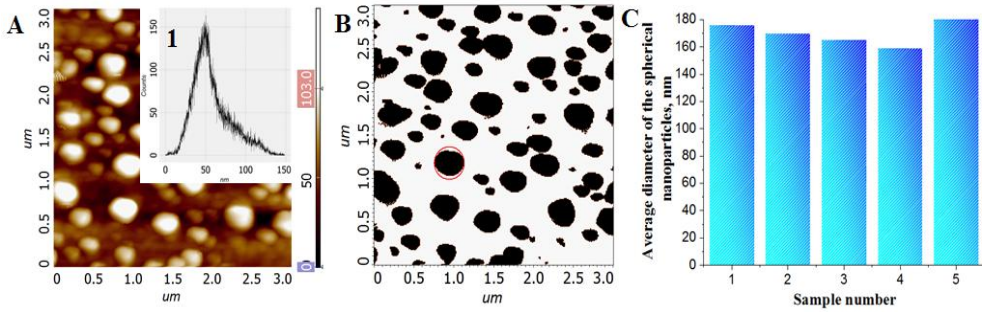

Fig. 3.8. The statistical evaluation of spherical silver nanoparticle formation repeatability: (A) AFM image of spherical silver nanoparticles and their height histogram (1); (B) grain image of spherical silver nanoparticles; (C) a graph showing the average diameter of spherical silver nanoparticles on 5 samples

Given that the nanoparticles on the silica films (prepared using the highest concentration of PEG 400) tend to form self-assembled networks the traditional statistical analysis for the evaluation of the repeatability of such structures is complicated. Therefore, for this purpose the fractal dimension was calculated using SPIP Image Processing software. The fractal dimension is an index describing the fractal patterns by assessing their complexity. This index is an indication of the statistical self-similarity. As seen in Fig. 3.9, the values of fractal dimensions of all 5 samples are similar indicating good repeatability of the nanostructures.

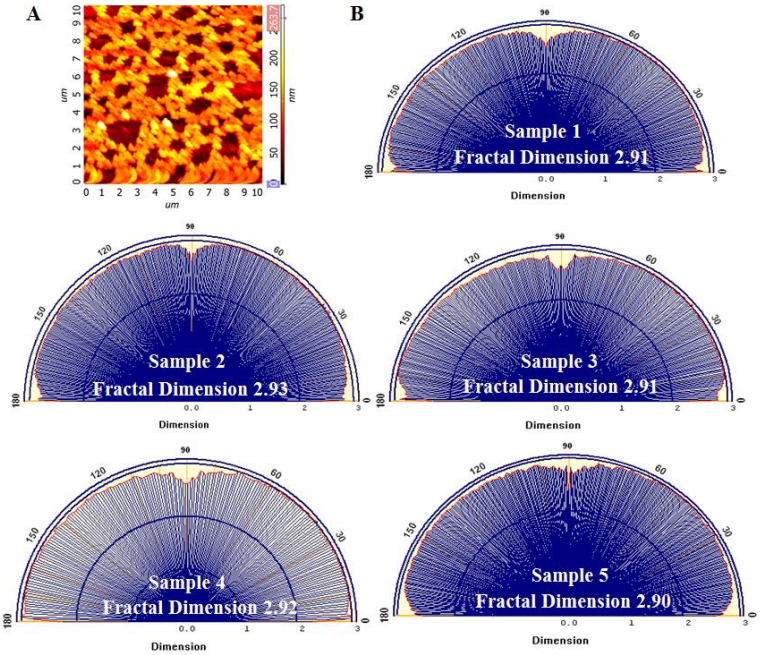

Fig 3.9. The statistical evaluation of silver self-assembled networks: (A) AFM image of self-assembled silver nanoparticles formed on the silica film; (B) fractal dimensions of roughness of 5 samples

3.1.4. The testing of the hybrid porous silica films decorated with silver nanoparticles for SERS

In order to evaluate the EF distribution on the SERS substrate and the EF, the theoretical simulation was performed for silver nanoring decorated SERS substrate. The results are presented in Fig. 3.10.

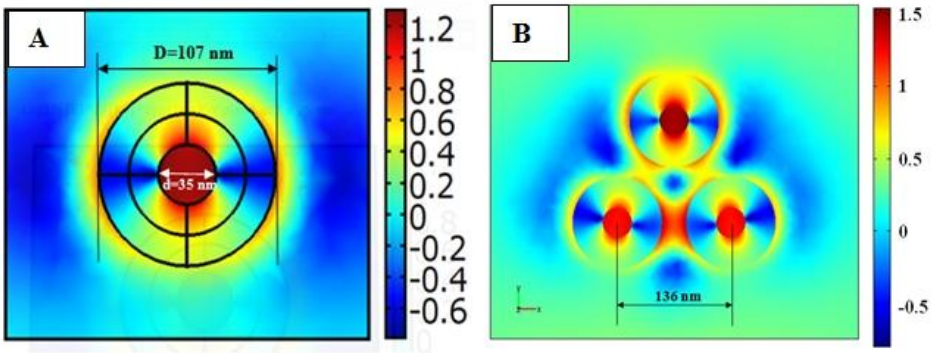

Fig. 3.10. The simulation of EM distribution: for a single silver nanoring (A); for a system consisting of three silver nanorings (B)

As seen in Fig. 3.10, the highest intensity of EM of the silver nanoring decorated SERS substrate occurs inside the rings. The theoretical enhancement of the Raman signal calculated according to the equation (2.2) was found to be 250 times. The experimental SERS measurements showed a relative enhancement of crystal violet analyte of around 200 times compared to the normal Raman Fig. 3.11 (B). Therefore, the experimental results agreed with theoretical calculations. The relatively low enhancement factor of nanosized silver rings can be explained by the large inner diameter of the nanorings (~35 nm) as well as the large distance between the separate nanorings (Fig. 3.4, B).

The SERS substrate decorated with spherical nanoparticles demonstrated an enhancement of the Raman signal for crystal violet analyte up to 100 times (Fig. 3.11, C), while the highest enhancement (around 270 times) was observed on the film decorated with self-assembled silver nanostructures (Fig. 3.11, D). The highest concentration of PEG 400 leads to the formation of close-packed silver nanoparticles and increases the content of the hot spots.

It is important to note that the Raman and SERS spectra presented in Fig. 3.11 show the relative enhancement of the Raman signal for a crystal violet analyte. It is not a “single molecule” enhancement spectrum.

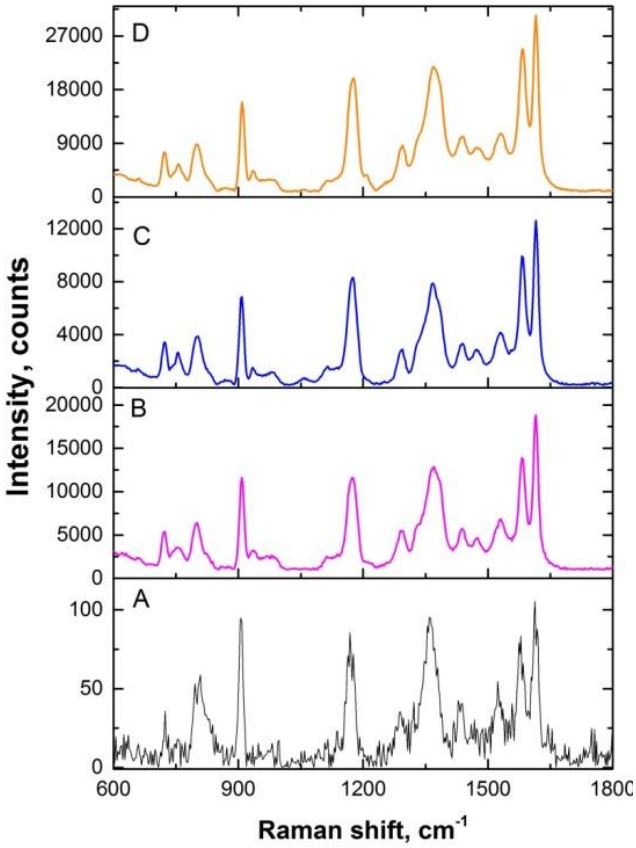

Fig. 3.11. The average spectra of crystal violet analyte collected at 50 randomly selected points of the sample: (A) Raman spectra obtained on microscopic glass; (B) SERS spectra obtained on silver nanoring decorated SERS substrate; (C) SERS spectra obtained on silver nanosphere decorated SERS substrate; (D) SERS spectra obtained on silver self-assembled nanoparticle decorated SERS substrate. The acquisition time for the collection of Raman and SERS spectra was 1s

Conclusions. A novel approach for the synthesis of silica films decorated with silver nanoparticles was demonstrated. It was found that the variation of PEG 400 concentrations in the sols allowed for the fabrication of different arrangements of silver nanoparticles on the films surfaces. The proposed method allowed for the synthesising of silver nanorings, spherical and networked self-assembled structures of silver nanoparticles. The fabricated films were applied for the SERS measurements using crystal violet dye as the target analyte. It was demonstrated that the highest relative enhancement of Raman signal (~270 times) can be obtained on the films decorated with a self-assembled network of silver nanoparticles. A similar result was observed on the silica films decorated with silver nanorings (~200). The synthesised silver nanostructures as the bifunctional film can be applied not only for SERS measurements. As the theoretical computation results show, the highest EM field is generated inside the silver nanorings. Therefore, such structures can act as

nanoreactors and open the possibility to perform local chemical reactions inside the nanorings.

3.2. The synthesis and characterisation of the SERS substrates prepared on silicon wafers

The synthesis of silver and gold SERS substrates was based on the direct silver/gold ion reduction on the HF etched silicon wafers. The selection of the method for the synthesis of the SERS substrates was based on the following factors:

A. Easy, inexpensive and fast preparation of the SERS sensors.

B. Minimum usage of chemical reagents allowing additional procedures for the removal of the residual reagents from the SERS substrate to be avoided. This is important for the trace detection because the additional reagents, such as organic reductants, stabilisers may have their own Raman spectra leading to the complicated identification of the analytes.

3.2.1. Silver nanoparticle decorated SERS substrates

The synthesis of silver SERS substrates was based on the direct silver ion reduction on HF etched silicon wafers. In the first case, the SERS substrates were prepared by synthesis protocol No. 1. (Table 2.2). In the first stage, HF dissolves the SiO_2 layer according to the following equation:

$$SiO_2(s) + 6HF(aq) \longrightarrow H_2SiF_6(aq) + 2H_2O(aq)$$

After the removal of the SiO_2 layer, silver ions capture electrons from the elemental silicon leading to the formation of silver atoms. Meanwhile, silicon is oxidised and lightly etched by the HF (Zaghouani et al., 2015). The formation mechanism of the silver nanoparticles can be described by the following equations:

$$\left.\begin{array}{l} Ag^+(aq) + e^- \longrightarrow Ag^0(s) \mid \times 2 \\ 2H^+(aq) + 2e^- \longrightarrow H_2\uparrow \end{array}\right\} \text{(reduction half-reactions)}$$

$$Si^0(s) + 6F^-(aq) \longrightarrow SiF_6^{2-}(aq) + 4e^- \text{ (oxidation half-reaction)}$$

$$Si^0(s) + 2Ag^+(aq) + 6F^-(aq) + 2H^+(aq) \longrightarrow SiF_6^{2-}(aq) + 2Ag^0(s) + H_2\uparrow$$

(overall redox reaction)

In order to determine their morphology, the synthesised silver SERS substrates were characterised by AFM. For the evaluation of the nanoparticles shapes repeatability, 10 SERS samples were prepared according to synthesis protocol No. 1. The AFM images and the height histograms of all 10 samples are presented in Fig. 3.12.

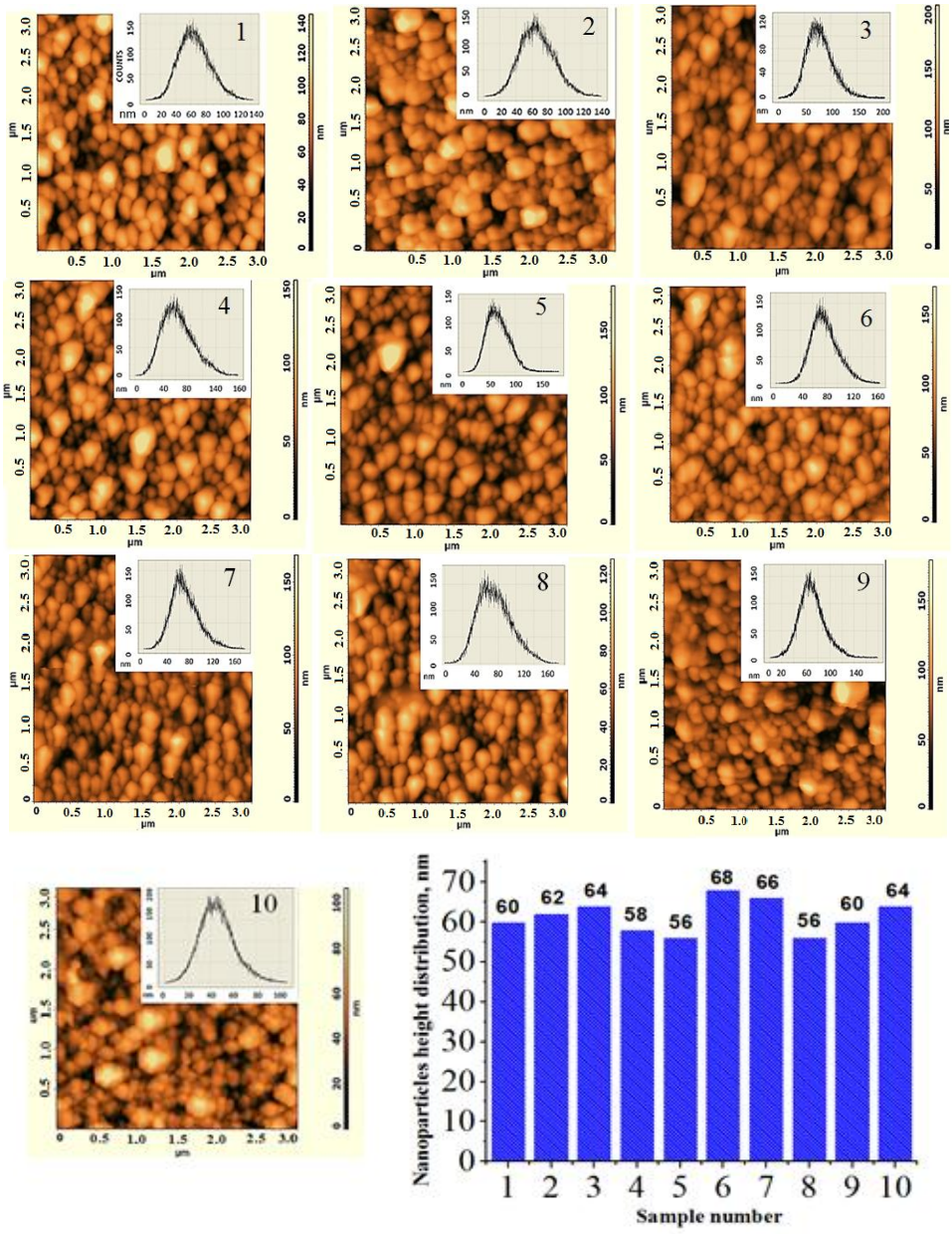

Fig. 3.12. The AFM images of the silver SERS substrates and the height histograms of silver nanoparticles distribution. For the evaluation of nanoparticles shapes and height repeatability, 10 samples (marked 1–10) were characterised in the scanning area of 3 × 3μm

As seen in Fig. 3.12, the silver nanoparticles of irregular shapes were formed on the silicon surface. The standard deviation (SD) of the nanoparticles height distribution of the SERS substrates was found to be 4 nm. The calculated average height of the nanoparticles of all 10 samples was ~61 nm. The SD was calculated according to the equation (3.1).

The SEM analysis confirmed the presence of the irregular-shaped silver nanoparticles and the EDX spectra revealed the presence of the silver element (Fig. 3.13, A and B). Meanwhile, UV-Vis spectra showed a plasmon at around 447 nm (Fig. 3.13, C), which is typical for the silver nanoparticles (Prabu and Johnson, 2015).

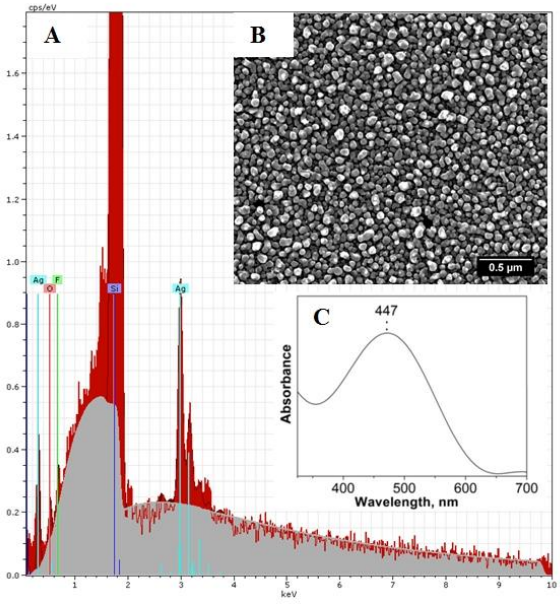

Fig. 3.13. EDX spectrum of silver SERS substrate (A); SEM image of the SERS substrate demonstrating the silver nanoparticles of irregular shapes (B) (magnification: 30000 ×; high vacuum mode ((30.00 kV)); UV-Vis spectra showing a plasmon at 447 nm that confirms the presence of silver nanoparticles

Under the particular conditions (such as reagents concentrations) the growth of silver nanoparticles on [111] oriented silicon wafers prefer the triangular shape with respect to the substrate lattice (Wall et al., 2011). Such nanostructures have edges at their vertexes that can concentrate the optical field within the narrow gaps between them leading to a high density of "hot spots". Therefore, silver nanotriangles have an advantage for the SERS applications compared to the spherical or irregular-shaped nanoparticles. However, no triangular nanoparticles were observed in the case when silver SERS substrates were prepared according to synthesis protocol No. 1 (Table 2.2). The reason for that can be explained by the high concentration of $AgNO_3$ and long exposure time of the silicon wafers in the reaction solution. The high concentration of $AgNO_3$ (10 mM) leads to the rapid formation of the primary silver nanoparticles (nucleation centres), whereas a long exposure time (10 s) determines the growth of irregular-shaped silver nanoparticles. In order to synthesise triangular silver nanoparticles, the next batch of SERS substrates was prepared according to synthesis protocol No. 2 (Table 2.2.). In this case, the concentration of $AgNO_3$ was reduced from 10 mM to 2.5 mM and the exposure time of the silicon wafers in the

synthesis solution was shortened from 10 s to 5 s. As seen in Fig. 3.14, the formation of silver nanotriangles on the silicon wafers was confirmed by AFM measurements.

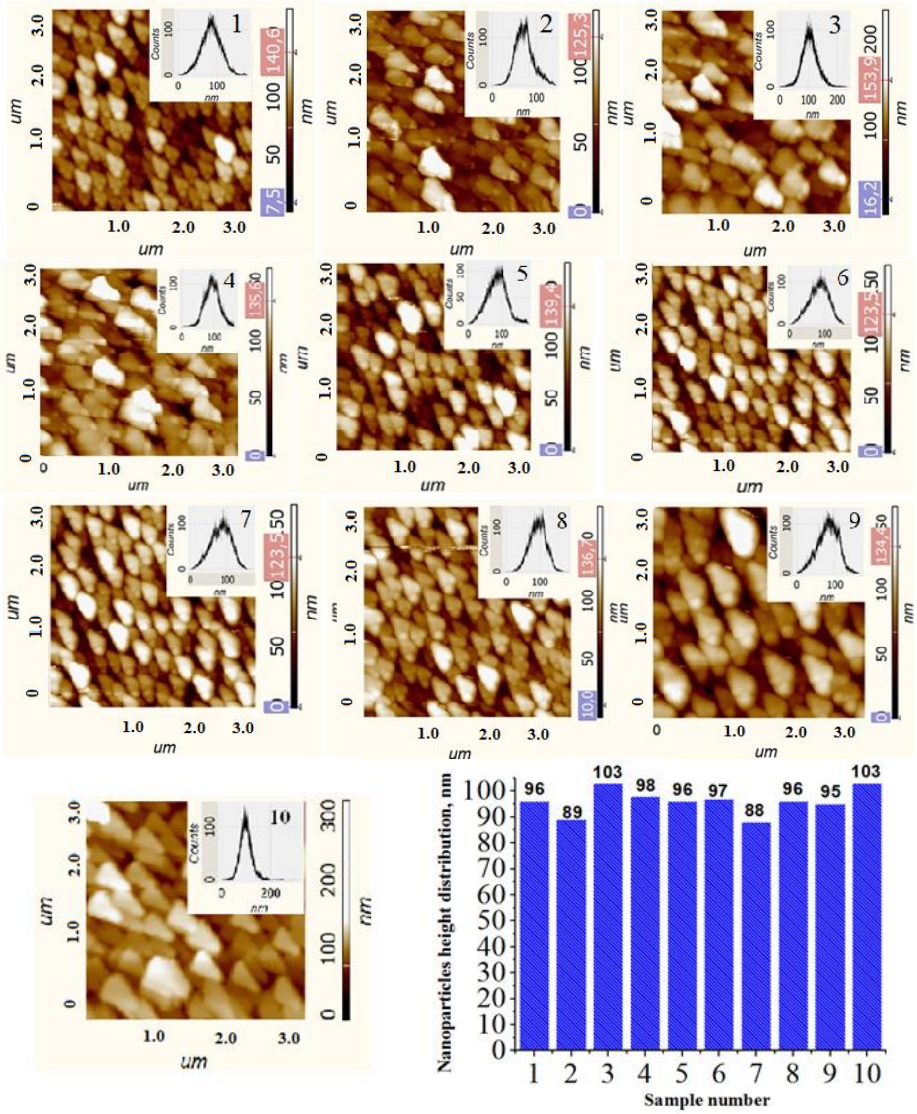

Fig. 3.14. The AFM images of the silver SERS substrates and the height histograms of silver nanoparticles distribution. For the evaluation of nanoparticles shapes and height repeatability, 10 samples (marked 1-10) were characterised in the scanning area of 3 × 3μm

The lower concentration of $AgNO_3$ leads to the slower formation of the primary silver nanoparticles that grow in accordance with the substrate lattice. After 5 seconds the SERS substrate is transferred to pure water that terminates any further growth of the silver nanoparticles thus preventing the formation of silver aggregates or irregular shapes. In order to evaluate the repeatability of the silver nanoparticles shape distribution, 10 SERS samples were prepared according to synthesis protocol

No. 2. The SD of the nanoparticles height distribution of the SERS substrates was found to be 5 nm. The calculated average height of the nanoparticles of all 10 samples was ~96 nm.

The SEM analysis confirmed the presence of the triangular nanoparticles, the EDX measurements revealed the presence of the silver element (Fig. 3.15, A and B) and UV-Vis spectra showed a plasmon at around 490 nm (Fig. 3.15, C). A broad peak in the UV-Vis spectra suggests the formation of the aggregates. However, in this case the broadened UV-Vis spectra can be a result of multiple plasmon resonances due to the specific shape of the silver nanoparticles.

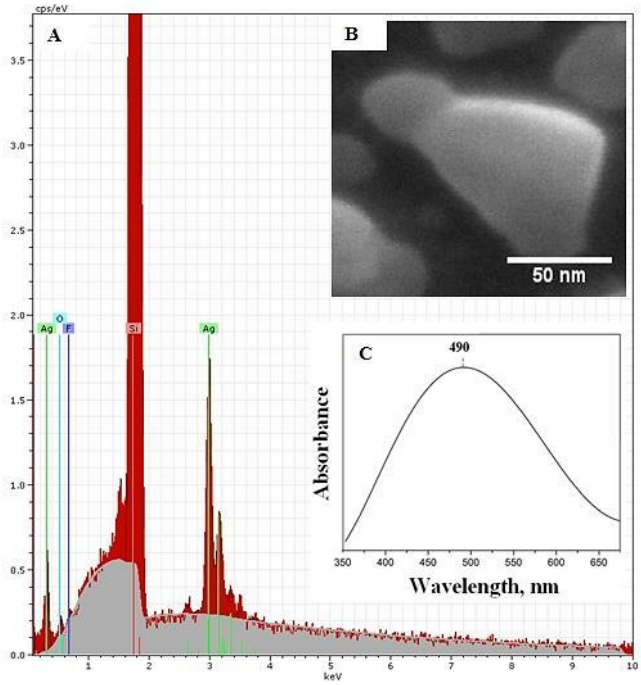

Fig. 3.15. EDX spectrum of silver SERS substrate (A); SEM image of silver nanotriangle (magnification: 400000 ×; high vacuum mode ((30.00 kV)); (B) UV-Vis spectra showing a plasmon at 490 nm that confirms the presence of silver nanoparticles

In order to determine the efficiency of the SERS substrates decorated with triangular silver nanoparticles, the theoretical simulation of the electromagnetic field distribution on such nanostructures has been performed. As seen in Fig. 3.16., the enhancement varies with height and is much greater in the z = 50 nm plane (B and D) than in the z = 0 plane (A and C). The enhancement also depends on polarisation: y-polarised light (C and D) produces a greater enhancement than the x-polarised light (A and B). The theoretical simulation results revealed that the intensity enhancement inside the gap for y-polarised light can result in Raman EF as high as 4×10^5.

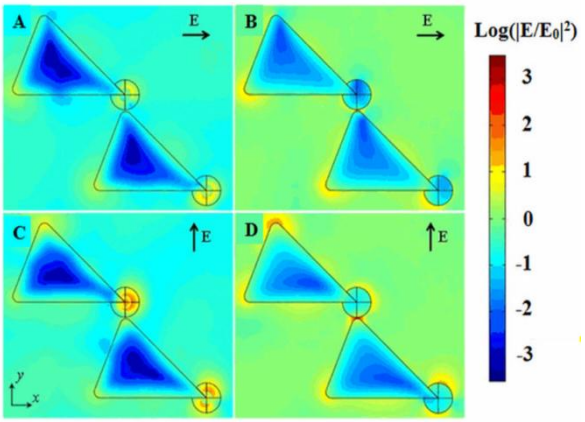

Fig. 3.16. Enhancement of electromagnetic field intensity in a logarithmic scale for a pair of nanotriangles in two cross-sections: (A) and (C) in the z = 0 plane, (B) and (D) in the z = 50 nm plane. The incident light is polarised in the x-axis for (A) and (B) and in the y-axis for (C) and (D)

3.2.2. Gold nanoparticle decorated SERS substrates

The synthesis of gold SERS substrates was based on the direct gold ions reduction on HF etched silicon wafers according to the method presented in Table 2.2. After the HF dissolves the SiO_2 layer, the elemental silicon reduces the metal complex leading to the formation of gold nanoparticles. The deposition of gold nanoparticles on the silicon wafers can be described by the following equations:

$$AuCl_4^-(aq) + 3e^- \longrightarrow Au^0(s) + 4Cl^-(aq)$$
$$2H^+(aq) + 2e^- \longrightarrow H_2\uparrow \quad | \times 1/2$$

(reduction half-reactions)

$$Si^0(s) + 6F^-(aq) \longrightarrow SiF_6^{2-}(aq) + 4e^-$$

(oxidation half-reaction)

$$Si^0(s) + AuCl_4^-(aq) + 6F^-(aq) + H^+(aq) \longrightarrow SiF_6^{2-}(aq) + Au^0(s) + 4Cl^-(aq) + 1/2H_2\uparrow$$

(overall redox reaction)

In order to determine their morphology, the synthesised gold SERS substrates were characterised by AFM. For the evaluation of the nanoparticles shapes repeatability, 10 gold SERS samples were prepared according to the synthesis protocol presented in Section 2.2.2. The AFM images and the height histograms of all 10 samples are presented in Fig. 3.17. As seen in Fig. 3.17, gold nanoparticles of irregular shapes were formed on the silicon wafers. The SD of the nanoparticles height distribution of the SERS substrates was found to be 8 nm. The calculated average height of the nanoparticles of all 10 samples was ~84 nm.

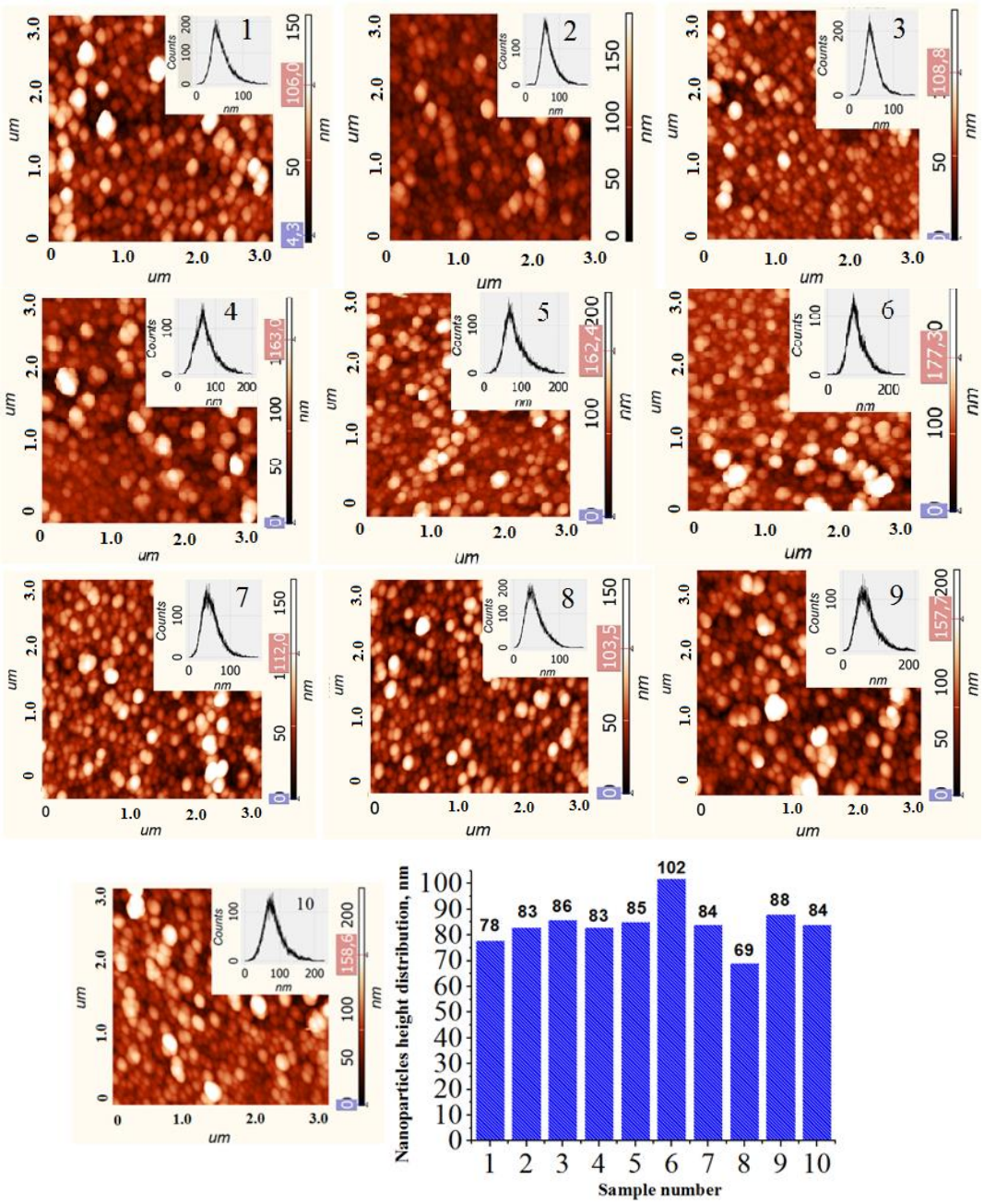

Fig. 3.17 The AFM images of the gold SERS substrates and the height histograms of gold nanoparticles distribution. For the evaluation of nanoparticles shapes and height repeatability, 10 samples (marked 1-10) were characterised in the scanning area of 3 × 3μm

The SEM analysis confirmed the presence of spherical nanoparticles formed on the silicon wafers, while the EDX spectra revealed the presence of the gold element (Fig. 3.18, A and B). The UV-Vis spectra of the synthesised gold SERS substrates showed a plasmon at around 544 nm (C), which is common for gold nanoparticles.

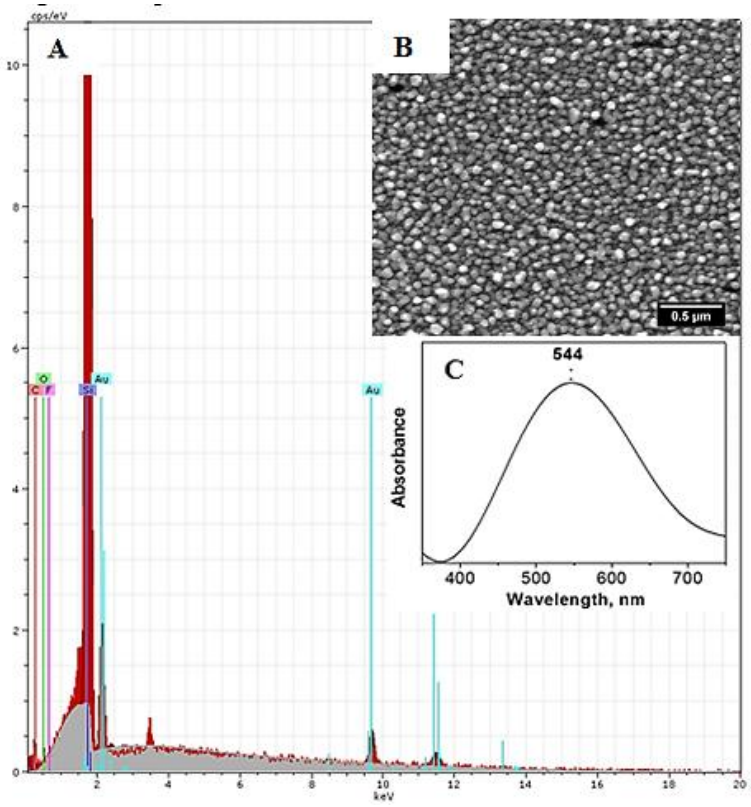

Fig. 3.18. EDX spectrum of gold SERS substrate (A); SEM image of gold SERS substrate (magnification: 30000 ×; high vacuum mode ((30.00 kV)); (B) UV–Vis spectra showing a plasmon at 490 nm that confirms the presence of silver nanoparticles

3.3. The determination of the relative enhancement factor of the silver and gold SERS substrates

In order to determine which type of SERS substrate shows the highest relative Raman signal enhancement, the pentacene monolayer was deposited on gold and silver SERS substrates. The results presented in Fig. 3.19 revealed that the highest relative enhancement of the Raman signal of pentacene was observed on the silver nanotriangle decorated SERS substrate (2.73×10^6). The SERS substrate decorated with irregular-shaped silver nanoparticles demonstrated the relative enhancement of the Raman signal of pentacene analyte of around 1.62×10^4, while the gold SERS substrate was 6.0×10^3.

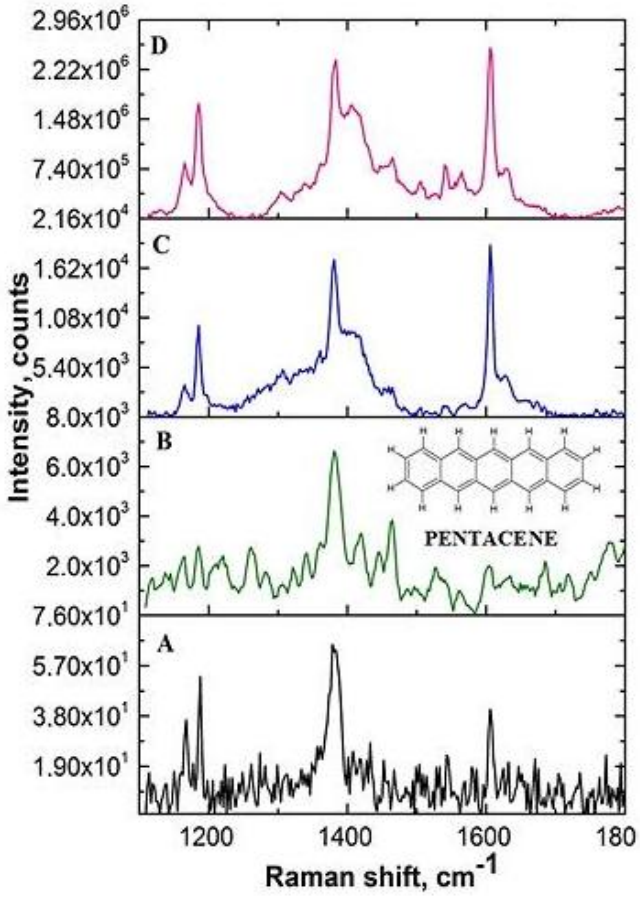

Fig. 3.19. Raman spectra of pentacene obtained on a blank silicon wafer (A); the SERS spectra of pentacene obtained on gold SERS substrate (B); the SERS spectra of pentacene obtained on a SERS substrate decorated with irregular shapes of silver nanoparticles (C); the SERS spectra of pentacene obtained on triangular silver nanoparticle decorated SERS substrate (D). In all the cases the acquisition time for Raman signal collection was 1 s

The synthesised SERS substrates were also tested with another analyte - R6G dye (Fig. 3.20). Again, the highest relative enhancement of the Raman signal of R6G dye was obtained on the silver nanotriangle decorated SERS substrate (2.25×10^7).

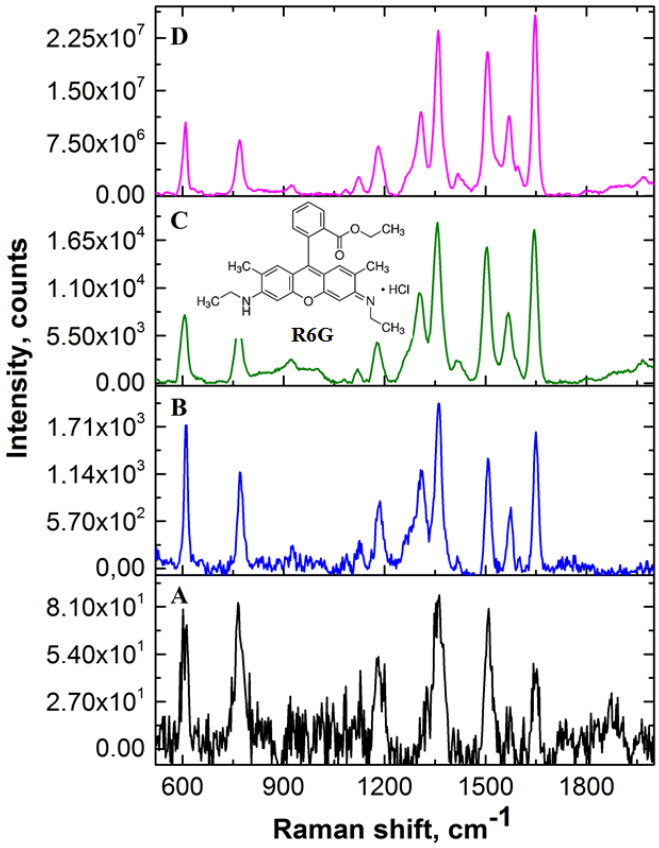

Fig. 3.20. Raman spectra of R6G obtained on a blank silicon wafer (A); the SERS spectra of R6G obtained on gold SERS substrate (B); the SERS spectra of R6G obtained on SERS substrate decorated with irregular shapes of silver nanoparticles (C); the SERS spectra of R6G obtained on triangular silver nanoparticle decorated SERS substrate (D). In all the cases the acquisition time for Raman signal collection was 1 s

Conclusions. In summary, it was determined that the highest relative enhancement of the Raman signal for pentacene and R6G analytes was observed on triangular silver nanoparticle decorated SERS substrates (Table 3.1).

Table 3.1. The relative enhancement of the Raman signal for pentacene and R6G analytes obtained on the different SERS substrates

SERS substrate	Analyte	Relative enhancement of Raman signal
Decorated with irregular shapes of silver nanoparticles	Pentacene	1.62×10^4
	R6G	1.65×10^4
Decorated with spherical gold nanoparticles	Pentacene	6.0×10^3
	R6G	1.7×10^3
Decorated with triangular silver nanoparticles	Pentacene	2.73×10^6
	R6G	2.25×10^7

3.4. Surface enhanced Raman spectroscopy of biomolecules

3.4.1. SERS-based detection of α-synuclein traces in liquid

The increasing amount of production using nanoparticles, such as cosmetics or household chemicals, causes concern on how they influence human health at the cellular level. When cells are exposed to nanoparticles, the cellular proteins tend to form aggregates and finally insoluble fibrils. The fibrillation may have significant effects on the induction / propagation of neurodegenerative diseases such as Parkinson's. α-synuclein is a Parkinson's disease-related protein abundant in the brain. It is not yet clearly understood what triggers the misfolding and aggregation of α-synuclein in the fibre like structures. Therefore, there is a need to develop new methodologies for the detection of its aggregates at low concentrations close to the physiological ones (nM). The SERS technique is an analytical tool finding a great application to study structural changes of biomolecules. Moreover, it provides information about the processes occurring at the bio-nano interface, such as nanoparticle interactions with lipid membranes.

In the living body, proteins are found in the biological fluids, such as blood, plasma, urine etc. Therefore, the aim of the current experiment was to detect and identify α-synuclein traces in water. As SERS substrates, triangular silver nanoparticle decorated silicon wafers were chosen because of their ability to exhibit a high SERS effect (10^7). The results revealed that the synthesised SERS substrates decorated with triangular silver nanoparticles are able to detect α-synuclein of femtomolar concentration in aqueous medium (Fig. 3.21). As seen in Fig.3.21, the spectra of α-synuclein slightly differ comparing them to each other. For example, amide I band observed at 1,652 cm^{-1} is well expressed in the control sample (dry), while in all the test samples this band is not clearly visible. This phenomenon is related to the motion of the protein: given that the SERS measurements are carried out in the solution, the protein does not lie in the plane. For this reason, the protein can easily move in the space. It means that at one point of the sample a particular fragment is located in close proximity (1-2 nm) to the SERS surface, while at another point the same fragment can be away (tens of nanometers) from the SERS surface. In this case, the particular vibrations of such fragment will be absent in the SERS spectra.

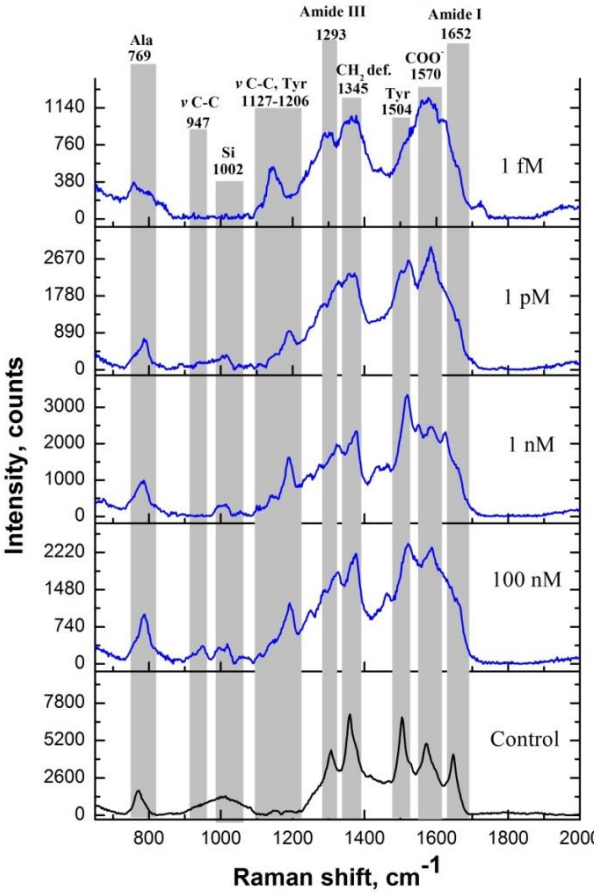

Fig. 3.21. SERS spectra of α-synuclein of different concentrations in aqueous solutions

Conclusion. The experiment has shown that silver SERS substrates decorated with triangular silver nanoparticles are able to detect the traces (1 fM) of α-synuclein in liquid.

3.4.2. The interaction of L-alanyl-L-tryptophan dipeptide with SERS surface

The detection of protein traces is as important as their interaction with the nanoparticles or nanostructured surfaces. The understanding of the protein binding mechanism is important for the development of the fundamental knowledge about their conformational changes induced by nanoparticles or nanostructured surfaces. The analysis of the protein-nanoparticle interaction mechanism is complicated due to the long chains of amino acid residues. Therefore, for the investigation of the interaction mechanism at the bio-nano interface, L-alanyl-L-tryptophan dipeptide was selected as the model biomolecule and triangular silver nanoparticle decorated SERS substrate, as a nanostructured surface. Few scientific publications include the study of the photo dissociation process (Fujihara et al., 2008) or fluorescence decay (Fleming et al., 1978) of L-alanyl-L-tryptophan. However, there are no publications

describing the structural characterisation of this dipeptide by Raman spectroscopy and its possible interaction with nanostructured surfaces. According to the Human Metabolome Database (HMD), L-alanyl-L-tryptophan is an incomplete destruction product of protein digestion or protein catabolism and has not yet been identified in human tissues or biofluids. For this reason it is referred to as an "expected" metabolite. However, peptides are assembled to form large polypeptides and proteins. Therefore, the investigation of short segments is a significant step towards the understanding of proteomics.

Proteins adsorption on nanostructured surfaces is mediated by several forces such as hydrogen bonds, solvation, Wan der Waals or electrostatic interaction between protein molecules and nanoparticles. These interactions may be strongly influenced by the morphology (Rechendorff et al., 2006; Scopelliti et al., 2010) and nature of nanostructured surfaces, the conditions of their preparation as well as the concentration and type of protein / peptide and pH value. It is important to mention that no acidification or alkalisation of dipeptide solution has been carried out in the current experiment. The change of pH by adding salts or acid results in the change of hydrogen ion concentrations in the solution and affects the hydrogen bonding within the dipeptide. Therefore, the structure of the dipeptide can be changed as well as its interaction with the nanostructured silver surface.

As seen in Fig. 3.22, the distances between silver triangular nanoparticles vary from ~120 to ~200 nm, this led to raise a hypothesis that dipeptide adsorption can take place both on the surface of nanoparticles and in the gaps between them.

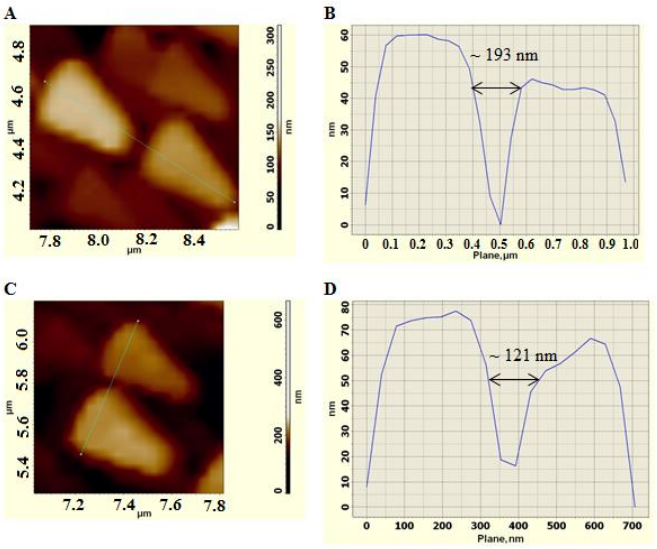

Fig. 3.22. AFM images of the silver nanotriangle decorated SERS substrate: (A) height image of silver nanotriangles measured at the first randomly selected point of the sample and the cross section between separate silver nanotriangles (B); (C) height image of silver nanotriangles measured at the second randomly selected point of the sample and the cross section between separate silver nanotriangles (D)

Fig. 3.23 shows Raman (control) and SERS spectra of the L-alanyl-L-tryptophan dipeptide recorded at 5 different randomly selected points of the sample. The proposed vibrational assignments of L-alanyl-L-tryptophan are represented in Table 3.2.

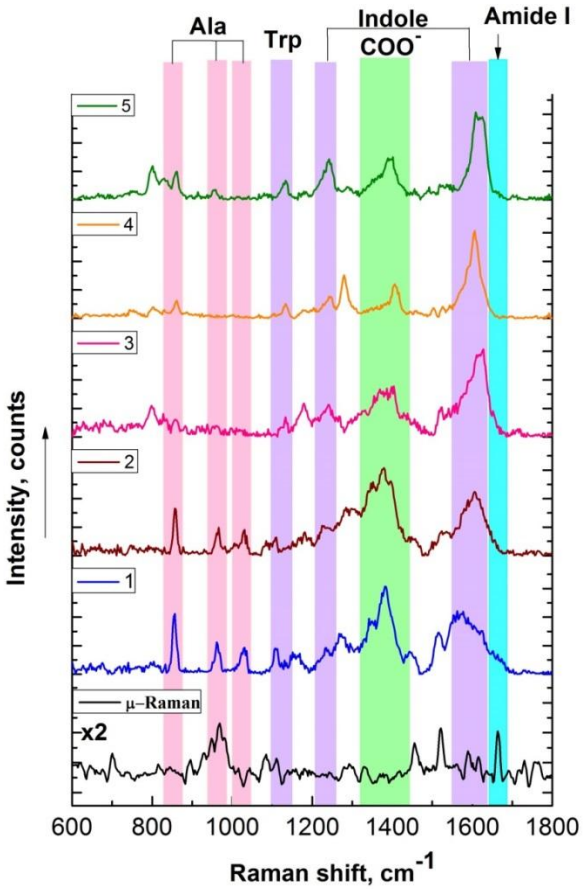

Fig. 3.23. Raman and SERS spectra of L-alanyl-L-tryptophan dipeptide recorded in liquid at randomly selected points of the sample. The acquisition time for the collection of Raman signal: 1 s

As seen in Fig. 3.23 all SERS spectra clearly demonstrate the difference in peak positions and intensities determined by the dipeptide orientation on the rough silver surface. Amide bands associated with vibrational modes of the peptide bond are the marker bands in the Raman and SERS spectra representing the secondary structure of peptides or proteins. However, the presence or absence of the amide I region at 1,640-1,678 cm^{-1} in SERS spectra also suggest the possible orientation of biomolecules on the nanostructured surfaces. In micro-Raman spectra, the amide I band is represented by a low intensity band at 1,666 cm^{-1}, whereas all SERS spectra show the silence of these vibrations. This phenomenon has been analysed before by other researchers both in SERS and TERS spectra (Kurouski et al., 2013; Blum et al.,

2012) of peptides and proteins. The amide I band is due to C = O stretching and N-H in plane bending modes and should be apparent in SERS spectra even if the peptide underwent conformational changes after adsorption on the rough silver surface. Considering this, the structural changes of the dipeptide should not determine the absence of the amide I band in SERS spectra. In the case of L-alanyl-L-tryptophan, the absence of the amide I band in SERS spectra can be determined by the large side chain of tryptophan that shields the peptide bond from the SERS surface (Kurouski et al., 2013). Other important regions in SERS spectra suggesting the possible arrangement of dipeptide molecules are located at 1,381-1,396 cm^{-1} and 1,570-1,608 cm^{-1} that correspond to -COO^- and indole ring vibrations respectively. According to the different intensities of these vibrations in all the SERS spectra, two possible options for L-alanyl-L-tryptophan orientation on the substrate surface were proposed (Fig. 3.24).

Table 3.2. Band assignments for Raman and SERS spectra of L-alanyl-L-tryptophan

Proposed assignment	Proposed residue	Peak position, cm^{-1}		Reference
		Raman	SERS	
C–C str.	alanine	702	–	–
-	tryptophan	–	798-805	Zhu et al. (2011)
C–C str.	alanine	–	855	Stewart and Fredericks (1999)
C–C str.	alanine	893	–	Stewart and Fredericks (1999)
CH_3 def.	alanine	967	962	Ushakumary et al. (2011)
C–N str.	alanine	–	1,030	Stewart and Fredericks (1999)
C–N str.	alanine	1,084	–	Stewart and Fredericks (1999)
C–N str., C-O str.	tryptophan	1,112	1,130-1,134	Aliaga et al. (2009)
C–H def., indole	tryptophan	–	1,232-1,241	Aliaga et al. (2009)
CH_2 wag.	tryptophan	1,283	1,275-1,282	Stewart and Fredericks (1999)
COO^- str.	tryptophan	–	1,378-1,381	Stewart and Fredericks (1999)
CH_2 asym.	alanine	1,459	1,451	Blum et al. (2012)
C=C, indole	tryptophan	–	1,570-1,620	Perna et al. (2013)
amide I	backbone	1,666	–	Stewart and Fredericks (1999)

*Abbreviations: str. = stretching, def. = deformation, wag. = wagging.

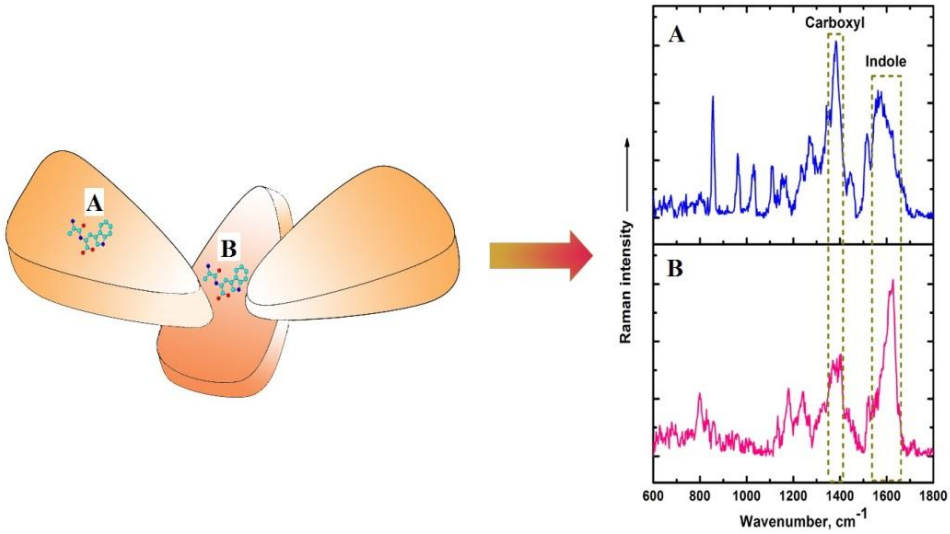

Fig. 3.24. The proposed L-alanyl-L-tryptophan dipeptide orientation on a silver SERS substrate: (A) adsorbance takes place on the surface of nanoparticles; (B) adsorbance takes place in between the nanoparticles

SERS spectra recorded at the first two points (Fig. 3.23, spectra 1 and 2) demonstrate the most intensive bands of carboxyl at 1,381 cm^{-1} and 1,378 cm^{-1} and suggest the close proximity of these groups to the SERS surface. In this case, dipeptide molecules are probably located on the surface of silver nanoparticles as shown in Fig. 3.24 (A). In SERS spectra obtained at the other three points (Fig. 3.23, spectra 3-5) the most enhanced bands appear at 1,620 cm^{-1}, 1,605 cm^{-1} and 1,570 cm^{-1} that correspond to the C = C aromatic ring vibration of indole (Perna et al., 2013). Increased intensity of aromatic ring vibrations suggests that L-alanyl-L-tryptophan is supposedly located in between the nanoparticles as shown in Fig.3.24 (B). Given that the dipeptide size is ~1 nm (Fig. 3.25) it can easily penetrate through the nanoscale gaps between silver nanoparticles. Therefore, it is very likely that the aromatic part of the dipeptide is located between silver nanotriangles acting as plasmonic dipole antennas and resulting in the enhanced Raman signal of indole ring vibrations.

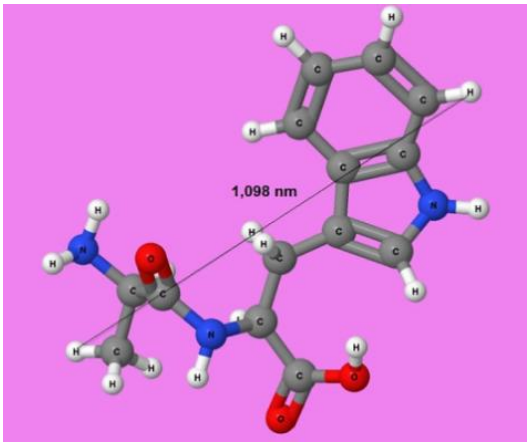

Fig. 3.25. The size of L-alanyl-L-tryptophan dipeptide measured using Jmol software

The amide III region is located at 1,230-1,300 cm^{-1} and arises from a combination of C-N stretching and N-H bending vibrations (Kurouski et al., 2013). However, the amide III bands overlap with C-H bending (Aliaga et al., 2009) and CH_2 wagging (Blum et al., 2012) vibrations. For this reason, the characterisation of peptides/proteins secondary structure based on the amide III region becomes complicated. In Raman spectra, no significant peaks in the amide III region are observed whereas in all SERS spectra low intensity shoulders appear at 1,232-1,241 cm^{-1} that are assigned for C-H vibrations of the indole fragment. This band is mostly expressed in the 3-5 SERS spectra and supports the hypothesis that an aromatic ring is situated in between the nanoparticles.

In SERS spectra, a marker band representing alanine residue is located at 855 cm^{-1} (Stewart, Fredericks, 1999). Other characteristic peaks of alanine in SERS spectra appear at ~1,030 cm^{-1} and 1,450 cm^{-1} and correspond to C-N stretching (Stewart and Fredericks (1999) and CH_2 deformation (Blum et al., 2012) modes respectively. A band at 967 cm^{-1} represents the CH_3 deformation vibrations (Ushakumary et al., 2011) that are visible both in Raman and SERS spectra. Alanine vibration modes are mostly enhanced in 1 and 2 spectra. Therefore, alanine is supposed to be very close (1-2 nm) to the nanostructured silver surface.

Conclusions. Raman and SERS spectra of the L-alanyl-L-tryptophan dipeptide were recorded for the first time. The analysis of SERS spectra of L-alanyl-L-tryptophan revealed that the dipeptide interacts with the nanostructured silver surface through carboxyl terminus. It was found that the most enhanced bands in SERS spectra correspond to carboxyl and indole ring vibrations. These results allowed it to be concluded that the SERS spectra of the dipeptide vary depending on which place of the SERS substrate (on the surface or in between the nanoparticles) it is adsorbed. The absence of the amide I bands in SERS spectra recorded at different points of the sample suggested that the peptide bond of L-alanyl-L-tryptophan has no direct contact with silver nanoparticles when the measurements are carried out in aqueous medium.

3.4.3. SERS-based detection of lipid membrane deposited on silver SERS substrate

Membranes are essential components of any living cell. The synthetic lipid membranes fabricated in the laboratory are the simplified planar models mimicking the natural ones. As it was shown before, Raman spectroscopy has been applied for the investigation of bulk lipids (Baeten et al., 2005; Sweetenham and Notingher, 2010). However, the Raman signal even of bulk lipids was found to be intrinsically weak and that complicates the analysis of the membranes at the nanoscale. SERS, as a non-destructive method, allows the investigation of the lipid membranes at a nano level and provides a better understanding of the influence of drugs, bacteria, nanoparticles etc., for membrane structures. Moreover, most of the neurodegenerative diseases, such as Alzheimer's, cystic fibrosis, muscular dystrophy or Parkinson's, are believed to be the result of cell membrane damage (Taylor et al., 2014). Therefore, the application of the SERS technique opens up the possibility to investigate such damage with a high sensitivity, which is essential for the analysis of the causes as well as for the early diagnostics of the above-mentioned diseases.

The aim of the current experiment was to apply triangular silver nanoparticle decorated SERS substrate for the detection of a synthetic lipid membrane. Therefore, the lipid membrane was deposited on the microscopic glass (control sample) and the silver SERS substrate (test sample) respectively. As seen in Fig. 3.26 (A), no peaks common for the lipid membrane deposited on blank microscopic glass were detected, while they were clearly seen in the SERS spectra (Fig. 3.26, B). The assignments of the bands in the SERS spectra characteristic for lipid membrane are listed in Table 3.3.

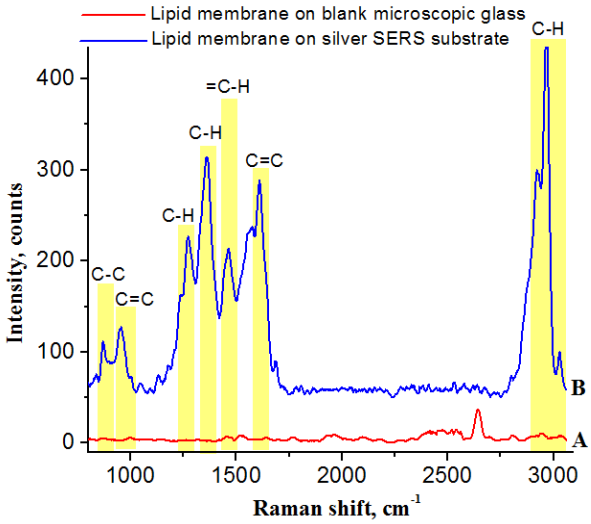

Fig. 3.26. Raman and SERS spectra of lipid membrane deposited on: (A) blank microscopic glass; (B) triangular silver nanoparticle decorated SERS substrate.
The acquisition time was 1 s

Table 3.3. Band assignments for Raman bands of phospholipids

Peak position in SERS spectra, cm^{-1}	Proposed assignment	Reference
800-920	C-C str.	Gunstone, Harwood and Padley (1994)
945-970	C=C in plane bend.	
1,060-1,136	C-C stretch.	
1,250-1,280	=C-H bend.	
1,295-1,305	C-H twist. def.	
1,400-1,500	C-H sciss. def.	
1,640-1,680	C=C stretch.	
1,730-1,750	C=O stretch.	
2700-3015	C-H stretch.	

*Abbreviations: bend. = bending, def. = deformation str. = stretching, sciss. = scissoring, twist. = twisting

Conclusion. The experiment has shown that the vibrations of lipid membrane deposited on blank microscopic glass were not detected in the Raman spectra. Meanwhile, the vibrations characteristic for a lipid membrane were clearly expressed in the SERS spectra. The results of the Raman and SERS measurements allowed it to be concluded that the SERS substrates decorated with triangular silver nanoparticles enhanced the spectra of lipid membrane thus opening the possibility for further structural analysis.

3.5. The detection of benzylpenicillin traces in cow's milk

Food quality and its safety is one of the most important issues of the modern food industry. The primary factor determining the quality of food products is raw materials. For example, milk is the main raw material for the production of cheese, yoghurt, butter etc. Moreover, milk as a nutritious drink, is used by most adults and children every day. However, is it really pure and safe?

Kang'ethe and Lang'a (2009) published an article in which they presented the shocking results of a milk investigation. Milk samples were obtained from urban centres in Kenya. Researchers found that 72% (315/439) of the milk from dairy farmers, 84% (71/85) from large and medium scale farmers and 99% (88/89) of the pasteurised marketed milk were positive for aflatoxin! Aflatoxin is a mycotoxin that is highly toxic and included in the list of carcinogenic substances. The reason aflatoxin was present in milk was the contaminated cow feed.

Other substances that can be found in milk and cause concern for human health is antibiotics. Antibiotics are used in most farms to treat the cows suffering from infections, such as mastitis. Milk obtained from the cows that were treated with antibiotics may have the residues of the antibiotics. Several types of the veterinary antibiotics are prohibited because of the side effects in humans. More recently, the residues of antibiotics were detected not only in milk but also in meat (Kennedy et al., 1998). Myllyniemi et al. (2000) analysed muscle and kidney taken from animals treated with antibiotics. They found that 68 out of 89 samples were positive for penicillin and enrofloxacin residues.

Andreou et al. (2015) successfully applied the SERS technique for the detection of ampicillin in milk. In their research, they proposed microfluidic-based SERS methodology and were able to detect ampicillin in low concentrations in milk (30 nM). In order to avoid the accumulation of lipid aggregates that impede the flow of the fluid, they removed the lipids from the milk. The experiment revealed that SERS is a sensitive technique for the detection and identification of ampicillin residues in the complex liquids such as milk.

Benzylpenicillin (known as penicillin G) is also a common antibiotic used in veterinary treatment. Therefore, the aim of the current experiment was to detect and identify the residues of benzylpenicillin (BP) in cow's milk obtained from the supermarket. In order to determine whether the vibrations of BP of trace concentrations (pM) are well expressed in the SERS spectra, the aqueous solutions of 5 pM, 2.5 pM, 1 pM, 0.5 pM and 0.25 pM of the antibiotic were prepared and SERS spectra were recorded. As seen in Fig. 3.27, the peaks common for BP (Table 3.4) are well seen even at the concentration of 0.25 pM. Therefore, the SERS measurements confirmed that selected SERS substrate is able to detect BP traces in water.

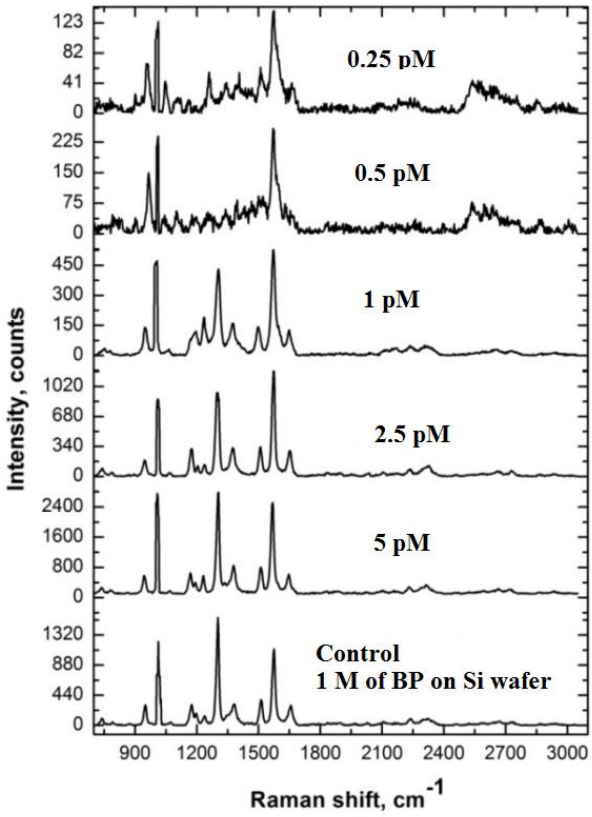

Fig. 3.27. Raman (control) and SERS spectra of BP. The acquisition time for Raman and SERS spectra collection was 1 s

Table 3.4. The assignments of BP vibrations observed in Raman and SERS spectra

Peak position, cm^{-1}	Proposed assignment	Reference
750	C-H benzene out of plane bend.	Reipa, Horvath, 1992
778	CH_3 wag.	
948	C-C stretch.	
1,004	Benzene ring breath.	
1,160	CCH in plane bend., benzene	
1,204	C–N stretch.	
1,237	C-C stretch., benzene	
1,294	Amide III	
1,383	COO^- symmetric stretch.	
1,505	C-C in plane stretch.	
1,584	C-C stretch., benzene	
1,654	Amide I, Benzene ring	

*Abbreviations: bend. = bending, breath. = breathing, stretch. = stretching, wag. = wagging.

The next step was to record the SERS spectra of milk. Two kinds of milk samples were selected:

- untreated raw milk of healthy cows obtained from an ecological farm (reference);
- pasteurised milk obtained from a supermarket.

The SERS measurements revealed that the SERS spectra of the milk obtained from the supermarket had strong fluorescence background (Fig. 3.28, A), whereas SERS spectra of the farm's milk did not (Fig. 3.28 B).

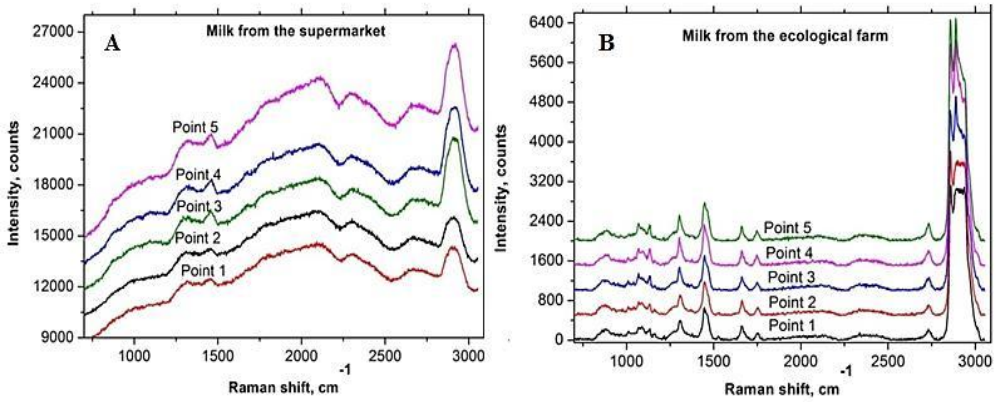

Fig. 3.28. The SERS spectra of (A) milk obtained from the supermarket and (B) obtained from the farmer recorded at five different points of the samples. The acquisition time for Raman and SERS spectra collection was 1 s

The fluorescence background in the Raman spectra of milk was also observed by other researchers (El-Abassy et al., 2012). However, what is the reason determining the presence of this phenomenon? In the milk industry, the raw cow's milk is processed before it is consumed. For example, commercial milk is

pasteurised at ultra-high temperatures in order to kill bacteria. However, this process induces the isomerisation and degradation reactions of lactose leading to the formation of fluorescent compounds in the milk (Morales, Romero and Jiménez-Pérez, 1996; Berg, 1993). Therefore, the presence of these compounds in commercial milk can be one of the reasons for the observation of the fluorescence background in SERS spectra. Additionally, the food additives such as preservatives or whitening agents can also give rise to the fluorescence background in Raman or SERS spectra. However, in order to determine the real reason for the presence of this phenomenon, detailed experiments and analyses must be carried out. Though, it is not one of the tasks of the current experiment.

In order to identify the peaks observed in milk SERS spectra, the fluorescent backgrounds were removed by CrystalSleuth software. As seen in Fig 3.29, the peaks observed at 878 cm^{-1} were assigned to tryptophan vibrations, while the bands at 1,072 cm^{-1}, 1,134 cm^{-1}, 1,450 cm^{-1}, and 2,858-2,911 cm^{-1} were characteristic for C-S, C-C, C-H and lipids respectively (Li-Chan, 2007). The bands representing the vibrations of peptide bonds were found to be located at 1,297 cm^{-1} (amide III) and 1,662 cm^{-1} (amide I).

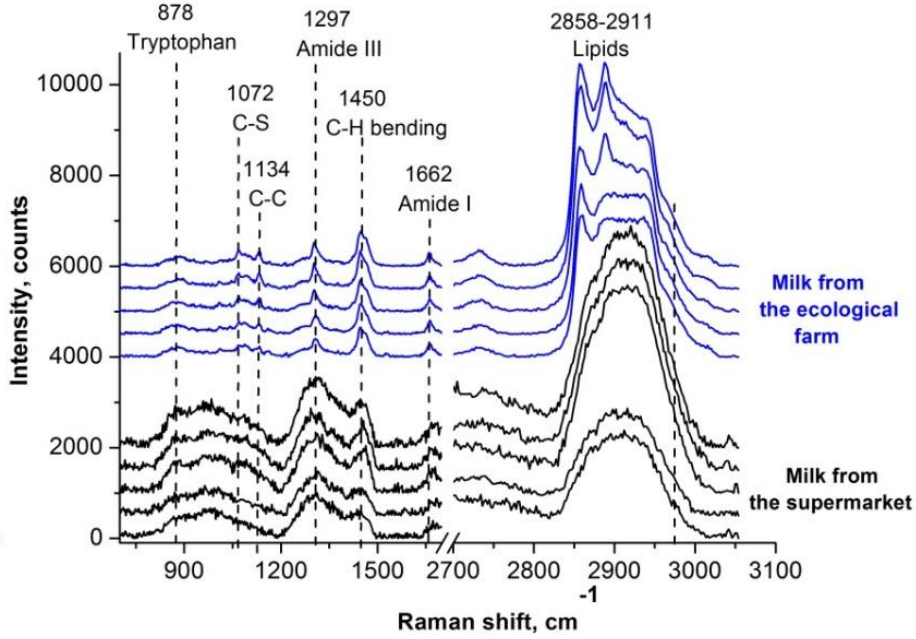

Fig. 3.29 The SERS spectra of milk with marked band positions and assignments. The backgrounds of the SERS spectra were removed by Crystal Sleuth software

The next step was to detect and identify the peaks of BP in milk. According to the milk obtained from the ecological farm in which the healthy cows are on natural feed, this kind of milk was selected as the reference. Milk samples were spiked with aqueous solutions of benzylpenicillin with trace concentrations of 5 pM, 2.5 pM, 1 pM, 0.5 pM and 0.25 pM. As seen in Fig. 3.30, four peaks, characteristic of

benzylpenicillin (at 778 cm^{-1}, 1,004 cm^{-1}, 1,204 cm^{-1} and 1,584 cm^{-1}), were detected in the spiked milk samples and not detected in the reference (control) milk sample. The marker band of BP showing its presence in milk was found to be located at 1,004 cm^{-1} which represents the vibrations of the benzene ring in BP molecules.

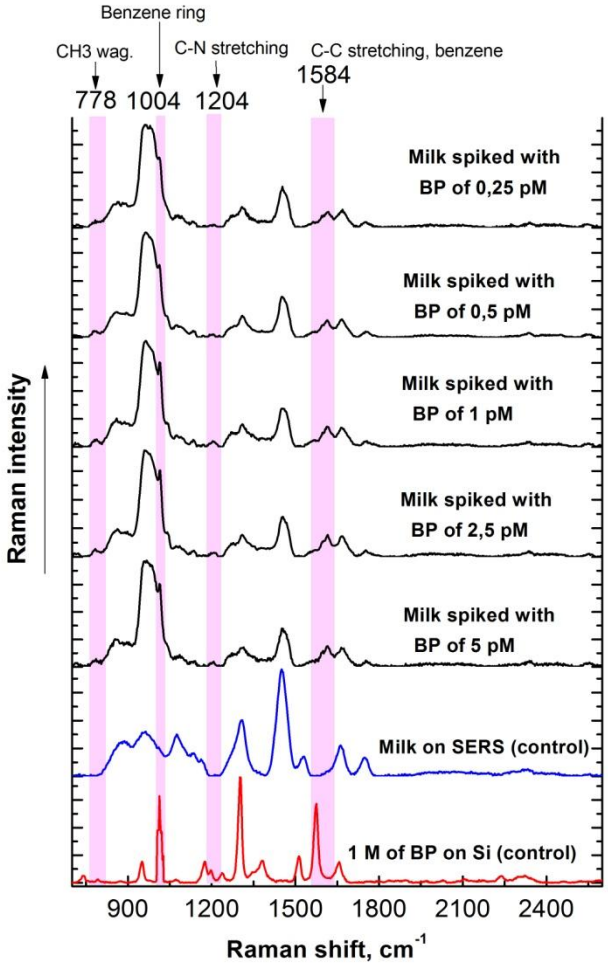

Fig. 3.30. Raman and SERS spectra of BP and milk spiked with trace concentrations of aqueous BP solutions respectively. The acquisition time for Raman and SERS spectra collection was 1 s

The final step of the experiment was to identify whether there are BP residues in the commercial milk. As shown in Fig 3.31, no BP peaks were detected in the test milk samples. However, the amide I and amide III band positions of BP were close to the amide I and amide III positions of milk. Accordingly, the peptide bond is common both for BP and milk, these bands were not the marker bands for the evaluation of BP traces in the milk.

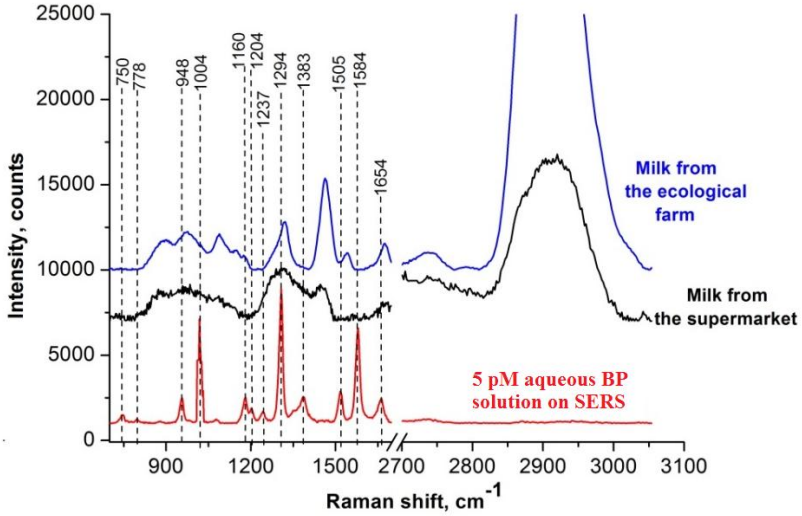

Fig. 3.31. The detection of BP traces in milk: SERS spectra of BP, commercial milk and milk obtained from the ecological farm. The acquisition time for Raman and SERS spectra collection was 1 s

Conclusions. In summary, the experiment was designed for the detection of BP traces in commercial milk obtained from the supermarket. As a reference, the untreated raw milk obtained from the ecological farm was selected. It was found that no traces of BP are present in the commercial milk. However, the strong fluorescence background was observed during the SERS measurements of the commercial milk. This phenomenon can be related to the degradation products of lactose occurring during the processing procedures of the milk, such as pasteurisation. However, the confirmation of this hypothesis requires detailed analysis and additional tests, which were not one of the tasks of the current experiment. The experiment confirmed that the silver SERS substrates decorated with triangular silver nanoparticles are able to detect trace concentration of BP (0.25 pM) in water as well as in milk.

3.6. Localised plasmon stimulated nanochemistry of graphene oxide on a SERS substrate

Graphene oxide (GO) is a carbon-based nanomaterial that can also be described as a monomolecular layer of graphite containing oxygen-rich species on its basal planes and edges. The presence of various functional groups (-hydroxyl, -epoxy, -carboxyl) makes GO attractive for the chemical functionalisation and further application in biology (Mei et al., 2015) optics (Loh et al., 2010) and medicine (Liu, Cui and Losic, 2013). However, contrary to graphene, the use of GO in the field of electronics, is restricted due to the disruption of its sp^2 bonding networks. In order to restore sp^2 structure and improve its electrical conductivity properties, the deoxygenation is required, which can be realised by the thermal (Song et al., 2014), electrochemical (Zhang et al., 2012) or chemical (Chua, Pumera, 2013) reduction of GO. Usually, these methods demand high temperatures and hazardous chemical

agents, such as hydrazine or sodium borohydride. Therefore, alternative, less time-consuming and cost-effective methods are desirable for the reduction, or even for the conversion of non-conductive GO to a material(s) with improved electrical properties. Recently, several groups have demonstrated that GO can be reduced by photoirradiation treatment, such as photocatalytic reduction under UV irradiation (Ding et al., 2011) or photothermal reduction upon exposure to a pulsed Xenon flash (Cote, Cruz-Silva and Huang, 2009). The advantage of these methods is that photoirradiation processes do not require the use of chemicals or long durations for the reaction to be completed. However, the energy generated by laser power is too low to disrupt the GO structure and produce, for example, polyaromatic hydrocarbons (PAHs), exhibiting semi-conducting behaviour (Feng, Pisula and Müllen, 2009). However, the local modification of GO deposited on the surface still remains a challenge.

In the current experiment, a new approach for the reduction of GO, deposited on a rough silver surface, and its further destruction to PAH-like compounds (similar to PAHs but with additional -OH or -COOH groups) driven by LSP is proposed. LSP, as collective oscillations of free electrons, can be generated in the nanometre–sized gaps between separate nanoparticles of noble metals and result in strong localised electric fields inside the gap. Three-dimensional (3D) nano-structures produce stronger LSP compared to two-dimensional ones. Therefore, chemical reactions can be facilitated and improved by the use of LSP. SERS and TERS techniques are the promising ways enabling the local modification of molecular features, thus opening new routes for the development of molecular semiconductors.

The aim of the current experiment was to perform the reduction and destruction of GO leading to the synthesis of PAHs on a SERS substrate. As a SERS substrate, the silver nanotriangle decorated silicon wafer was selected. As it has been shown in the previous experiments (Sections 3.3, 3.4.1 and 3.5), the silver SERS substrates decorated with triangular silver nanoparticles are able to detect trace concentrations of the substances and exhibit a relative enhancement of the Raman signal of 10^7. Therefore, it was hypothesised that GO, entrapped inside the nano-gaps acting as dipole-type nanoantennas and producing an electromagnetic field of high intensity, could be reduced and moreover, decomposed to PAH-like compounds. For this purpose, GO was deposited on the SERS substrate from an aqueous medium and fifty Raman spectra have been collected every second at the same point of the sample. As seen in Fig. 3.32 (A), the GO spectra changed completely after 12 seconds of irradiation indicating the essential changes of GO structure, while these changes were not observed when GO was deposited on the blank silicon wafer (Fig. 3.32, B and C).

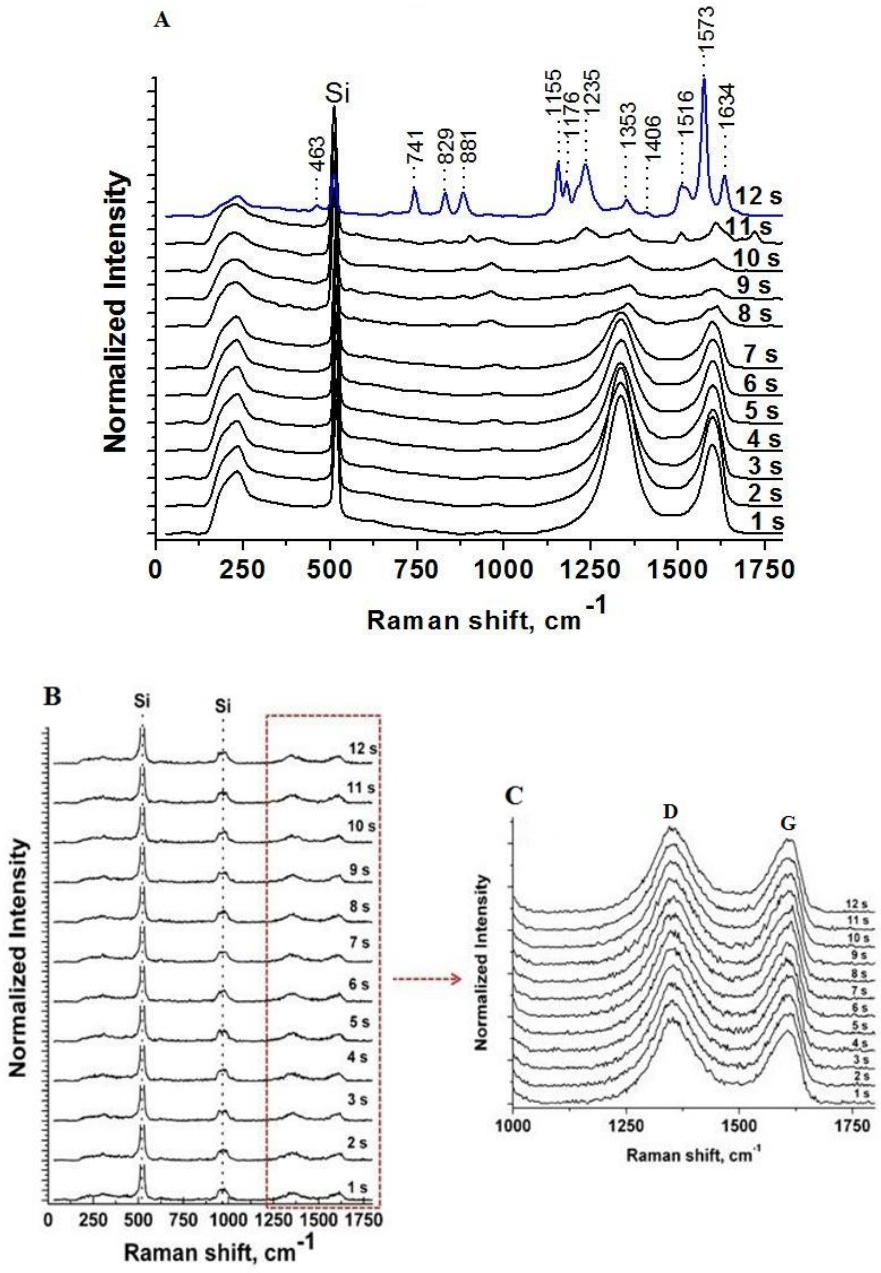

Fig. 3.32. (A) Raman spectra of GO deposited on a SERS substrate showing the changes of GO structure during irradiation with the laser; (B) Raman spectra of GO deposited on a blank Si wafer showing no changes of the GO spectra during irradiation with the laser and indicating that the reduction of GO and the synthesis of PAHs-like compounds do not take place; (C) the enlarged Raman spectra of GO deposited on a blank Si wafer

The mechanism via which the structure of GO changes during the irradiation involves two possible steps: first, the reduction and then the destruction of GO. An important agent playing a key role in these processes is water. According to Pei and Cheng (2012), the partial removal of GO functional groups could be influenced by the superheated supercritical (SC) water occurring in a sealed system, where the solvent (water) is brought to a temperature above its boiling point by the increase of pressure resulting from heating. Similar conditions could be obtained on a SERS substrate in cases when water molecules are located inside the nano-gaps and covered by GO flakes. Another interesting mechanism for the reduction and breakage of GO was suggested by Concalves et al. (2014) who proposed that under the ultrasound treatment, the thermal reduction of GO is mainly governed through the formation of radicals by the decomposition of water. In the case of the current experiment, the high energy induced by LSP promotes the decomposition of water molecules to hydroxyl radicals which have a great potential to reduce oxygen-rich species of GO (Concalves et al., 2014). In order to confirm the raised hypothesis, there was a need to confirm the presence of water, possibly remaining inside the nano-gaps after the deposition of GO from aqueous medium, in the reaction system. As seen in Fig. 3.33 (A), two peaks were observed in Raman spectra at ≈3,362 cm^{-1} and ≈3,456 cm^{-1} that are assigned to hydroxyl stretching and hydrogen bond vibrations of water molecules, respectively. Therefore, the appearance of these peaks in SERS spectra supports the idea that hydroxyl radicals induce the reduction of GO. The presence of water was also detected on the control sample where GO was deposited on the blank Si wafer (Fig. 3.33, B). The reduction process of GO can manifest itself in Raman spectra by the changes in relative intensity of its D and G peaks (Sobon et al., 2012). A progressive decrease of ID/IG ratio shown in Fig. 3.34 (A) suggests the GO conversion to reduced GO (rGO), while these observations are absent in the control sample (Fig. 3.34 B). Obvious changes of ID/IG ratio are also observed in Raman spectra until the 10^{th} second of irradiation.

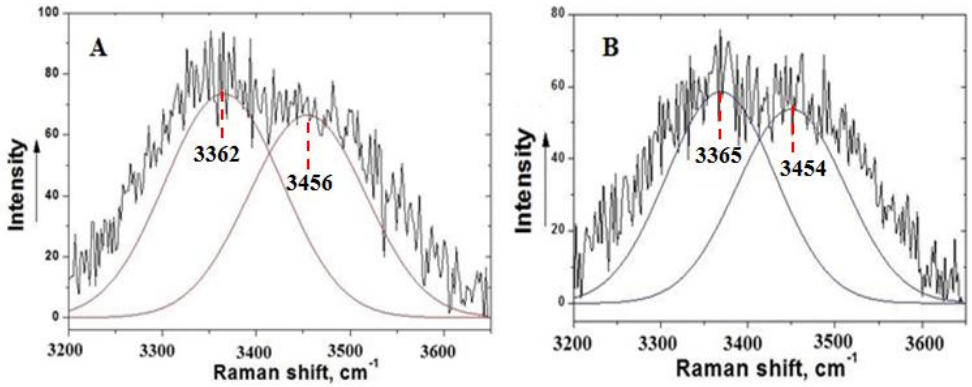

Fig. 3.33. Raman spectra of water obtained on the same spot of the sample where the irradiation of GO has been carried out: (A) on a SERS substrate (B) on a blank Si wafer

Afterwards, hydroxyl radicals as a part of the photocatalytic reaction continue attacking the already formed rGO which finally undergo the fragmentation to the

PAH-like compounds (Fig. 3.32, A (12 s)). These compounds were found to be the final products of the reaction because no further changes have been observed after the 12 seconds of irradiation. The schematic illustration of the reduction and decomposition processes of GO is represented in Fig. 3.35.

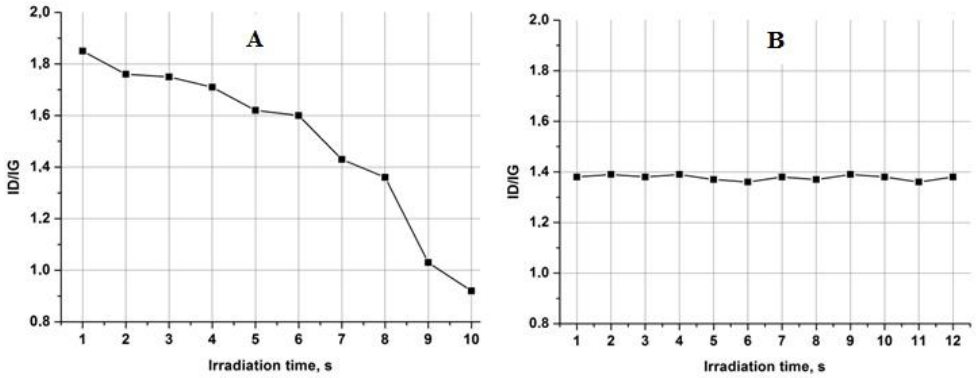

Fig.3.34. Graphical illustration of GO ID/IG ratio evolution on a SERS substrate (A) and on the blank Si wafer (B) indicating and not indicating the changes in GO structure during the laser irradiation respectively

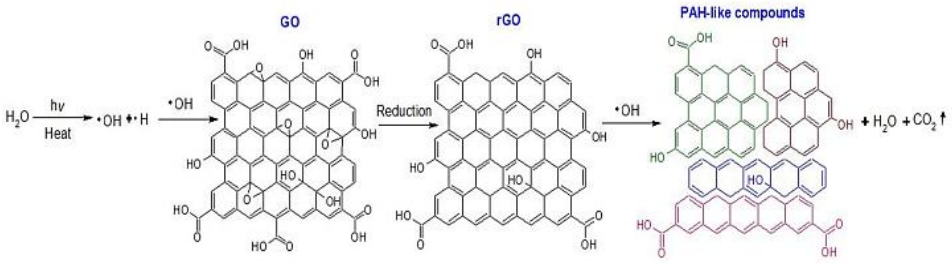

Fig. 3.35. The mechanism of GO reduction and its further decomposition to PAH-like compounds

The reduction and decomposition of GO were carried out in the area with a diameter of about 500 nm in the plane where the laser beam is focused. However, the destruction of GO and the synthesis of PAHs were observed only in the "hot spots" where the distance between separate silver nanoparticles was < 10 nm (Fig. 3.36).

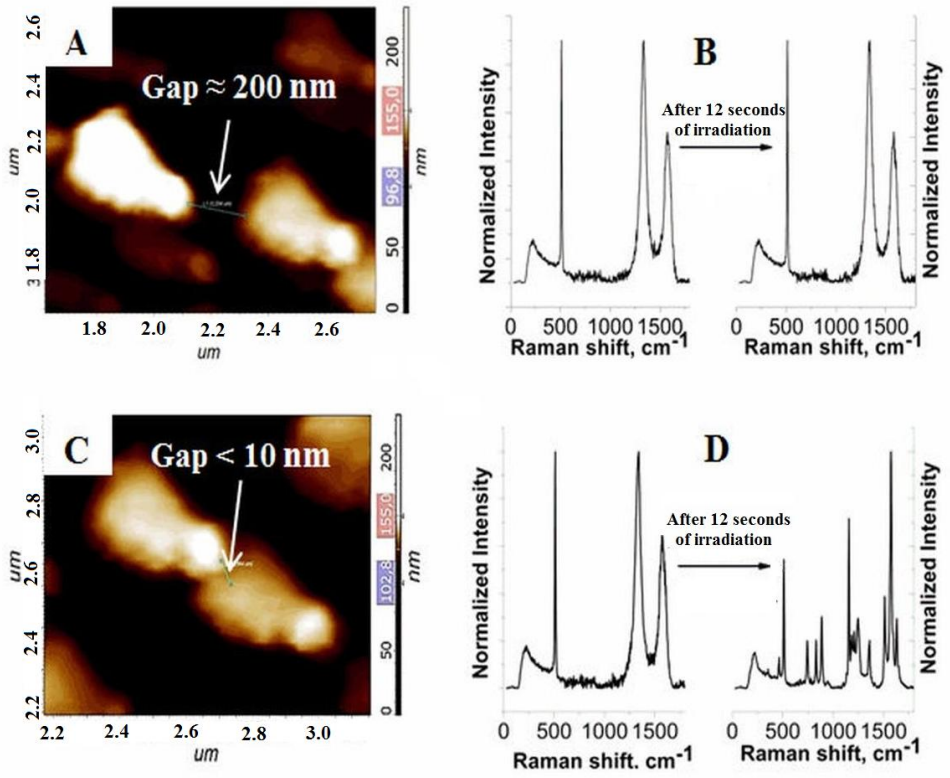

Fig. 3.36. Raman spectra of GO recorded through real-time in the different sizes of nanogaps between triangular silver nanoparticles: (A) AFM image of two silver nanotriangles with a gap of ≈200 nm and Raman spectra of GO showing no spectral changes after 12 seconds of irradiation with a laser in this nanogap (B); AFM image of two silver nanotriangles with a gap of < 10 nm (C) and Raman spectra of GO showing the presence of new compounds formed after 12 seconds of irradiation with a laser in this nanogap (D)

The clear identification of individual compounds was complicated due to the limits of the instruments and the methods allowing measurements to be made at the same point of the sample. However, the vibrations common for PAHs (Alajtal et al., 2010; Leyton et al., 2005; Adil and Guha, 2012; Zhou et al., 2012; Pouchaname et al., 2012; Colangeli et al., 1992) were assigned and are presented in Table 3.5.

Table 3.5. Band assignments for Raman spectra of PAH-like compounds

Peak position, cm^{-1}	Proposed assignment	Proposed molecule
463	Out of plane C-H bend.	Ethylnaphtalene
741	Out of plane C-H bend.	Pentacene
829	C-C stretch.	Phenanthrene
881	Out of plane C-H bend.	Chrysene
1,155	C-H in plane bend.	Pentacene
1,176	C-H in plane bend.	Pentacene, benzene
1,235	C-H in plane def.	Pyrene
1,353	C-C stretch. H-C-C bend.	Phenanthrene, coronene
1,406	C-C aromatic stretch.	Pentacene, phenanthrene
1,516	COO^- stretch.	–
1,573	C-C aromatic stretch.	Chrysene, phenanthrene, perylene
1,634	C=C stretch.	Ethylnaphtalene, benzo[α]pyrene

*Abbreviations: bend. = bending, def. = deformation, stretch. = stretching.

In order to elucidate the changes of electrical properties of GO after its decomposition, the measurements of the local I-V characteristics in the area of the laser spot were performed. The integrated Raman and AFM platform allowed the Raman laser spot and AFM cantilevers tip position to be controlled. As shown in Fig. 3.37 (A), experimentally obtained I-V characteristics of the blank SERS substrate coated with Ag nanoparticles, demonstrate a strong linear behaviour with applied voltage indicating an ohmic conductivity, common for noble metals. Fig. 3.37 (B) shows the I-V characteristics of GO, deposited on a SERS substrate before the irradiation. As it is seen, the conductivity is in the range of pA, typical for GO, while slight nonlinearity is probably due to the current sensitivity to contact force. The dramatic changes of I-V curves occur after the decomposition of GO. As seen in Fig. 3.34 (C), all the curves obtained at three points of the sample show the increase of conductivity (more than 10 times) which confirms the changes of GO structure and formation of molecular conductivity, likely PAHs, as supported by Raman spectra. I-V curves are asymmetrical indicating unequal flow of the current in opposite directions. This phenomenon can be due to the spatial symmetry of the molecules, formed after the destruction of GO: I-Vs of the symmetric molecules are usually highly symmetric, while the I-Vs of the asymmetric molecules are clearly asymmetric (Reichert et al., 2002). Similar results of I-V measurements of PAHs have been shown in the previous work (Böhme et al., 2007) where the increase of asymmetry in I-V curves has been explained as a result of the increased size of the aromatic core.

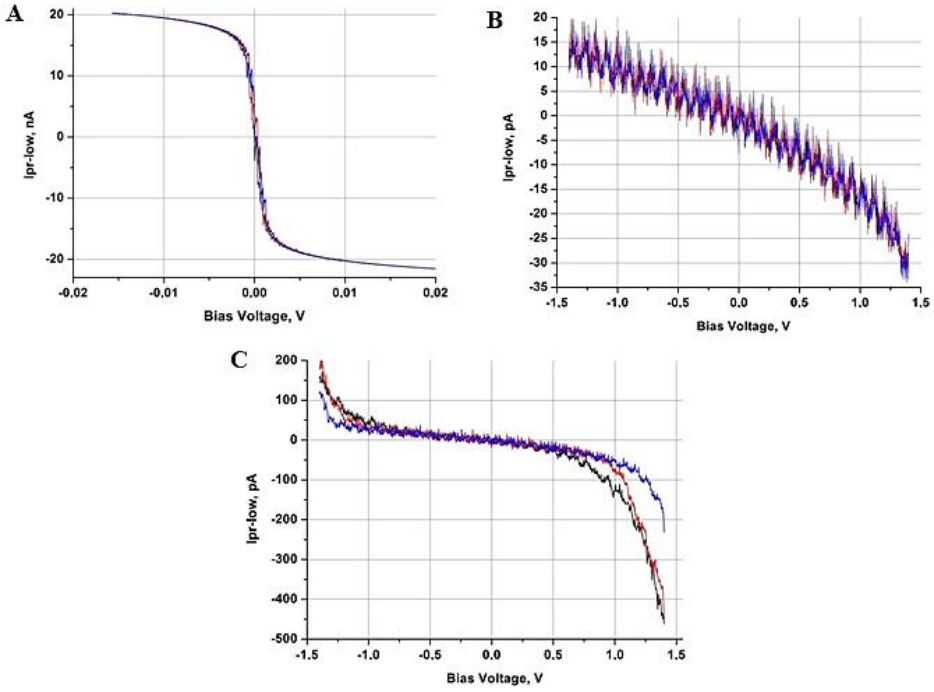

Fig. 3.37. I-V characteristics of blank SERS substrate (A), GO deposited on a SERS substrate before (B) and after (C) the laser irradiation. In all cases, the measurements were carried out at three randomly selected points where irradiation has been carried out

Conclusions. In summary, a novel way stimulated by LSP for the reduction and destruction of GO to PAH-like compounds on a SERS substrate has been demonstrated. It was found that •OH radicals as a result of water decomposition induce the reduction of GO and the synthesis of PAHs. This was confirmed by Raman measurements and I-V characteristics which were found to be common for PAHs. The used method allowed the local modification of electrical conductivity of GO which can be used for the further development of nanostructured organic semiconductors on graphene substrate.

CONCLUSIONS

1. A novel approach for the sol-gel based 3D nanostructured hybrid film synthesis decorated with silver nanoparticles has been developed. It was demonstrated that the control of PEG 400 concentrations in the sols allows the synthesising of the SERS substrates decorated with ring-shaped, spherical and self–assembled silver nanoparticles. The formation of such structures was confirmed by AFM and SEM measurements. The presence of silver nanoparticles was confirmed by UV-Vis measurements showing the plasmon at 472-478 nm common for silver nanoparticles. The highest relative enhancement of Raman signal for crystal violet analyte was observed on self-assembled silver nanoparticle decorated SERS substrate (~270 times), while the SERS substrates decorated with silver nanorings and spherical nanoparticles exhibited the relative enhancement of the Raman signal for the same analyte of ~200 and 120 times, respectively.

2. A novel methodology for the synthesis of silver and gold plasmonic nanostructures (SERS substrates) based on the direct silver ions reduction on HF etched silicon wafers has been developed. It was demonstrated that the control of $AgNO_3$ concentration as well as exposure time of the silicon wafers in the reaction solution allows the synthesising of the SERS substrates decorated with irregular-shapes and triangular silver nanoparticles. The fabricated SERS substrates were characterised by AFM and SEM that confirmed the formation of such nanostructures. The EDX and UV-Vis measurements revealed the presence of silver/gold nanoparticles formed on the silicon wafers. The relative enhancement of the Raman signal was tested with two target analytes: pentacene and R6G. It was demonstrated that the highest enhancement for both analytes was observed on silver nanotriangle decorated SERS substrates: 2.73×10^6 for pentacene and 2.25×10^7 for R6G.

3. It has been shown that silver SERS substrates decorated with triangular silver nanoparticles are able to detect the traces of α-synuclein in water (up to 1 fM). It was also demonstrated that the same substrates are able to detect trace concentrations (up to 0.25 pM) of benzylpenicillin in water and milk samples. It was demonstrated that the silver SERS substrates decorated with triangular silver nanoparticles are able to detect the vibrations of the lipid membrane on which it is deposited.

4. The interaction of L-alanyl-L-tryptophan dipeptide with a nanostructured silver surface has been investigated. The characterisation of L-alanyl-L-tryptophan dipeptide by Raman and surface enhanced Raman spectroscopies has been carried out for the first time. It was found that the SERS spectra of the dipeptide differ at the different points of the sample when the measurements are carried out in water. It was determined that this phenomenon is related to the orientation as well as its location on the SERS surface. SERS measurements revealed that in the case when the dipeptide is adsorbed on the silver nanoparticle, the most enhanced vibrations of carboxyl in the SERS spectra are observed; in the case when the dipeptide is located in between the nanoparticles, the most enhanced vibrations of the indole ring are

seen in the SERS spectra. The absence of amide I vibrations in all the SERS spectra revealed that the dipeptide has no direct contact with the silver SERS surface.

5. A mechanism of the nanochemical reactions driven by LSP has been investigated. A novel approach for the local reduction of graphene oxide on silver SERS substrate has been developed. It was found that the reduction of GO and the synthesis of PAHs was driven by LSP. The key ingredient inducing the reduction of GO and the synthesis of PAHs was found to be •OH radicals. The presence of new compounds was confirmed by the appearance of new peaks in the SERS spectra as well as by the measurements of I-V characteristics.

ACKNOWLEDGEMENTS

First of all I would like to express my appreciation to my Supervisor Prof. Habil. Dr Valentinas Snitka for his guidance and support throughout the time of my dissertation research. It was a great pleasure to work with him.

I would also like to thank Dr Denys Naumenko and Dr Huizhong Xu for their help and comprehensive support. Thanks also go to the team of KTU Research Centre for Microsystems and Nanotechnology, especially to Nora Šlekienė, Dr Leopoldas Limanauskas, Dr Raminta Rodaitė-Rišević̆ienė , Dr Danutė Batiuškaitė and Dr Egidijus Griškonis.

I express the deepest gratitude to my family – Mother, Grandmother and Brother.

Finally, I would like to thank my dear friends Benas Trakšelis, Agnė Valatkienė, Dovydas Valatka, Dainora Morkūnaitė, Dovilė Nagaitytė, Rasa Sabutienė, Meda Bukauskė, Robertas Bukauskas and Karigailė Bukauskaitė. Without you none of this would indeed be possible.

REFERENCES

1. Abdelsalam, M. E., Mahajan, S., Bartlett, P. N., Baumberg, J. J., & Russell, A. E. (2007). SERS at structured palladium and platinum surfaces. *Journal of the American Chemical Society*, *129*(23), 7399-7406.
2. Abrahamsson, K. (2001). Feasibility of quantitative determination of doxorubicin with surface-enhanced Raman spectroscopy. *J. Raman Spectrosc*, *32*, 971-974.
3. Adil, D., & Guha, S. (2012). Surface-enhanced Raman spectroscopic studies of metal–semiconductor interfaces in organic field-effect transistors. *The Journal of Physical Chemistry C*, *116*(23), 12779-12785.
4. Agarwal, N. R., Fazio, E., Neri, F., Trusso, S., Castiglioni, C., Lucotti, A., ... & Ossi, P. M. (2011). Ag and Au nanoparticles for SERS substrates produced by pulsed laser ablation. *Crystal Research and Technology*, *46*(8), 836-840.
5. Ahmed, S., Ahmad, M., Swami, B. L., & Ikram, S. (2016). A review on plants extract mediated synthesis of silver nanoparticles for antimicrobial applications: a green expertise. *Journal of Advanced Research*, *7*(1), 17-28.
6. Alajtal, A. I., Edwards, H. G. M., Elbagerma, M. A., & Scowen, I. J. (2010). The effect of laser wavelength on the Raman Spectra of phenanthrene, chrysene, and tetracene: Implications for extra-terrestrial detection of polyaromatic hydrocarbons. *Spectrochimica Acta Part A: Molecular and Biomolecular Spectroscopy*, *76*(1), 1-5.
7. Aliaga, A. E., Osorio-Román, I., Leyton, P., Garrido, C., Carcamo, J., Caniulef, C., ... & Campos-Vallette, M. M. (2009). Surface-enhanced Raman scattering study of L-tryptophan. *Journal of Raman Spectroscopy*, *40*(2), 164-169.
8. Andreou, C., Mirsafavi, R., Moskovits, M., & Meinhart, C. D. (2015). Detection of low concentrations of ampicillin in milk. *Analyst*, *140*(15), 5003-5005.
9. Anthony, K. J. P., Murugan, M., Jeyaraj, M., Rathinam, N. K., & Sangiliyandi, G. (2014). Synthesis of silver nanoparticles using pine mushroom extract: A potential antimicrobial agent against E. coli and B. subtilis. *Journal of Industrial and Engineering Chemistry*, *20*(4), 2325-2331.
10. Baeten, V., Fernández Pierna, J. A., Dardenne, P., Meurens, M., García-González, D. L., & Aparicio-Ruiz, R. (2005). Detection of the presence of hazelnut oil in olive oil by FT-Raman and FT-MIR spectroscopy. *Journal of agricultural and food chemistry*, *53*(16), 6201-6206.
11. Banaee, M. G., & Crozier, K. B. (2010). Gold nanorings as substrates for surface-enhanced Raman scattering. *Optics letters*, *35*(5), 760-762.
12. Banchelli, M., Tiribilli, B., Pini, R., Dei, L., Matteini, P., & Caminati, G. (2016). Controlled graphene oxide assembly on silver nanocube monolayers for SERS detection: dependence on nanocube packing procedure. *Beilstein Journal of Nanotechnology*, *7*(1), 9-21.
13. Bao, Z., Sun, Z., Xiao, M., Chen, H., Tian, L., & Wang, J. (2011). Transverse oxidation of gold nanorods assisted by selective end capping of silver oxide. *Journal of Materials Chemistry*, *21*(31), 11537-11543.

14. Bechelany, M., Brodard, P., Philippe, L., & Michler, J. (2009). Extended domains of organized nanorings of silver grains as surface-enhanced Raman scattering sensors for molecular detection. *Nanotechnology*, *20*(45), 455302.
15. Bell, S. E., & McCourt, M. R. (2009). SERS enhancement by aggregated Au colloids: effect of particle size. *Physical Chemistry Chemical Physics*, *11*(34), 7455-7462.
16. Benítez–Martínez, S., López-Lorente, Á. I., & Valcárcel, M. (2015). Multilayer graphene–gold nanoparticle hybrid substrate for the SERS determination of metronidazole. *Microchemical Journal*, *121*, 6-13.
17. Berg, H. E. (1993). *Reactions of lactose during heat treatment of milk: a quantitative study*. Landbouwuniversiteit te Wageningen.
18. Bi, L., Dong, J., Xie, W., Lu, W., Tong, W., Tao, L., & Qian, W. (2013). Bimetallic gold–silver nanoplate array as a highly active SERS substrate for detection of streptavidin/biotin assemblies. *Analytica chimica acta*, *805*, 95-100.
19. Blum, C., Schmid, T., Opilik, L., Metanis, N., Weidmann, S., & Zenobi, R. (2012). Missing amide I mode in gap-mode tip-enhanced Raman spectra of proteins. *The Journal of Physical Chemistry C*, *116*(43), 23061-23066.
20. Böhme, T., Simpson, C. D., Müllen, K., & Rabe, J. P. (2007). Current–voltage characteristics of a homologous series of polycyclic aromatic hydrocarbons. *Chemistry–A European Journal*, *13*(26), 7349-7357.
21. Boitor, R. A., Tódor, I. S., Leopold, L. F., & Leopold, N. (2015). Room Temperature Synthesis of Highly Monodisperse and Sers-Active Glucose-Reduced Gold Nanoparticles. *Journal of Applied Spectroscopy*, *82*(3), 415-419.
22. Buividas, R., Day, D. J., & Juodkazis, S. (2012, October). Surface patterning by ripples using femtosecond laser for sensing and opto-fluidics. In *SPIE NanoScience+ Engineering* (pp. 845728-845728). International Society for Optics and Photonics.
23. Buividas, R., Stoddart, P. R., & Juodkazis, S. (2012). Laser fabricated ripple substrates for surface-enhanced Raman scattering. *Annalen der Physik*, *524*(11), L5-L10.
24. Bumbrah, G. S., Sharma, R. M. (2015). Raman spectroscopy – Basic principle, instrumentation and selected applications for the characterization of drugs of abuse. *Egyptian Journal of Forensic Sciences*.
25. Butler, H. J., Fogarty, S. W., Kerns, J. G., Martin-Hirsch, P. L., Fullwood, N. J., & Martin, F. L. (2015). Gold nanoparticles as a substrate in bio-analytical near-infrared surface-enhanced Raman spectroscopy. *Analyst*, *140*(9), 3090-3097.
26. Caglayan, M. G., Torul, H., Onur, F., & Tamer, U. (2015). SERS-based assays for sensitive detection of modafinil. *Journal of Raman Spectroscopy*, *46*(9), 802-806.
27. Camargo, P. H., Au, L., Rycenga, M., Li, W., & Xia, Y. (2010). Measuring the SERS enhancement factors of dimers with different structures constructed from silver nanocubes. *Chemical physics letters*, *484*(4), 304-308.
28. Castro, J. L., Ramırez, M. L., Tocon, I. L., & Otero, J. C. (2003). Vibrational study of the metal–adsorbate interaction of phenylacetic acid and α-phenylglycine on silver surfaces. *Journal of colloid and interface science*, *263*(2), 357-363.

29. Cejkova, J., Prokopec, V., Brazdova, S., Kokaislova, A., Matejka, P., & Stepanek, F. (2009). Characterization of copper SERS-active substrates prepared by electrochemical deposition. *Applied Surface Science*, *255*(18), 7864-7870.
30. Chaney, S. B., Shanmukh, S., Dluhy, R. A., & Zhao, Y. P. (2005). Aligned silver nanorod arrays produce high sensitivity surface-enhanced Raman spectroscopy substrates. *Applied Physics Letters*, *87*(3), 031908.
31. Chen, H., Wei, G., Ispas, A., Hickey, S. G., & Eychmüller, A. (2010). Synthesis of palladium nanoparticles and their applications for surface-enhanced Raman scattering and electrocatalysis. *The Journal of Physical Chemistry C*, *114*(50), 21976-21981.
32. Chen, L., Wu, M., Jing, Q., Yu, Y., Huang, J., Liu, Y., ... & Qiu, G. (2015). Gallium/gold composite microspheres fixed on a silicon substrate for surface enhanced Raman scattering. *RSC Advances*, *5*(82), 67134-67140.
33. Chikkaraddy, R., Singh, D., & Kumar, G. P. (2012). Plasmon assisted light propagation and Raman scattering hot-spot in end-to-end coupled silver nanowire pairs. *Applied Physics Letters*, *100*(4), 043108.
34. Choi, C. J., Xu, Z., Wu, H. Y., Liu, G. L., & Cunningham, B. T. (2010). Surface-enhanced Raman nanodomes. *Nanotechnology*, *21*(41), 415301.
35. Chou, A., Jaatinen, E., Buividas, R., Seniutinas, G., Juodkazis, S., Izake, E. L., & Fredericks, P. M. (2012). SERS substrate for detection of explosives. *Nanoscale*, *4*(23), 7419-7424.
36. Chou, I. H., Benford, M., Beier, H. T., Coté, G. L., Wang, M., Jing, N., ... & Good, T. A. (2008). Nanofluidic biosensing for β-amyloid detection using surface enhanced Raman spectroscopy. *Nano letters*, *8*(6), 1729-1735.
37. Chua, C. K., & Pumera, M. (2013). Reduction of graphene oxide with substituted borohydrides. *Journal of Materials Chemistry A*, *1*(5), 1892-1898.
38. Chung, T., Lee, S. Y., Song, E. Y., Chun, H., & Lee, B. (2011). Plasmonic nanostructures for nano-scale bio-sensing. *Sensors*, *11*(11), 10907-10929.
39. Cîntă Pînzaru, S., Pavel, I., Leopold, N., & Kiefer, W. (2004). Identification and characterization of pharmaceuticals using Raman and surface-enhanced Raman scattering. *Journal of Raman Spectroscopy*, *35*(5), 338-346.
40. Ciou, S. H., Cao, Y. W., Huang, H. C., Su, D. Y., & Huang, C. L. (2009). SERS enhancement factors studies of silver nanoprism and spherical nanoparticle colloids in the presence of bromide ions. *The Journal of Physical Chemistry C*, *113*(22), 9520-9525
41. Colangeli, L., Mennella, V., Baratta, G. A., Bussoletti, E., & Strazzulla, G. (1992). Raman and infrared spectra of polycyclic aromatic hydrocarbon molecules of possible astrophysical interest. *The Astrophysical Journal*, *396*, 369-377.
42. Colthup, N. (2012). *Introduction to infrared and Raman spectroscopy*. Elsevier.
43. Cote, L. J., Cruz-Silva, R., & Huang, J. (2009). Flash reduction and patterning of graphite oxide and its polymer composite. *Journal of the American Chemical Society*, *131*(31), 11027-11032.
44. Creanga, I., Fagadar-Cosma, G., Palade, A., Lascu, A., Enache, C., Birdeanu, M., & Fagadar-Cosma, E. (2013). New hybrid silver colloid-A3B potphyrin complex exhibiting wide band absorption. *Digest Journal of Nanomaterials & Biostructures (DJNB)*, *8*(2).

45. Csizmadia, T., Hopp, B., Smausz, T., Kopniczky, J., Hanyecz, I., Sipos, Á., ... & Szabó, G. (2013). Possible application of laser-induced backside dry etching technique for fabrication of SERS substrate surfaces. *Applied Surface Science*, *278*, 234-240.
46. Cui, L., Wang, P., Chen, X., Fang, Y., Zhang, Z., & Sun, M. (2014). Plasmon-driven dimerization via SS chemical bond in an aqueous environment. *Scientific reports*, *4*.
47. Dai, Z. G., Xiao, X. H., Wu, W., Zhang, Y. P., Liao, L., Guo, S. S., ... & Jiang, C. Z. (2015). Plasmon-driven reaction controlled by the number of graphene layers and localized surface plasmon distribution during optical excitation. *Light: Science & Applications*, *4*(10), e342.
48. Dendisová-Vyškovská, M., Prokopec, V., Člupek, M., & Matějka, P. (2012). Comparison of SERS effectiveness of copper substrates prepared by different methods: what are the values of enhancement factors?. *Journal of Raman Spectroscopy*, *43*(2), 181-186.
49. Ding, G., Xie, S., Liu, Y., Wang, L., & Xu, F. (2015). Graphene oxide-silver nanocomposite as SERS substrate for dye detection: Effects of silver loading amount and composite dosage. *Applied Surface Science*, *345*, 310-318.
50. Ding, Y. H., Zhang, P., Zhuo, Q., Ren, H. M., Yang, Z. M., & Jiang, Y. (2011). A green approach to the synthesis of reduced graphene oxide nanosheets under UV irradiation. *Nanotechnology*, *22*(21), 215601.
51. Domenici, F., Bizzarri, A. R., & Cannistraro, S. (2012). Surface-enhanced Raman scattering detection of wild-type and mutant p53 proteins at very low concentration in human serum. *Analytical biochemistry*, *421*(1), 9-15.
52. Dong, B., Fang, Y., Chen, X., Xu, H., & Sun, M. (2011). Substrate-, wavelength-, and time-dependent plasmon-assisted surface catalysis reaction of 4-nitrobenzenethiol dimerizing to p, p′-dimercaptoazobenzene on Au, Ag, and Cu films. *Langmuir*, *27*(17), 10677-10682.
53. Dong, R., Weng, S., Yang, L., & Liu, J. (2015). Detection and direct readout of drugs in human urine using dynamic surface-enhanced Raman spectroscopy and support vector machines. *Analytical chemistry*, *87*(5), 2937-2944.
54. Dong, S., Tang, C., Zhou, H., & Zhao, H. (2004). Photochemical synthesis of gold nanoparticles by the sunlight radiation using a seeding approach. *Gold bulletin*, *37*(3-4), 187-195.
55. Drogat, N., Granet, R., Sol, V., & Krausz, P. (2010). One-Pot Silver Nanoring Synthesis. *Nanoscale research letters*, *5*(3), 566-569.
56. Dutta, B. K., Ellateif, T. M. A., & Maitra, S. (2011). Development of a porous silica film by sol–gel process. *World Acad. Sci. Eng. Technol*, *73*, 308-312.
57. El-Abassy, R. M., Eravuchira, P. J., Donfack, P., Von Der Kammer, B., & Materny, A. (2012). Direct determination of unsaturation level of milk fat using Raman spectroscopy. *Applied spectroscopy*, *66*(5), 538-544.
58. Eom, S. Y., Ryu, S. L., Kim, H. L., & Kwon, C. H. (2013). Systematic preparation of colloidal silver nanoparticles for effective SERS substrates. *Colloids and Surfaces A: Physicochemical and Engineering Aspects*, *422*, 39-43.

59. Fan, M., & Brolo, A. G. (2009). Silver nanoparticles self-assembly as SERS substrates with near single molecule detection limit. *Physical Chemistry Chemical Physics*, *11*(34), 7381-7389.
60. Fan, M., Lai, F. J., Chou, H. L., Lu, W. T., Hwang, B. J., & Brolo, A. G. (2013). Surface-enhanced Raman scattering (SERS) from Au: Ag bimetallic nanoparticles: the effect of the molecular probe. *Chemical Science*, *4*(1), 509-515.
61. Fan, S. Q., Li, C. J., Li, C. X., Liu, G. J., Yang, G. J., & Zhang, L. Z. (2006). Preliminary study of performance of dye-sensitized solar cell of nano-TiO2 coating deposited by vacuum cold spraying. *Materials transactions*, *47*(7), 1703-1709.
62. Farquharson, S., Shende, C., Sengupta, A., Huang, H., & Inscore, F. (2011). Rapid detection and identification of overdose drugs in Saliva by surface-enhanced Raman scattering using fused gold colloids. *Pharmaceutics*, *3*(3), 425-439.
63. Faulds, K., Hernandez-Santana A., Ewen Smith W. (2010). The inorganic chemistry of surface enhanced Raman scattering (SERS). *Spectroscopic Properties of Inorganic and Organometallic Compounds*., *41*, 1-21.
64. Feng, L., Ma, R., Wang, Y., Xu, D., Xiao, D., Liu, L., & Lu, N. (2015). Silver-coated elevated bowtie nanoantenna arrays: Improving the near-field enhancement of gap cavities for highly active surface-enhanced Raman scattering. *Nano Research*, *8*(11), 3715-3724.
65. Feng, X., Pisula, W., & Müllen, K. (2009). Large polycyclic aromatic hydrocarbons: synthesis and discotic organization. *Pure and Applied Chemistry*, *81*(12), 2203-2224.
66. Fleger, Y., & Rosenbluh, M. (2009). Surface plasmons and surface enhanced Raman spectra of aggregated and alloyed gold-silver nanoparticles. *International Journal of Optics*, *2009*.
67. Fleischmann, M., Hendra, P. J., McQuillan, A. J. (1974). Raman spectra of pyridine adsorbed at a silver electrode. *Chemical Physics Letters*, *26*(2), 163-166.
68. Fleming, G. R., Morris, J. M., Robbins, R. J., Woolfe, G. J., Thistlethwaite, P. J., & Robinson, G. W. (1978). Nonexponential fluorescence decay of aqueous tryptophan and two related peptides by picosecond spectroscopy. *Proceedings of the National Academy of Sciences*, *75*(10), 4652-4656.
69. Frano, K. A., Mayhew, H. E., Svoboda, S. A., & Wustholz, K. L. (2014). Combined SERS and Raman analysis for the identification of red pigments in cross-sections from historic oil paintings. *Analyst*, *139*(24), 6450-6455.
70. Fu, Q., Wong, K. M., Zhou, Y., Wu, M., & Lei, Y. (2015). Ni/Au hybrid nanoparticle arrays as a highly efficient, cost-effective and stable SERS substrate. *RSC Advances*, *5*(8), 6172-6180.
71. Fujihara, A., Matsumoto, H., Shibata, Y., Ishikawa, H., & Fuke, K. (2008). Photodissociation and spectroscopic study of cold protonated dipeptides. *The Journal of Physical Chemistry A*, *112*(7), 1457-1463.
72. García-Macedo, J. A., Valverde, G., Lockard, J., & Zink, J. I. (2004, June). SERS on mesostructured thin films with silver nanoparticles. In *Integrated Optoelectronic Devices 2004* (pp. 117-124). International Society for Optics and Photonics.
73. Gaware, U., Kamble, V., & Ankamwar, B. (2012). Ecofriendly synthesis of anisotropic gold nanoparticles: a potential candidate of SERS studies. *International Journal of Electrochemistry*, *2012*.

74. Gonçalves, G., Vila, M., Bdikin, I., de Andrés, A., Emami, N., Ferreira, R. A., ... & Marques, P. A. (2014). Breakdown into nanoscale of graphene oxide: Confined hot spot atomic reduction and fragmentation. *Scientific reports*, *4*.
75. Gopal, J., Abdelhamid, H. N., Huang, J. H., & Wu, H. F. (2016). Non-destructive detection of the freshness of fruits and vegetables using gold and silver nanoparticle mediated graphene enhanced Raman spectroscopy. *Sensors and Actuators B: Chemical*, *224*, 413-424.
76. Gordon, K. C., & McGoverin, C. M. (2011). Raman mapping of pharmaceuticals. *International journal of pharmaceutics*, *417*(1), 151-162.
77. Grinceviciute, N., Verdes, D., & Snitka, V. (2015). Effect of zinc oxide and titanium dioxide nanoparticles on supported lipid bilayers. *J. Nanomed. Res*, *2*, 00030.
78. Gunstone, F. D., Harwood, J. L., & Padley, F. B. (1994). Marine oils: fish and whale oils. *Gunstone, FD The lipid handbook. Lon-don: Chapman & Hall*.
79. Haiza, H., Azizan, A., Mohidin, A. H., & Halin, D. S. C. (2013, June). Green synthesis of silver nanoparticles using local honey. In *Nano Hybrids* (Vol. 4, pp. 87-98).
80. Han, Z., Liu, H., Meng, J., Yang, L., Liu, J., & Liu, J. (2015). Portable Kit for Identification and Detection of Drugs in Human Urine Using Surface-Enhanced Raman Spectroscopy. *Analytical chemistry*, *87*(18), 9500-9506.
81. Hanlon, E. B., Manoharan, R., Koo, T., Shafer, K. E., Motz, J. T., Fitzmaurice, M., Kramer J. R., Itzkan I., Dasari R. R., Feld, M. S. (2000). Prospects for in vivo Raman spectroscopy. *Physics in medicine and biology*. 45(2), 1-59.
82. Harraz, F. A., Ismail, A. A., Bouzid, H., Al-Sayari, S. A., Al-Hajry, A., & Al-Assiri, M. S. (2015). Surface-enhanced Raman scattering (SERS)-active substrates from silver plated-porous silicon for detection of crystal violet. *Applied Surface Science*, *331*, 241-247.
83. He, S., Xie, W., Zhang, W., Zhang, L., Wang, Y., Liu, X., ... & Du, C. (2015). Multivariate qualitative analysis of banned additives in food safety using surface enhanced Raman scattering spectroscopy. *Spectrochimica Acta Part A: Molecular and Biomolecular Spectroscopy*, *137*, 1092-1099.
84. Herrera, G. M., Padilla, A. C., & Hernandez-Rivera, S. P. (2013). Surface enhanced Raman scattering (SERS) studies of gold and silver nanoparticles prepared by laser ablation. *Nanomaterials*, *3*(1), 158-172.
85. Hong, S., & Li, X. (2013). Optimal size of gold nanoparticles for surface-enhanced Raman spectroscopy under different conditions. *Journal of Nanomaterials*, *2013*, 49.
86. Hsu, H., El-Sayed, M., & Eustis, S. (2004). Photochemical synthesis of gold nanoparticles with interesting shapes. *NNIN REU Research accomplishments*, 68-69.
87. http://atoid.com/ [accessed 2016-02-16]
88. http://oceanoptics.com/product/sers/ [accessed 2016-02-16]
89. http://www.altechna.com/download/catalog/Altechna_Catalog_2014.pdf [accessed 2016-02-16]
90. http://www.silmeco.com/products/sers-substrate-serstrate [accessed 2016-02-16]
91. http://www.spl-tech.cn/UploadPic/2012/05/22/20120522161540321378.pdf [accessed 2016-02-16]

92. Huebner, U., Schneidewind, H., Cialla, D., Weber, K., Zeisberger, M., Mattheis, R., ... & Popp, J. (2010, April). Fabrication of regular patterned SERS arrays by electron beam lithography. In *SPIE Photonics Europe* (pp. 771536-771536). International Society for Optics and Photonics.
93. Indrasekara, A. S. D. S., Meyers, S., Shubeita, S., Feldman, L. C., Gustafsson, T., & Fabris, L. (2014). Gold nanostar substrates for SERS-based chemical sensing in the femtomolar regime. *Nanoscale*, *6*(15), 8891-8899.
94. Iravani, S. (2014). Bacteria in nanoparticle synthesis: Current status and Future prospects. *International Scholarly Research Notices*, *2014*.
95. Iravani, S., Korbekandi, H., Mirmohammadi, S. V., & Zolfaghari, B. (2014). Synthesis of silver nanoparticles: chemical, physical and biological methods. *Research in pharmaceutical sciences*, *9*(6), 385.
96. Israelsen, N. D., Hanson, C., & Vargis, E. (2015). Nanoparticle properties and synthesis effects on surface-enhanced Raman scattering enhancement factor: an introduction. *The Scientific World Journal*, *2015*.
97. Jiang, X., Zeng, Q., & Yu, A. (2006). A self-seeding coreduction method for shape control of silver nanoplates. *Nanotechnology*, *17*(19), 4929.
98. Jiwei, Q., Yudong, L., Ming, Y., Qiang, W., Zongqiang, C., Jingyang, P., ... & Jingjun, X. (2013). Fabrication of nanowire network AAO and its application in SERS. *Nanoscale research letters*, *8*(1), 1-6.
99. Jung, H. Y., Gupta, R. K., Oh, E. O., Kim, Y. H., & Whang, C. M. (2005). Vibrational spectroscopic studies of sol–gel derived physical and chemical bonded ORMOSILs. *Journal of non-crystalline solids*, *351*(5), 372-379.
100. Kahraman, M., Aydin, Ö., & Culha, M. (2009). Size Effect of 3D Aggregates Assembled from Silver Nanoparticles on Surface-Enhanced Raman Scattering. *ChemPhysChem*, *10*(3), 537-542.
101. Kahrilas, G. A., Wally, L. M., Fredrick, S. J., Hiskey, M., Prieto, A. L., & Owens, J. E. (2013). Microwave-assisted green synthesis of silver nanoparticles using orange peel extract. *ACS Sustainable Chemistry & Engineering*, *2*(3), 367-376.
102. Kang, J. S., Lee, C. J., Kim, M. S., & Lee, M. S. (2003). New routes to the preparation of silver-doped sol-gel films for a SERS Study. *BULLETIN-KOREAN CHEMICAL SOCIETY*, *24*(11), 1599-1604.
103. Kang, L., Han, X., Chu, J., Xiong, J., He, X., Wang, H. L., & Xu, P. (2015). In Situ Surface-Enhanced Raman Spectroscopy Study of Plasmon-Driven Catalytic Reactions of 4-Nitrothiophenol under a Controlled Atmosphere. *ChemCatChem*, *7*(6), 1004-1010.
104. Kang'ethe, E. K., & Lang'a, K. A. (2009). Aflatoxin B1 and M1 contamination of animal feeds and milk from urban centers in Kenya. *African Health Sciences*, *9*(4).
105. Karvonen, L., Chen, Y., Säynätjoki, A., Taiviola, K., Tervonen, A., & Honkanen, S. (2011). SERS-active silver nanoparticle aggregates produced in high-iron float glass by ion exchange process. *Optical Materials*, *34*(1), 1-5.
106. Kashmery, H. A., Thompson, D. G., Dondi, R., Mabbott, S., Graham, D., Clark, A. W., & Burley, G. A. (2015). SERS enhancement of silver nanoparticles prepared by a template-directed triazole ligand strategy. *Chemical Communications*, *51*(65), 13028-13031.

107. Kast, S. C. T. R. E., Auner, K. V. H. G. W. (2015). Agricultural and Environmental Management with Raman Spectroscopy.

108. Kausaite, A., van Dijk, M., Castrop, J., Ramanaviciene, A., Baltrus, J. P., Acaite, J., & Ramanavicius, A. (2007). Surface plasmon resonance label-free monitoring of antibody antigen interactions in real time. *Biochemistry and Molecular Biology Education*, *35*(1), 57-63.

109. Kelly, K. L., Coronado, E., Zhao, L. L., & Schatz, G. C. (2003). The optical properties of metal nanoparticles: the influence of size, shape, and dielectric environment. *The Journal of Physical Chemistry B*, *107*(3), 668-677.

110. Kennedy, D. G., McCracken, R. J., Cannavan, A., & Hewitt, S. A. (1998). Use of liquid chromatography–mass spectrometry in the analysis of residues of antibiotics in meat and milk. *Journal of chromatography A*, *812*(1), 77-98

111. Khlebtsov, B. N., Khanadeev, V. A., Panfilova, E. V., Bratashov, D. N., & Khlebtsov, N. G. (2015). Gold nanoisland films as reproducible SERS substrates for highly sensitive detection of fungicides. *ACS applied materials & interfaces*, *7*(12), 6518-6529.

112. Krpetić, Ž., Guerrini, L., Larmour, I. A., Reglinski, J., Faulds, K., & Graham, D. (2012). Importance of Nanoparticle Size in Colorimetric and SERS-Based Multimodal Trace Detection of Ni (II) Ions with Functional Gold Nanoparticles. *Small*, *8*(5), 707-714.

113. Kumar, G. P. (2012). Plasmonic nano-architectures for surface enhanced Raman scattering: a review. *Journal of Nanophotonics*, *6*(1), 064503-1.

114. Kumar, P. S., Pastoriza-Santos, I., Rodríguez-González, B., de Abajo, F. J. G., & Liz-Marzan, L. M. (2007). High-yield synthesis and optical response of gold nanostars. *Nanotechnology*, *19*(1), 015606

115. Kuraoka, K., Ueda, T., Sato, M., Okamoto, T., & Yazawa, T. (2005). Preparation and properties of organic–inorganic hybrid flexible hardcoat films. *Journal of materials science*, *40*(13), 3577-3579.

116. Kurouski, D., & Van Duyne, R. P. (2015). In Situ detection and identification of hair dyes using surface-enhanced Raman spectroscopy (SERS). *Analytical chemistry*, *87*(5), 2901-2906.

117. Kurouski, D., Postiglione, T., Deckert-Gaudig, T., Deckert, V., & Lednev, I. K. (2013). Amide I vibrational mode suppression in surface (SERS) and tip (TERS) enhanced Raman spectra of protein specimens. *Analyst*, *138*(6), 1665-1673.

118. Kvítek, L., Prucek, R., Panáček, A., Novotný, R., Hrbáč, J., & Zbořil, R. (2005). The influence of complexing agent concentration on particle size in the process of SERS active silver colloid synthesis. *Journal of Materials Chemistry*, *15*(10), 1099-1105.

119. Lai-Kwan, C., & Chang, H. T. (Eds.). (2012). *From bioimaging to biosensors: noble metal nanoparticles in biodetection*. Crc Press.

120. Lee, D., & Yoon, S. (2015). Gold Nanocube–Nanosphere Dimers: Preparation, Plasmon Coupling, and Surface-Enhanced Raman Scattering. *The Journal of Physical Chemistry C*, *119*(14), 7873-7882.

121. Lee, D., Choe, Y. J., Lee, M., Jeong, D. H., & Paik, S. R. (2011). Protein-Based SERS Technology Monitoring the Chemical Reactivity on an α-Synuclein-Mediated Two-Dimensional Array of Gold Nanoparticles. *Langmuir*, *27*(21), 12782-12787.

122. Lee, K. M., Herrman, T. J., Yun, U. (2014). Application of Raman spectroscopy for qualitative and quantitative analysis of aflatoxins in ground maize samples. *Journal of Cereal Science*, *59*(1), 70-78.

123. Leng, W., Yasseri, A. A., Sharma, S., Li, Z., Woo, H. Y., Vak, D., ... & Kelley, A. M. (2006). Silver nanocrystal-modified silicon nanowires as substrates for surface-enhanced Raman and hyper-Raman scattering. *Analytical chemistry*, *78*(17), 6279-6282.

124. Leopold, N., Chiş, V., Mircescu, N. E., Marişca, O. T., Buja, O. M., Leopold, L. F., ... & Berindan-Neagoe, I. (2013). One step synthesis of SERS active colloidal gold nanoparticles by reduction with polyethylene glycol. *Colloids and Surfaces A: Physicochemical and Engineering Aspects*, *436*, 133-138.

125. Levin, C. S. (2009). Influence of Varying Analyte Concentration, Environment, and Composition on Nanoshell-based SERS. ProQuest.

126. Leyton, P., Domingo, C., Sanchez-Cortes, S., Campos-Vallette, M., & Garcia-Ramos, J. V. (2005). Surface enhanced vibrational (IR and Raman) spectroscopy in the design of chemosensors based on ester functionalized p-tert-butylcalix [4] arene hosts. *Langmuir*, *21*(25), 11814-11820.

127. Li, C., Li, D., Wan, G., Xu, J., & Hou, W. (2011). Facile synthesis of concentrated gold nanoparticles with low size-distribution in water: temperature and pH controls. *Nanoscale research letters*, *6*(1), 1-10.

128. Li, D., Lin, Y. S., & Guliants, V. V. (2010). Synthesis and Characterization of Ordered Meso-Macro-Porous Silica Membranes on a Porous Alumina Support. *Tsinghua Science & Technology*, *15*(4), 377-384.

129. Li, D., Ouyang, Y., Chen, L., Cao, W., & Shi, S. (2011). SERS spectra of pyridine adsorbed on nickel film prepared by magnetron sputtering. *Indian Journal of Physics*, *85*(2), 293-299.

130. Li, L., Liu, J., Yang, X., Huang, J., He, D., Guo, X., ... & Wang, K. (2016). Biomimetic synthesis of highly biocompatible gold nanoparticles with amino acid-dithiocarbamate as a precursor for SERS imaging. *Nanotechnology*, *27*(10), 105603.

131. Li, W., Camargo, P. H., Lu, X., & Xia, Y. (2008). Dimers of silver nanospheres: facile synthesis and their use as hot spots for surface-enhanced Raman scattering. *Nano letters*, *9*(1), 485-490.

132. Li-Chan, E. C. (2007). Vibrational spectroscopy applied to the study of milk proteins. *Le Lait*, *87*(4-5), 443-458.

133. Lin-jun, H., Yan-xin, W., Jian-guo, T., Yao, W., Ji-xian, L., Ji-qing, J., & Wei, W. (2016). Preparation of Graphene/Silver Nanohybrid Composite with Good Surface-Enhanced Raman Scattering Characteristics. *Int. J. Electrochem. Sci*, *11*, 398-405.

134. Liu, J. W., Wang, J. L., Huang, W. R., Yu, L., Ren, X. F., Wen, W. C., & Yu, S. H. (2012). Ordering Ag nanowire arrays by a glass capillary: A portable, reusable and durable SERS substrate. *Scientific reports*, *2*.

135. Liu, J., Cui, L., & Losic, D. (2013). Graphene and graphene oxide as new nanocarriers for drug delivery applications. *Acta biomaterialia*, *9*(12), 9243-9257.

136. Liu, Y. J., Chu, H. Y., & Zhao, Y. P. (2010). Silver nanorod array substrates fabricated by oblique angle deposition: morphological, optical, and SERS characterizations. *The Journal of Physical Chemistry C*, *114*(18), 8176-8183.

137. Livingstone, R., Quagliano, L. G., Perez-Paz, N., Munoz, M., Tamargo, M. C., Jean-Mary, F., & Lombardi, J. R. (2005, November). SERS as sensing method for bio-molecules on MBE-grown quantum dots. In *Optics East 2005* (pp. 60080A-60080A). International Society for Optics and Photonics.

138. Loh, K. P., Bao, Q., Eda, G., & Chhowalla, M. (2010). Graphene oxide as a chemically tunable platform for optical applications. *Nature chemistry*, *2*(12), 1015-1024.

139. Loo, Y. Y., Chieng, B. W., Nishibuchi, M., & Radu, S. (2012). Synthesis of silver nanoparticles by using tea leaf extract from Camellia sinensis. *International journal of nanomedicine*, *7*, 4263.

140. Luo, C., Zhang, Y., Zeng, X., Zeng, Y., & Wang, Y. (2005). The role of poly (ethylene glycol) in the formation of silver nanoparticles. *Journal of colloid and interface science*, *288*(2), 444-448.

141. Macijauskienė, B., & Griškoni, E. (2015). Ultrasound assisted modification of graphite felt with electroless silver-Part 1: composition, morphology, structure and electrical conductivity. *Chemija*, *26*(1).

142. Manara, D., Grandjean, A., & Neuville, D. R. (2009). Advances in understanding the structure of borosilicate glasses: A Raman spectroscopy study. *American Mineralogist*, *94*(5-6), 777-784.

143. Manikprabhu, D., & Lingappa, K. (2013). Microwave assisted rapid and green synthesis of silver nanoparticles using a pigment produced by Streptomyces coelicolor klmp33. *Bioinorganic chemistry and applications*, *2013*.

144. Mansouri, S. S., & Ghader, S. (2009). Experimental study on effect of different parameters on size and shape of triangular silver nanoparticles prepared by a simple and rapid method in aqueous solution. *Arabian Journal of Chemistry*, *2*(1), 47-53.

145. Mavani, K., & Shah, M. (2013). Synthesis of silver nanoparticles by using sodium borohydride as a reducing agent. *International Journal of Engineering Research & Technology*, *2*(3).

146. Mei, K. C., Rubio, N., Costa, P. M., Kafa, H., Abbate, V., Festy, F., ... & Al-Jamal, K. T. (2015). Synthesis of double-clickable functionalised graphene oxide for biological applications. *Chemical Communications*, *51*(81), 14981-14984.

147. Mevold, A. H., Hsu, W. W., Hardiansyah, A., Huang, L. Y., Yang, M. C., Liu, T. Y., & Wang, J. K. (2015). Fabrication of Gold Nanoparticles/Graphene-PDDA Nanohybrids for Bio-detection by SERS Nanotechnology. *Nanoscale research letters*, *10*(1), 1-7.

148. Mikac, L., Ivanda, M., Gotić, M., Mihelj, T., & Horvat, L. (2014). Synthesis and characterization of silver colloidal nanoparticles with different coatings for SERS application. *Journal of nanoparticle research*, *16*(12), 1-13.

149. Milea, C. A., Bogatu, C., & Duta, A. (2011). The influence of parameters in silica sol-gel process. *Bulletin of TheTransilvania University of Brasov*, *4*, 53.

150. Morales, F. J., Romero, C., & Jiménez-Pérez, S. (1996). Fluorescence associated with Maillard reaction in milk and milk-resembling systems. *Food Chemistry*, *57*(3), 423-428.

151. Muniz-Miranda, M., Gellini, C., & Giorgetti, E. (2011). Surface-enhanced Raman scattering from copper nanoparticles obtained by laser ablation. *The Journal of Physical Chemistry C*, *115*(12), 5021-5027.

152. Myllyniemi, A. L., Rannikko, R., Lindfors, E., Niemi, A., & Bäckman, C. (2000). Microbiological and chemical detection of incurred penicillin G, oxytetracycline, enrofloxacin and ciprofloxacin residues in bovine and porcine tissues. *Food Additives & Contaminants*, *17*(12), 991-1000.

153. Nam, S., Parikh, D. V., Condon, B. D., Zhao, Q., & Yoshioka-Tarver, M. (2011). Importance of poly (ethylene glycol) conformation for the synthesis of silver nanoparticles in aqueous solution. *Journal of Nanoparticle Research*, *13*(9), 3755-3764.

154. Ngo, Y. H., Li, D., Simon, G. P., & Garnier, G. (2012). Gold nanoparticle–paper as a three-dimensional surface enhanced raman scattering substrate. *Langmuir*, *28*(23), 8782-8790.

155. Nickel, U., zu Castell, A., Pöppl, K., & Schneider, S. (2000). A silver colloid produced by reduction with hydrazine as support for highly sensitive surface-enhanced Raman spectroscopy. *Langmuir*, *16*(23), 9087-9091.

156. Novara, C., Petracca, F., Virga, A., Rivolo, P., Ferrero, S., Chiolerio, A., Giorgis, F. (2014). SERS active silver nanoparticles synthesized by inkjet printing on mesoporous silicon. *Nanoscale research letters*, *9*(1), 1-7.

157. O'Connell, M. L., Ryder, A. G., Leger, M. N., Howley, T. (2010). Qualitative analysis using Raman spectroscopy and chemometrics: a comprehensive model system for narcotics analysis. *Applied spectroscopy*, *64*(10), 1109-1121.

158. Oh, C., Lee, Y. G., Choi, T. S., Jon, C. U., & Oh, S. G. (2009). Facile synthesis of PEG–silica hybrid particles using one-step sol–gel reaction in aqueous solution. *Colloids and Surfaces A: Physicochemical and Engineering Aspects*, *349*(1), 145-150.

159. Oh, M. K., Shin, Y. S., Lee, C. L., De, R., Kang, H., Yu, N. E., ... & Yang, J. K. (2015). Morphological and SERS properties of silver nanorod array films fabricated by oblique thermal evaporation at various substrate temperatures. *Nanoscale research letters*, *10*(1), 1-9.

160. Oshikiri, T., Ueno, K., & Misawa, H. (2014). Plasmon-Induced Ammonia Synthesis through Nitrogen Photofixation with Visible Light Irradiation. *Angewandte Chemie*, *126*(37), 9960-9963.

161. Osorio-Román, I. O., Ortega-Vásquez, V., Vargas, C. V., & Aroca, R. F. (2011). Surface-Enhanced Spectra on D-Gluconic Acid Coated Silver Nanoparticles. *Applied spectroscopy*, *65*(8), 838-843.

162. Owens, P., Phillipson, N., Perumal, J., O'Connor, G. M., & Olivo, M. (2015). Sensing of p53 and EGFR Biomarkers Using High Efficiency SERS Substrates. *Biosensors*, *5*(4), 664-677.

163. Pastoriza-Santos, I., & Liz-Marzán, L. M. (1999). Formation and stabilization of silver nanoparticles through reduction by N, N-dimethylformamide. *Langmuir*, *15*(4), 948-951.

164. Pei, S., & Cheng, H. M. (2012). The reduction of graphene oxide. *Carbon*, *50*(9), 3210-3228.

165. Perna, G., Lasalvia, M., Gallo, C., Quartucci, G., & Capozzi, V. (2013). Vibrational characterization of synthetic eumelanin by means of raman and surface enhanced raman scattering. *The Open Surface Science Journal*, *5*(1).

166. Petryayeva, E., & Krull, U. J. (2011). Localized surface plasmon resonance: Nanostructures, bioassays and biosensing—A review. *Analytica chimica acta*, *706*(1), 8-24.

167. Petti, L., Capasso, R., Rippa, M., Pannico, M., La Manna, P., Peluso, G., ... & Musto, P. (2016). A plasmonic nanostructure fabricated by electron beam lithography as a sensitive and highly homogeneous SERS substrate for bio-sensing applications. *Vibrational Spectroscopy*, *82*, 22-30.

168. Philip, D. (2009). Honey mediated green synthesis of gold nanoparticles. *Spectrochimica Acta Part A: Molecular and Biomolecular Spectroscopy*, *73*(4), 650-653.

169. Podstawka, E., Ozaki, Y., & Proniewicz, L. M. (2005). Part III: surface-enhanced raman scattering of amino acids and their homodipeptide monolayers deposited onto colloidal gold surface. *Applied spectroscopy*, *59*(12), 1516-1526.

170. Pouchaname, V., Tinabaye, A., Madivanane, R., Renukadevi, Dr Vibrational Analysis (Experimental & Ab initio Computation) of 2-ethylnaphthalene. IRACST – *Engineering Science and Technology: An International Journal*. 2012, *2*, 752-758.

171. Prabu, H. J., & Johnson, I. (2015). Plant-mediated biosynthesis and characterization of silver nanoparticles by leaf extracts of Tragia involucrata, Cymbopogon citronella, Solanum verbascifolium and Tylophora ovata. *Karbala International Journal of Modern Science*, *1*(4), 237-246.

172. Pratiwi, D., Fawcett, J. P., Gordon, K. C., Rades, T. (2002). Quantitative analysis of polymorphic mixtures of ranitidine hydrochloride by Raman spectroscopy and principal components analysis. *European journal of pharmaceutics and biopharmaceutics*, *54*(3), 337-341.

173. Pris, M. (2014). Influence of different parameters on wet synthesis of silver nanoparticles.

174. Ramírez-Santos, Á. A., Acevedo-Peña, P., & Córdoba, E. M. (2012). Enhanced photocatalytic activity of TiO2 films by modification with polyethylene glycol. *Quimica Nova*, *35*(10), 1931-1935.

175. Rashid, M. U., Bhuiyan, M. K. H., & Quayum, M. E. (2013). Synthesis of silver nano particles (Ag-NPs) and their uses for quantitative analysis of vitamin C tablets. *Dhaka University Journal of Pharmaceutical Sciences*, *12*(1), 29-33.

176. Rechendorff, K., Hovgaard, M. B., Foss, M., Zhdanov, V. P., & Besenbacher, F. (2006). Enhancement of protein adsorption induced by surface roughness. *Langmuir*, *22*(26), 10885-10888.

177. Reichert, J., Ochs, R., Beckmann, D., Weber, H. B., Mayor, M., & Löhneysen, H. V. (2002). Driving current through single organic molecules. *Physical Review Letters*, *88*(17), 176804.

178. Reipa, V., & Horvath, J. J. (1992). Surface-enhanced Raman study of benzylpenicillin. *Applied spectroscopy*, *46*(6), 1009-1013.

179. Rodrigues, D. C., Andrade, G. F. S., & Temperini, M. L. A. (2013). SERS performance of gold nanotubes obtained by sputtering onto polycarbonate track-etched membranes. *Physical Chemistry Chemical Physics*, *15*(4), 1169-1176.

180. Rodríguez-Lorenzo, L., Alvarez-Puebla, R. A., Pastoriza-Santos, I., Mazzucco, S., Stéphan, O., Kociak, M., ... & García de Abajo, F. J. (2009). Zeptomol detection

through controlled ultrasensitive surface-enhanced Raman scattering. *Journal of the American Chemical Society*, *131*(13), 4616-4618.

181. Rösch, P., Harz, M., Schmitt, M., Popp, J. (2005). Raman spectroscopic identification of single yeast cells. *Journal of Raman Spectroscopy*, *36*(5), 377-379.

182. Rycenga, M., McLellan, J. M., & Xia, Y. (2008). Controlling the assembly of silver nanocubes through selective functionalization of their faces. *Advanced Materials*, *20*(12), 2416-2420.

183. Rycenga, M., Xia, X., Moran, C. H., Zhou, F., Qin, D., Li, Z. Y., & Xia, Y. (2011). Generation of Hot Spots with Silver Nanocubes for Single-Molecule Detection by Surface-Enhanced Raman Scattering. *Angewandte Chemie*, *123*(24), 5587-5591

184. Saini, A., Maurer, T., Lorenzo, I. I., Santos, A. R., Beal, J., Goffard, J., ... & Plain, J. (2015). Synthesis and SERS application of SiO2@ Au nanoparticles. *Plasmonics*, *10*(4), 791-796.

185. Sajanlal, P. R., & Pradeep, T. (2009). Electric field assisted growth of highly surface enhanced Raman active gold nanotriangles. *Journal of nanoscience and nanotechnology*, *9*(9), 5283.

186. Samal, A. K., Polavarapu, L., Rodal-Cedeira, S., Liz-Marzán, L. M., Pérez-Juste, J., & Pastoriza-Santos, I. (2013). Size Tunable Au@ Ag core–shell nanoparticles: synthesis and surface-enhanced Raman scattering properties. *Langmuir*, *29*(48), 15076-15082.

187. Samanta, A., Jana, S., Das, R. K., & Chang, Y. T. (2014). Wavelength and shape dependent SERS study to develop ultrasensitive nanotags for imaging of cancer cells. *RSC Advances*, *4*(24), 12415-12421.

188. Sathyavathi, R., Krishna, M., & Rao, D. N. (2011). Biosynthesis of silver nanoparticles using Moringa oleifera leaf extract and its application to optical limiting. *Journal of nanoscience and nanotechnology*, *11*(3), 2031-2035.

189. Sato-Berrú, R., Redón, R., Vázquez-Olmos, A., & Saniger, J. M. (2009). Silver nanoparticles synthesized by direct photoreduction of metal salts. Application in surface-enhanced Raman spectroscopy. *Journal of Raman Spectroscopy*, *40*(4), 376-380.

190. Scarabelli, L., Coronado-Puchau, M., Giner-Casares, J. J., Langer, J., & Liz-Marzán, L. M. (2014). Monodisperse gold nanotriangles: size control, large-scale self-assembly, and performance in surface-enhanced Raman scattering. *ACS nano*, *8*(6), 5833-5842.

191. Schulz, F., Homolka, T., Bastús, N. G., Puntes, V., Weller, H., & Vossmeyer, T. (2014). Little adjustments significantly improve the Turkevich synthesis of gold nanoparticles. *Langmuir*, *30*(35), 10779-10784.

192. Schwartzberg, A. M., Grant, C. D., Wolcott, A., Talley, C. E., Huser, T. R., Bogomolni, R., & Zhang, J. Z. (2004). Unique gold nanoparticle aggregates as a highly active surface-enhanced Raman scattering substrate. *The Journal of Physical Chemistry B*, *108*(50), 19191-19197.

193. Scopelliti, P. E., Borgonovo, A., Indrieri, M., Giorgetti, L., Bongiorno, G., Carbone, R., ... & Milani, P. (2010). The effect of surface nanometre-scale morphology on protein adsorption. *PloS one*, *5*(7), e11862.

194. Seballos, L., Richards, N., Stevens, D. J., Patel, M., Kapitzky, L., Lokey, S., ... & Zhang, J. Z. (2007). Competitive binding effects on surface-enhanced Raman scattering of peptide molecules. *Chemical physics letters*, *447*(4), 335-339.

195. Sen, I. K., Mandal, A. K., Chakraborti, S., Dey, B., Chakraborty, R., & Islam, S. S. (2013). Green synthesis of silver nanoparticles using glucan from mushroom and study of antibacterial activity. *International journal of biological macromolecules*, *62*, 439-449.

196. Seol, S. K., Kim, D., Jung, S., Chang, W. S., & Kim, J. T. (2013). One-step synthesis of PEG-coated gold nanoparticles by rapid microwave heating. *Journal of Nanomaterials*, *2013*.

197. Shameli, K., Ahmad, M. B., Jazayeri, S. D., Shabanzadeh, P., Sangpour, P., Jahangirian, H., & Gharayebi, Y. (2012). Investigation of antibacterial properties silver nanoparticles prepared via green method. *Chem Cent J*, *6*(1), 73.

198. Shen, J., Su, J., Yan, J., Zhao, B., Wang, D., Wang, S., ... & Fan, C. (2015). Bimetallic nano-mushrooms with DNA-mediated interior nanogaps for high-efficiency SERS signal amplification. *Nano Research*, *8*(3), 731-742.

199. Shi, X., Liu, S., Han, X., Ma, J., Jiang, Y., & Yu, G. (2015). High-Sensitivity Surface-Enhanced Raman Scattering (SERS) Substrate Based on a Gold Colloid Solution with a pH Change for Detection of Trace-Level Polycyclic Aromatic Hydrocarbons in Aqueous Solution. *Applied spectroscopy*, *69*(5), 574-579.

200. Shivaji, S., Madhu, S., & Singh, S. (2011). Extracellular synthesis of antibacterial silver nanoparticles using psychrophilic bacteria. *Process Biochemistry*, *46*(9), 1800-1807.

201. Sinkó, K. (2010). Influence of chemical conditions on the nanoporous structure of silicate aerogels. *Materials*, *3*(1), 704-740.

202. Sivanesan, A., Witkowska, E., Adamkiewicz, W., Dziewit, Ł., Kamińska, A., & Waluk, J. (2014). Nanostructured silver–gold bimetallic SERS substrates for selective identification of bacteria in human blood. *Analyst*, *139*(5), 1037-1043.

203. Sivera, M., Kvitek, L., Soukupova, J., Panacek, A., Prucek, R., Vecerova, R., & Zboril, R. (2014). Silver nanoparticles modified by gelatin with extraordinary pH stability and long-term antibacterial activity. *PloS one*, *9*(8), e103675.

204. Skoog D. A., Holler F. J., Nieman T. A. (1998), Principles of Instrumental Analysis, 5th Edition, Saunders College Publishing, Philadelphia.

205. Smith, E., Dent, G. (2005). Introduction, basic theory and principles. *Modern Raman Spectroscopy-A Practical Approach*, 1-21.

206. Smith, E., Dent, G. (2013). Modern Raman spectroscopy: a practical approach. John Wiley & Sons.

207. Snitka, V., Naumenko, D. O., Ramanauskaite, L., Kravchenko, S. A., & Snopok, B. A. (2012). Generation of diversiform gold nanostructures inspired by honey's components: Growth mechanism, characterization, and shape separation by the centrifugation-assisted sedimentation. *Journal of colloid and interface science*, *386*(1), 99-106.

208. Snitka, V., Naumenko, D., Ramanauskaite, L., Kravchenko, S. A., & Snopok, B. A. (2011). Composite silicate films with gold nanoparticles for surface-enhanced Raman spectroscopy: synthesis using natural products. *Theoretical and Experimental Chemistry*, *47*(5), 296-302.

209. Sobczak-Kupiec, A., Malina, D., Wzorek, Z., & Zimowska, M. (2011). Influence of silver nitrate concentration on the properties of silver nanoparticles. *Micro & Nano Letters, IET*, *6*(8), 656-660.

210. Sobon, G., Sotor, J., Jagiello, J., Kozinski, R., Zdrojek, M., Holdynski, M., ... & Abramski, K. M. (2012). Graphene oxide vs. reduced graphene oxide as saturable absorbers for Er-doped passively mode-locked fiber laser. *Optics express*, *20*(17), 19463-19473.

211. Song, H., Li, X., Yoo, S., Wu, Y., Liu, W., Wang, X., & Liu, H. (2014). Highly Sensitive Surface Enhanced Raman Spectroscopy from Ag Nanoparticle Decorated Graphene Sheet. *Journal of Nanomaterials*, *2014*.

212. Song, N. J., Chen, C. M., Lu, C., Liu, Z., Kong, Q. Q., & Cai, R. (2014). Thermally reduced graphene oxide films as flexible lateral heat spreaders. *Journal of Materials Chemistry A*, *2*(39), 16563-16568.

213. Stamplecoskie, K. G., Scaiano, J. C., Tiwari, V. S., & Anis, H. (2011). Optimal size of silver nanoparticles for surface-enhanced Raman spectroscopy. *The Journal of Physical Chemistry C*, *115*(5), 1403-1409.

214. Stevenson, A. P., Bea, D. B., Civit, S., Contera, S. A., Cerveto, A. I., & Trigueros, S. (2012). Three strategies to stabilise nearly monodispersed silver nanoparticles in aqueous solution. *Nanoscale research letters*, *7*(1), 1-8.

215. Stewart, S., & Fredericks, P. M. (1999). Surface-enhanced Raman spectroscopy of amino acids adsorbed on an electrochemically prepared silver surface. *Spectrochimica Acta Part A: Molecular and Biomolecular Spectroscopy*, *55*(7), 1641-1660.

216. Stiufiuc, R., Iacovita, C., Lucaciu, C. M., Stiufiuc, G., Dutu, A. G., Braescu, C., & Leopold, N. (2013). SERS-active silver colloids prepared by reduction of silver nitrate with short-chain polyethylene glycol. *Nanoscale research letters*, *8*(1), 1-5.

217. Stone, N., Kendall, C., Smith, J., Crow, P., Barr, H. (2004). Raman spectroscopy for identification of epithelial cancers. *Faraday discussions*, *126*, 141-157.

218. Strachan, C. J., Rades, T., Gordon, K. C., Rantanen, J. (2007). Raman spectroscopy for quantitative analysis of pharmaceutical solids. *Journal of pharmacy and pharmacology*, *59*(2), 179-192.

219. Su, Q., Ma, X., Dong, J., Jiang, C., & Qian, W. (2011). A reproducible SERS substrate based on electrostatically assisted APTES-functionalized surface-assembly of gold nanostars. *ACS applied materials & interfaces*, *3*(6), 1873-1879.

220. Sugawa, K., Akiyama, T., Tanoue, Y., Harumoto, T., Yanagida, S., Yasumori, A., ... & Otsuki, J. (2015). Particle size dependence of the surface-enhanced Raman scattering properties of densely arranged two-dimensional assemblies of Au (core)–Ag (shell) nanospheres. *Physical Chemistry Chemical Physics*, *17*(33), 21182-21189.

221. Sun, J., Fan, W., Wu, D., & Sun, Y. (1998). Structure Control of SiO 2 Sol-Gels via Addition of PEG. *Studies in Surface Science and Catalysis*, *118*, 617-624.

222. Sun, M., Zhang, Z., Zheng, H., & Xu, H. (2012). In-situ plasmon-driven chemical reactions revealed by high vacuum tip-enhanced Raman spectroscopy. *Scientific reports*, *2*.

223. Sweetenham, C. S., & Notingher, I. (2010). Raman spectroscopy methods for detecting and imaging supported lipid bilayers. *Journal of Spectroscopy*, *24*(1-2), 113-117

224. Sweetenham, C. S., & Notingher, I. (2011). Combined atomic force microscopy-Raman mapping of electric field enhancement and surface-enhanced Raman scattering hot-spots for nanosphere lithography substrates. *Journal of Nanophotonics*, *5*(1), 059504-059504.

225. Tao, A., Kim, F., Hess, C., Goldberger, J., He, R., Sun, Y., ... & Yang, P. (2003). Langmuir-Blodgett silver nanowire monolayers for molecular sensing using surface-enhanced Raman spectroscopy. *Nano Letters*, *3*(9), 1229-1233.

226. Taylor, R. W., Benz, F., Sigle, D. O., Bowman, R. W., Bao, P., Roth, J. S., ... & Baumberg, J. J. (2014). Watching individual molecules flex within lipid membranes using SERS. *Scientific reports*, *4*.

227. Tian, Z. Q., Ren, B., Li, J. F., & Yang, Z. L. (2007). Expanding generality of surface-enhanced Raman spectroscopy with borrowing SERS activity strategy. *Chemical Communications*, (34), 3514-3534.

228. Tsvetkov, M. Y., Khlebtsov, B. N., Khanadeev, V. A., Bagratashvili, V. N., Timashev, P. S., Samoylovich, M. I., & Khlebtsov, N. G. (2013). SERS substrates formed by gold nanorods deposited on colloidal silica films. *Nanoscale research letters*, *8*(1), 1-9.

229. Turkevich, J., Stevenson, P. C., & Hillier, J. (1951). A study of the nucleation and growth processes in the synthesis of colloidal gold. *Discussions of the Faraday Society*, *11*, 55-75.

230. Tüysüz, H., Chan, C. K. (2015). Solar Energy for Fuels.

231. Ushakumary L., Sheena Mary. Y, Shyma Mary. Y, Yohannan Panicker C., Hema Tresa Varghese, Jojo P. J. (2011). Infrared Raman, surface enhanced Raman scattering and computational study of L-Alanine. *Global Journal of Analytical Chemistry*, 2 (1), 15-20.

232. Vinod, M., & Gopchandran, K. G. (2014). Au, Ag and Au: Ag colloidal nanoparticles synthesized by pulsed laser ablation as SERS substrates. *Progress in Natural Science: Materials International*, *24*(6), 569-578.

233. Wall, D., Tikhonov, S., Sindermann, S., Spoddig, D., Hassel, C., Hoegen, M., & Heringdorf, F. J. (2011). Shape, orientation, and crystalline composition of silver islands on Si (111). *IBM Journal of Research and Development*, *55*(4), 9-1.

234. Wang, M., De Vivo, B., Lu, W., & Muniz-Miranda, M. (2014). Sensitive Surface-Enhanced Raman Scattering (SERS) Detection of Nitroaromatic Pollutants in Water. *Applied spectroscopy*, *68*(7), 784-788.

235. Wang, Q. (2013). Raman spectroscopic characterization and analysis of agricultural and biological systems.

236. Wang, Y. Q., Ma, S., Yang, Q. Q., & Li, X. J. (2012). Size-dependent SERS detection of R6G by silver nanoparticles immersion-plated on silicon nanoporous pillar array. *Applied Surface Science*, *258*(15), 5881-5885.

237. Weaver, M. J., Zou, S., Chan, H. Y. H. (2000). Peer reviewed: the new interfacial ubiquity of surface-enhanced Raman spectroscopy. *Analytical chemistry*, *72*(1), 38-A.

238. Wei, G., Wang, J., & Chen, Y. (2015). Electromagnetic enhancement of ordered silver nanorod arrays evaluated by discrete dipole approximation. *Beilstein journal of nanotechnology*, *6*(1), 686-696.

239. Wu, P. C., Khoury, C. G., Kim, T. H., Yang, Y., Losurdo, M., Bianco, G. V., & Everitt, H. O. (2009). Demonstration of surface-enhanced Raman scattering by tunable, plasmonic gallium nanoparticles. *Journal of the American Chemical Society*, *131*(34), 12032-12033.

240. Xia, N., Cai, Y., Jiang, T., & Yao, J. (2011). Green synthesis of silver nanoparticles by chemical reduction with hyaluronan. *Carbohydrate Polymers*, *86*(2), 956-961.

241. Xia, X., Li, W., Zhang, Y., & Xia, Y. (2013). Silica-coated dimers of silver nanospheres as surface-enhanced Raman scattering tags for imaging cancer cells. *Interface focus*, *3*(3), 20120092.

242. Xie, Y., Zhu, X., Sun, Y., Wang, H., Qian, H., & Yao, W. (2012). Rapid detection method for nitrofuran antibiotic residues by surface-enhanced Raman Spectroscopy. *European Food Research and Technology*, *235*(3), 555-561.

243. Xu, S, Wang J., Zou Y., Liu H., Wang G., Zhang X, Jiang S, Li Z., Cao D. and Tang R. (2015). High performance SERS active substrates fabricated by directly growing graphene on Ag nanoparticles. *RCS Advances*, *5*, 90457-90465.

244. Xu, W., Mao, N., & Zhang, J. (2013). Graphene: A Platform for Surface-Enhanced Raman Spectroscopy. *Small*, *9*(8), 1206-1224.

245. Xue, B., Wang, D., Zuo, J., Kong, X., Zhang, Y., Liu, X., ... & Zeng, Q. (2015). Towards high quality triangular silver nanoprisms: improved synthesis, six-tip based hot spots and ultra-high local surface plasmon resonance sensitivity. *Nanoscale*, *7*(17), 8048-8057.

246. Yan, Z. X., Zhang, Y. L., Wang, W., Fu, X. Y., Jiang, H. B., Liu, Y. Q., ... & Sun, H. B. (2015). Superhydrophobic SERS Substrates Based on Silver-Coated Reduced Graphene Oxide Gratings Prepared by Two-Beam Laser Interference. *ACS applied materials & interfaces*, *7*(49), 27059-27065.

247. Yang, B., Liu, Z., Guo, Z., Zhang, W., Wan, M., Qin, X., & Zhong, H. (2014). In situ green synthesis of silver–graphene oxide nanocomposites by using tryptophan as a reducing and stabilizing agent and their application in SERS. *Applied Surface Science*, *316*, 22-27.

248. Yang, J., Li, J., Du, Z., Gong, Q., Teng, J., & Hong, M. (2014). Laser hybrid micro/nano-structuring of Si surfaces in air and its applications for SERS detection. *Scientific reports*, *4*, 6657.

249. Yang, S., Dai, X., Stogin, B. B., & Wong, T. S. (2016). Ultrasensitive surface-enhanced Raman scattering detection in common fluids. *Proceedings of the National Academy of Sciences*, *113*(2), 268-273.

250. Yang, Y., Zhang, Q., Fu, Z. W., & Qin, D. (2014). Transformation of Ag Nanocubes into Ag–Au Hollow Nanostructures with Enriched Ag Contents to Improve SERS Activity and Chemical Stability. *ACS applied materials & interfaces*, *6*(5), 3750-3757.

251. Yi, Z., Luo, J., Yi, Y., Kang, X., Ye, X., Bi, P., ... & Tang, Y. (2015). Study of strong dipole and quadrupole plasmon resonance in Ag nanorings antenna. *Optical Materials Express*, *5*(2), 210-217.

252. Yi, Z., Xu, X., Luo, J., Li, X., Yi, Y., Jiang, X., ... & Tang, Y. (2014). Size controllable synthesis of ultrafine spherical gold particles and their simulation of plasmonic and SERS behaviours. *Physica B: Condensed Matter*, *438*, 22-28.

253. Yi, Z., Zhang, J. B., Chen, Y., Chen, S. J., Luo, J. S., Tang, Y. J., ... & Yi, Y. G. (2011). Triangular Au-Ag framework nanostructures prepared by multi-stage replacement and their spectral properties. *Transactions of the Nonferrous Metals Society of China*, *21*(9), 2049-2055.

254. Yuan, H., Fales, A. M., Khoury, C. G., Liu, J., & Vo-Dinh, T. (2013). Spectral characterization and intracellular detection of Surface-Enhanced Raman Scattering (SERS)-encoded plasmonic gold nanostars. *Journal of Raman Spectroscopy*, *44*(2), 234-239.

255. Zaghouani, R. B., Manai, L., Rezgui, B. D., & Bessais, B. (2015). Study of silver nanoparticles electroless growth and their impact on silicon properties. *Chemistry*, *1*(3), 90-94.

256. Zhang, Q., Lee, J. Y., Yang, J., Boothroyd, C., & Zhang, J. (2007). Size and composition tunable Ag–Au alloy nanoparticles by replacement reactions. *Nanotechnology*, *18*(24), 245605.

257. Zhang, T., Song, Y. J., Zhang, X. Y., & Wu, J. Y. (2014). Synthesis of silver nanostructures by multistep methods. *Sensors*, *14*(4), 5860-5889.

258. Zhang, X., Wang, P., Zhang, Z., Fang, Y., & Sun, M. (2014). Plasmon-driven sequential chemical reactions in an aqueous environment. *Scientific reports*, *4*.

259. Zhang, X., Zhang, D., Chen, Y., Sun, X., & Ma, Y. (2012). Electrochemical reduction of graphene oxide films: preparation, characterization and their electrochemical properties. *Chinese Science Bulletin*, *57*(23), 3045-3050

260. Zhang, Y., Walkenfort, B., Yoon, J. H., Schlücker, S., & Xie, W. (2015). Gold and silver nanoparticle monomers are non-SERS-active: a negative experimental study with silica-encapsulated Raman-reporter-coated metal colloids. *Physical Chemistry Chemical Physics*, *17*(33), 21120-21126.

261. Zheng, Y., Wang, W., Fu, Q., Wu, M., Shayan, K., Wong, K. M., ... & Lei, Y. (2014). Surface-Enhanced Raman Scattering (SERS) Substrate Based on Large-Area Well-Defined Gold Nanoparticle Arrays with High SERS Uniformity and Stability. *ChemPlusChem*, *79*(11), 1622-1630.

262. Zhou, M., Wang, K., Men, Z., Gao, S., Li, Z., & Sun, C. (2012). Study of high-pressure Raman intensity behaviour of aromatic hydrocarbons: Benzene, biphenyl and naphthalene. *Spectrochimica Acta Part A: Molecular and Biomolecular Spectroscopy*, *97*, 526-531.

263. Zhu, G., Zhu, X., Fan, Q., & Wan, X. (2011). Raman spectra of amino acids and their aqueous solutions. *Spectrochimica Acta Part A: Molecular and Biomolecular Spectroscopy*, *78*(3), 1187-1195.

264. Zong, Y., Guo, Q., Xu, M., Yuan, Y., Gu, R., & Yao, J. (2014). Plasmon-induced decarboxylation of mercaptobenzoic acid on nanoparticle film monitored by surface-enhanced Raman spectroscopy. *RSC Advances*, *4*(60), 31810-31816.

265. Zou, S., & Schatz, G. C. (2006). Combining Micron-Size Glass Spheres with Silver Nanoparticles to Produce Extraordinary Field Enhancements for Surface-Enhanced Raman Scattering Applications. *Israel Journal of Chemistry*, *46*(3), 293-297.

A LIST OF PUBLICATIONS

1. Ramanauskaite, L., Xu, H., & Snitka, V. (2016). Localized Plasmon-Stimulated Nanochemistry of Graphene Oxide on a SERS Substrate. *ChemPhysChem*.(IF: 3.419)

2. Ramanauskaite, L., & Snitka, V. (2015). Surface enhanced Raman spectroscopy of L-alanyl-L-tryptophan dipeptide adsorbed on Si substrate decorated with triangular silver nanoplates. *Chemical Physics Letters*, *623*, 46-50. (IF: 1,897)

3. Ramanauskaite, L., & Snitka, V. (2015). The synthesis of controlled shape nanoplasmonic silver-silica structures by combining sol-gel technique and direct silver reduction. *Nanoscale research letters*,*10*(1), 1. (IF: 2,779)

4. Snitka, V., Naumenko, D. O., Ramanauskaite, L., Kravchenko, S. A., & Snopok, B. A. (2012). Generation of diversiform gold nanostructures inspired by honey's components: Growth mechanism, characterization, and shape separation by the centrifugation-assisted sedimentation. *Journal of colloid and interface science*, *386*(1), 99-106. (IF: 1,217)

5. Snitka, V., Naumenko, D., Ramanauskaite, L., Kravchenko, S. A., & Snopok, B. A. (2011). Composite silicate films with gold nanoparticles for surface-enhanced Raman spectroscopy: synthesis using natural products. *Theoretical and Experimental Chemistry*, *47*(5), 296-302. (IF:0,637)

A LIST OF INTERNATIONAL CONFERENCES

1. BIT's 2nd Annual World Congress of Smart Materials (2016), Singapore. Presentation theme: Photonic Nanostructures for Surface Enhanced Raman Spectroscopy. Authors: Valentinas Snitka, Lina Ramanauskaitė. *Invited talk*.

2. EMN Hong Kong meeting, Energy Materials Nanotechnology (2015), Hong Kong. Presentation theme: Synthesis of hybrid Graphene-Porphyrin nanofiber structures by ionic self-assembly. Authors: Valentinas Snitka, Lina Ramanauskaitė, Nora Grincevičiūtė. *Invited talk.*

3. META'15, the 6th International Conference on Metamaterials, Photonic Crystals and Plasmonics (2015), New York. Presentation theme: Investigation of amyloidogenic proteins interaction with lipid bilayers using local plasmonic probes. Authors: V. Snitka, L. Ramanauskaite, N. Grinceviciute and H. Xu.

4. EMN Phuket Meeting (2015), Phuket, Thailand. Presentation theme: Plasmonic Nanoprobes for Surface Enhanced Raman Spectroscopy of Biological Molecules. Authors: Valentinas Snitka, Lina Ramanauskaitė, N. Grincevičiūtė, H. Xu. *Invited talk.*

5. ImagineNano2015 Bio&Med (2015), Bilbao, Spain. Presentation theme: Investigation of bilayer lipid membranes on nanostructured Au and Ag substrates by surface enhanced Raman spectroscopy. Authors: Nora Grincevičiūtė, Lina Ramanauskaitė, Valentinas Snitka.

6. ImagineNano2015 PPM (2015), Bilbao, Spain. Presentation theme: Novel plasmonic probes for Tip- Enhanced Raman Spectroscopy. Authors: Valentinas Snitka, Lina Ramanauskaitė, H. Xu, Rasa Žūkienė, Tomas Gadišauskas.

7. ImagineNano2015_Chemistry (2015), Bilbao, Spain. Presentation theme: The synthesis of nano-wedge decorated substrates for the detection of molecular traces by surface enhanced Raman spectroscopy. Authors: Lina Ramanauskaitė, H. Xu, Rasa Žūkienė, Valentinas Snitka.

8. 2nd International Workshop on Metallic Nano-Objects: From Fundamentals to Applications (2014), Lille, France. Presentation theme: Ring type plasmonic nanostructures for Surface Enhanced Raman Spectroscopy. Authors: Lina Ramanauskaitė, Valentinas Snitka.

9. 13th International Conference on Near Field Optics, Nanophotonics, and Related Techniques (2014), Salt Lake City, Utah, USA. Presentation theme: Surface Enhanced Raman Spectroscopy of L-alanyl-L-tryptophan dipeptide. Authors: Lina Ramanauskaitė, Valentinas Snitka.

10. XIIIth International Conference of Lithuanian Biochemical Society (2014), Birštonas, Lithuania. Presentation theme: The effect of bovine serum albumin-coated zinc oxide nanoparticles on cell viability and ROS generation. Authors: Rasa Žūkienė, Nora Grincevičiūtė, Lina Ramanauskaitė, Valentinas Snitka.

11. Nanotechnology: Research and Development (2014), Lithuania. Presentation theme: State-of-the art review in bionanotechnology imaging. Authors: V. Snitka, D. Verdes, L. Ramanauskaitė.

12. 5th international conference on Advanced Nanomaterials (2014), Aveiro, Portugal. Presentation theme: Sol-Gel Derived Nanostructured Silica Films Decorated with Silver Nanoparticles. Authors: L. Ramanauskaitė, V. Snitka.

13. ENM spring meeting / Energy materials nanotechnology (2014), Las Vegas, USA. Presentation theme: Photonic nanostructures for surface enhanced Raman spectroscopy. Authors: Valentinas Snitka, Lina Ramanauskaitė. *Invited talk*.

A LIST OF SEMINARS

1. The application of scanning probe microscopy for the investigation of biological structures (2015), Kaunas, Lithuania. The themes of oral presentations:
   - Investigation of L-alanyl-L-tryptophan dipeptide adsorbed on the nanostructured silver surface by surface enhanced Raman spectroscopy.
   - The synthesis of controlled plasmonic nanostructures by sol-gel technology and direct silver ions reduction on the silica films.

2. The application of innovative nanoscopic methods for the investigation of proteins (2014), Vilnius, Lithuania. The theme of oral presentation:
   - The functionalization and application of the substrates for surface enhanced Raman spectroscopy.

INTERNSHIPS

1. University of Zurich, Department of Chemistry (Switzerland, Zurich, 2014). Duration: one week.

2. Instituto Officina dei Materiali CNR (Trieste, Italy, 2015). Duration: one week.

PARTICIPATION IN RESEARCH PROJECTS

1. Nanoscopic investigation of structural transformations of proteins at the nano-bio-interfaces (NanoProt) funded by European Social Fund (Successfully implemented). Duration: 26 months (2013–2015).

2. Development of advanced methods for molecular contamination analysis by surface and tip enhanced Raman for space applications (CONRAM,) funded in collaboration between European Space Agency (ESA) and Lithuanian Ministry of Economy. Duration: 24 months (2016–2017).

SL344. 2016-11-18, 13,75 leidyb. apsk. l. Tiražas 10 egz. Užsakymas 422.
Išleido Kauno technologijos universitetas, K. Donelaičio g. 73, 44249 Kaunas
Spausdino leidyklos „Technologija“ spaustuvė, Studentų g. 54, 51424 Kaunas